

© <2018>. This manuscript version is made available under the CC-BY-NC-ND 4.0 license <http://creativecommons.org/licenses/by-nc-nd/4.0/>

This document is the Accepted Manuscript version of a Published Work that appeared in final form in [Cyclometalated iridium(III) luminescent complexes in therapy and phototherapy]. To access the final edited and published work see [https://doi.org/10.1016/j.ccr.2018.01.010].

Review

Cyclometalated iridium(III) luminescent complexes in therapy and phototherapy

Ana Zamora,[‡] Gloria Viguera,[‡] Venancio Rodríguez, M. Dolores Santana and José Ruiz*

Departamento de Química Inorgánica, Universidad de Murcia, and Institute for Bio-Health Research of Murcia (IMIB-Arrixaca), E-30071 Murcia, Spain.

*Corresponding author: Tel: +34 868 887455.

E-mail address: jruiz@um.es. (J. Ruiz)

[‡]These authors contributed equally to this work.

Contents

1. Introduction.....	
2. Cyclometalated Ir(III) anticancer theranostic agents.	
2.1. Organelle targeted and membrane disruptor agents	
2.1.1. DNA binders and nucleus-targeted	
2.1.2. Mitochondria-targeted	
2.1.3. Localization in lysosomes.	
2.1.4. Localization in membrane.	
2.2. Protein-targeted inhibitors	
2.2.1. Receptors-targeted	
2.2.2. Protein binders and enzyme inhibitors.....	
2.2.3. Protein–protein interactions inhibitors as anticancer agents	
3. Cyclometalated Ir(III) complexes for phototherapy: from the visible to the NIR light activation	
3.1. General	
3.2. One photon PDT	
3.2.1. Mitochondria and lysosome-targeted PS	

3.2.2. ER and nucleus-targeted PS	
3.2.3. Cytoplasm-targeted PS.....	
3.2.4. Towards NIR activation.....	
3.2.4.a Conjugation of bulky organic fluorophores.....	
3.2.4.b Use of π -expansive ligands.....	
3.2.4.c Conjugation to UCNPs.....	
3.3. Two photon PDT.....	
3.4. PACT.....	
4. Cyclometalated Ir(III) complexes in bacterial infections, inflammatory diseases, and neurological disorders	
4.1. Antibacterial agents	
4.2. Alzheimer's disease	
4.3. Chronic inflammatory diseases	
5 Overall structure activity relationships of some representative complexes	
6. Conclusions.....	
Abbreviations.....	
Acknowledgments.....	
References.....	

Abstract

Octahedral Ir(III) complexes bearing cyclometalated ligands exhibit a great stability in biological media and are excellent therapeutical and phototherapeutical candidates for some major human ailments. Interesting examples of the use of luminescent iridium compounds in the area of cancer diagnosis and treatment have been recently reported, including modulators in protein-protein interactions, membrane-disruptors or mitochondria-targeted agents. Likewise, the scope of their conjugation to targeting vehicles as well as to smart nanoplatfoms has been studied as a mean for an adequate delivery to cancer cells. Furthermore, several Ir(III) compounds have recently been found to be promising photodynamic therapy (PDT) agents both for cancer and Alzheimer's disease. Additionally, their use as photoactive species in photoactivated chemotherapy (PACT) has also been explored in spite of their high photostability. Finally, new developments of Ir(III)-based drugs in infectious and inflammatory diseases, and neurological disorders, will be also discussed, including a direct inhibitor of *S. aureus*, containing one amino group in the N^N ligand, a TACE inhibitor (an enzyme involved in the formation of the biologically active form of TNF- α) and a photosensitizer inducing oxidation of amyloidogenic peptides and controlling their aggregation pathways under mild conditions. The mechanism of action of Ir(III) agents together with the relationship between their structures and biomedical activities will be discussed.

Keywords: Medicinal; Cyclometalated iridium(III) complex; Anticancer; Luminiscence; Alzheimer's disease; Antibacterial; Theranostic; PDT; PACT; Nanomaterial; Drug delivery

1. Introduction

Iridium is a transition metal of the platinum group that possesses interesting photophysical properties that have given rise to important applications [1]. One of the most outstanding functions of iridium compounds is its use as catalysts [2] in hydrogenation reactions [3], water oxidation [4] or metathesis of alkanes [5], among others [6]. Other very important industrial applications of Ir(III) complexes are their use in electronic devices, such as photoelectronic sensors, photochemistry and luminescent chemosensors [7]. The increase in the number of articles related to these applications has been growing exponentially during the last five years whereas in comparison, the use of Ir(III) compounds in biomedicine is still in its infancy (Fig. 1). However, there is an increasing interest in developing Ir(III)-based compounds with biomedical purposes. This is because Ir(III) complexes present physicochemical properties that allow the modulation of their reactivity from kinetically labile species to others practically inert [8]. Moreover, Ir(III) compounds display several advantages with respect to platinum and ruthenium compounds that reinforce their medicinal chemistry potential, such as their easy synthesis, air and moisture stability [8].

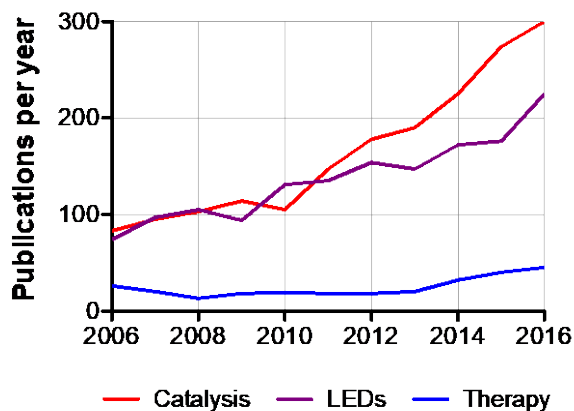


Fig. 1. Published articles on iridium therapy and other applications between 2006-2016 (Web of Science, core collection, 2017-september)

In the 70s, the chemistry of iridium anti-cancer compounds was centered on d^8 square-planar 1,5-cyclooctadiene Ir(I) complexes (Fig. 2), due to their similarity to those of Pt(II) [9]. More recently, 'half-sandwich' cyclometalated Ir(III) complexes have demonstrated promising antiproliferative activity towards a range of cancer cell lines [10]. In this context, Sadler and co-workers [10-13] have extensively investigated pseudo-octahedral Ir(III) complexes of the type $[(\eta^5\text{-Cp}^x)\text{Ir}(\text{X}^{\wedge}\text{Y})\text{L}]^{0/+}$ (Fig. 2), where Cp^x is pentamethylcyclopentadienyl Cp^* or its phenyl or biphenyl derivative, $\text{X}^{\wedge}\text{Y}$ is a chelating $\text{N}^{\wedge}\text{N}$ or $\text{C}^{\wedge}\text{N}$ bidentate ligand and L an anionic chloride or a neutral pyridyl ligand. The structural and electronic properties of these species are usually governed by the ligands. Thence, metal complexes offer enormous scope for the design of anticancer candidates due to their versatile structures, potential redox features, and wide range of ligand substitution rates. Consequently, it is now generally accepted that even simple modifications of organometallic scaffolds dictate target preferences [11, 14-19]. For example, the ligand exchange reactions of some Cp^*Ir complexes, which can take place in a few seconds, are directly related to their anticancer activities due to their ability to bind to DNA. Likewise, these complexes can have redox mechanisms of action and function as catalytic drugs [10, 11a]. Furthermore, organometallic Ir(III) compounds have been used as structural scaffold for the specific inhibition of biologically relevant enzymes [15a,19]. Even more interestingly, smart design and efficient synthesis of cyclopentadienyl

organoiridium(III) complexes have given rise to a range of the biological activities. Thus, benzimidazole Ir(III) cyclometalated complexes have demonstrated promising dual cytotoxic and anti-angiogenesis activities [20]. Furthermore, the use or the conjugation of fluorogenic reporters such as BODIPY has provided either the visualization of transfer hydrogenation iridium catalysts [21] as real-time monitoring of Ir(III) distribution inside living cells [22]. For example, the judicious positioning of the BODIPY entity in complex **1** increased the lipophilicity of the complexes and slowed down the hydrolysis rate, which in turn enhanced its cytotoxicity.

On the other hand, octahedral cyclometalated Ir(III) complexes are notable for their intrinsic luminescence properties and have been recently reviewed as biomolecular probes and cellular imaging reagents by Lo and Tso [23]. In addition to their usefulness as luminescent probes and sensors, other interesting therapeutic properties have been described against different biomolecular targets. Thus, compounds of the formula $[\text{Ir}(\text{C}^{\wedge}\text{N})_2(\text{N}^{\wedge}\text{N})]^+$ (Fig. 2) can exhibit good anticancer activity, generate singlet oxygen when photoactivated or act as modulators in protein-protein interactions, such as tumor necrosis factor- α (TNF- α), signal transducer and activator of transcription 3 (STAT3) and mammalian target of rapamycin (mTOR) [24].

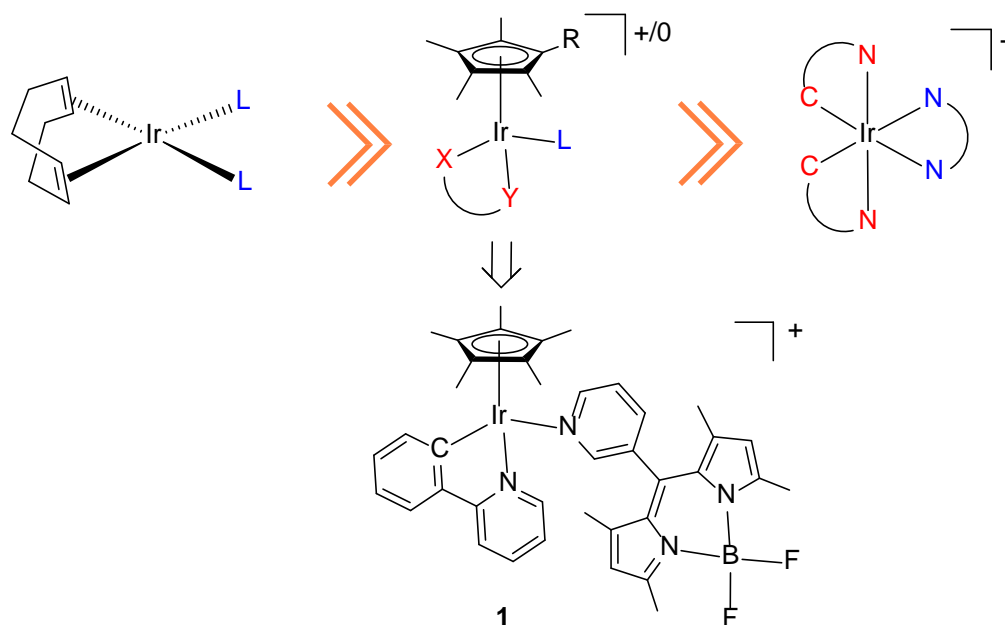


Fig. 2. Main geometries for organometallic Ir(I) and Ir(III) therapeutic agents (up). A half-sandwich Ir(III) teranostic agent (bottom).

The photophysical properties of polypyridyl complexes of Ir(III) can be also suitably fine-tuned through the coordination of different types of ligands to encompass a wide range of emission colors in the visible and the near-infrared (NIR) region of the spectrum [25]. As in other heavy transition metal complexes the emissions may be produced from various excited states including $^3\text{MLCT}$, $^3\text{ILCT}$, $^3\text{LLCT}$, $^3\text{LMMCT}$, $^3\text{MMLCT}$, $^3\text{MLLCT}$. All of them are influenced by the effect of the heavy atom and therefore the excited state is a triplet state in nature, what favors high quantum yields, long lifetimes, large Stokes' shifts and high photostability. In addition, luminescence from triplet emitting states can be quenched by oxygen, and in this sense Ir(III) complexes can be used in intracellular environments as hypoxia sensors [26] or to sensitize molecular oxygen. Therefore, using the appropriate ligands Ir(III) complexes have found application as probes of ions, molecules and organelles [27], as well as efficient photosensitizers for photodynamic therapy (PDT).

Although relatively unexplored, the rich organoiridium chemistry offers unique features that can be exploited to generate novel diagnostic and therapeutic agents or even more importantly, compounds possessing both therapeutic and diagnostic functions. In this review, we highlight in three big sections the most important applications of luminescent cyclometalated Ir(III) complexes as therapeutic agents. First, we covered their antitumor potential together with their structure–activity relationships (SARs) and the proposed mechanism of actions. Following, their most recent applications in PDT are discussed, including its surprising role in photoactivated chemotherapy (PACT). Finally, we collected some of their less studied applications, such as its use in antibacterial resistance, Alzheimer's, and autoinflammatory diseases. In addition, their activity in some nanomaterial systems and some *in vivo* studies are also highlighted.

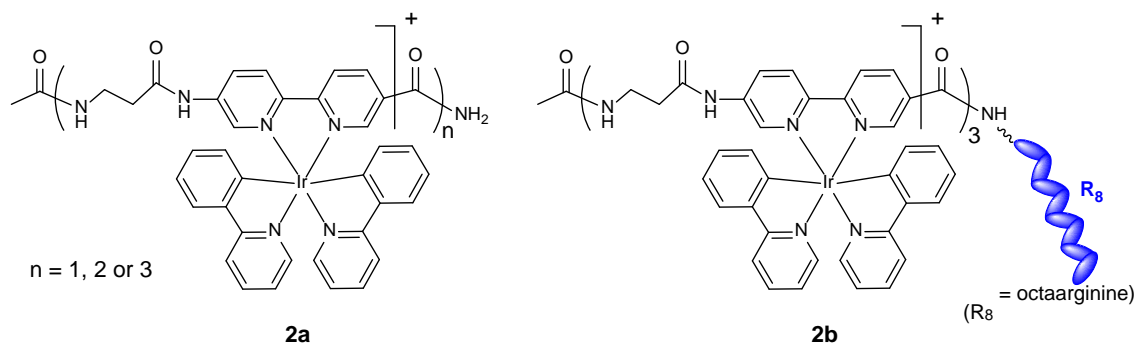
2. Cyclometalated Ir(III) anticancer theranostic agents

Cancer is one of the leading causes of death, and therefore a serious public health problem around the world. To get an idea, the American Cancer Society estimates about 1,7 million new cancer cases to be diagnosed in 2017 and about 600,000 cancer death this year in the United States [28]. Chemotherapy, together with surgery and radiation therapy, is the most common form of cancer treatment. However, systemic chemotherapy is often the only treatment option for metastasized tumors and nearly 50% of patients are being treated with platinum-based drug. In spite of their clinical success, the efficacy of traditional Pt(II) anticancer drugs is badly compromised by resistance problems and severe systemic toxicities due to its indiscriminate body distribution [29]. As an alternative to the FDA-approved Pt(II) complexes, numerous metal-based drugs targeting DNA or proteins via covalent interactions have been screened as antitumor agents. Instead, metallodrugs exhibiting non-traditional mechanism of action have not been historically considered. In this section, it is demonstrated the importance given in the recent literature to the development of kinetically inert Ir(III) complexes as theranostic anticancer agents as well as selective inhibitors against biologically relevant targets. We have divided this section into different groups according to the primary target to which the luminescent $[\text{Ir}(\text{C}^{\wedge}\text{N})_2(\text{N}^{\wedge}\text{N})]^+$ complexes are directed.

2.1. Organelle-targeted and membrane disruptor agents

2.1.1. DNA binders and nucleus-targeted

Nucleus-targeted drug delivery is a promising strategy for anticancer therapy [30], but targeting nucleus *in vivo* still presents great challenges. Vázquez and co-workers have recently prepared a series of organometallopeptides **2a** showing low DNA affinity [31]. This might be explained by the reduced charge of $[\text{Ir}(\text{ppy})_2(\text{bpy})]^+$ fragments (+1 charge in each complex) in comparison to that of the $[\text{Ru}(\text{bpy})_3]^{2+}$ DNA complexes (+2). With the aim of introducing additional positively charged groups to enhance the electrostatic interactions with the negatively charged DNA, the octaarginine derivatives bis-cyclometalated Ir(III) **2b** were synthesized. Interestingly, the octaarginine derivatives exhibited high DNA binding affinity, sequence selectivity, and high cytotoxicity towards a set of cancer cell lines [31]. The binding affinity was heavily dependent on the nuclearity of the metallopeptides, so that the trinuclear oligoarginine derivative **2b** displayed association constants with the DNA hairpin 100 times higher than those typically reported for common mononuclear intercalating Ru(II) complexes, 1000 times stronger than those observed for other non-intercalating DNA binding metal complexes, and in the order of that of the Hoechst 33258, a widely used organic DNA minor-groove binder. The cytotoxicity of the octaarginine derivatives **2b** was explained by the induction of highly supercoiled DNA as observed in AFM studies, and the resulting obstruction of processes requiring the access of proteins to the DNA.



Chen and co-workers have recently reported [32] large nanoparticles (ca. 150 nm) composed of PEG-benzoic imine-oligo-*l*-lysine/Ir(III) metallodrug complex **3a** (Fig. 3), with a detachable PEG shell when internalized into intracellular acidic endo/lysosomes of HeLa cancer cells. The small nanoparticles (ca. 40 nm), with exposure of the oligo-*l*-lysine after the detachment of the PEG shield, then translocate into the nucleus *via* the nucleopore due to the small size and nuclear localization ability of the oligo-*l*-lysine **3b**. The PEG chains were detached due to the cleavage of the benzoic imine bond at low pH. The intranuclear drug release was confirmed by the real-time observation of the intranuclear nanoparticles, as recorded by confocal fluorescent microscopy in 10-min intervals for 40 min after 6 h incubation. It was found that the luminescence intensity of Ir(dfppy)²⁺ moiety was progressively enhanced over time due to the interaction with histidine residues in the nucleus. The intranuclear release of the metallodrug provided a highly effective way to kill HeLa cells. Greater tumor suppression in a mice model compared to the native drug was also observed.

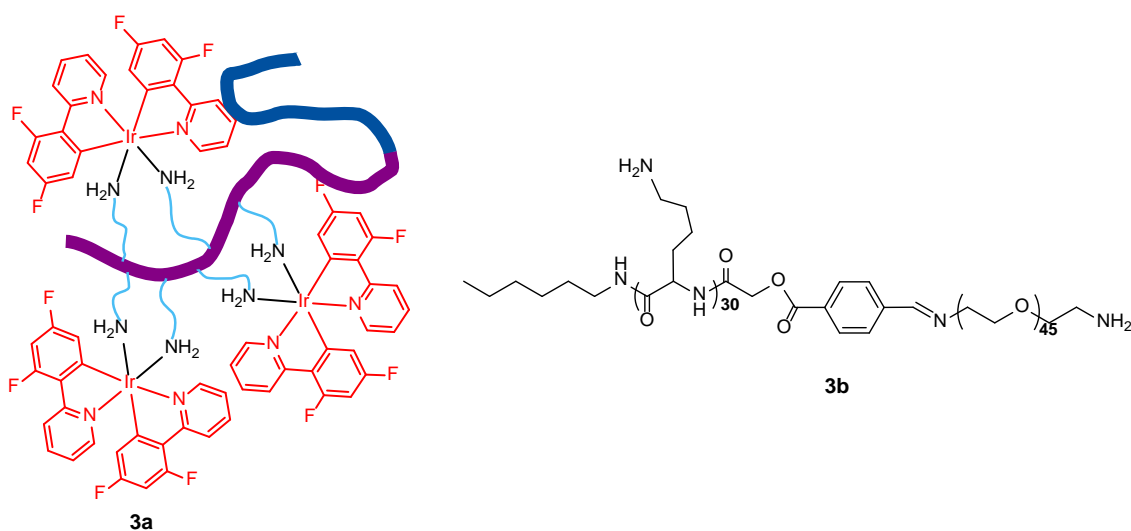


Fig. 3. PEG-*b*-oligo-*L*-Lys/Ir(III) amphiphilic conjugate (left) and the PEG detachable block copolymer to give NH₂-PEG-imine-Lys₃₀ (right).

2.1.2. Mitochondria-targeted

As one of the most important cell signaling center, mitochondria are essential organelles required for cellular energy production. They are involved in many other cellular activities, one of which is to

produce ROS and lead to mitochondria-mediated apoptosis. Because of mitochondrial-targeted compounds represent a promising approach to eradicate chemotherapy-refractory cancer cells, the interest in developing mitochondria-targeted luminescent therapeutic agents has increased [33-38], which provides the possibility for *in situ* monitoring the therapeutic effect. Mao and co-workers have reported several series of mitochondria-targeted theranostic agents. Coumarin-appended phosphorescent cyclometalated Ir(III) complexes such as **4a** and **4b** specifically target mitochondria and demonstrated theranostic functions by simultaneously inducing and monitoring morphological changes in the organelle [33]. The influence of C^N ligands on their cytotoxicity was negligible, as they showed comparable *in vitro* antiproliferative activity. Genome-wide transcriptional and connectivity map analyses revealed that the cytotoxicity of **4b** was associated with pathways involved in mitochondrial dysfunction and apoptosis [33]. A library of ester-modified cyclometalated Ir(III) complexes as **4c** have been also reported by Mao *et al.* [34]. The cytotoxicity of these Ir(III) complexes were correlated with the length of their ester groups. They initiate a series of events associated with mitochondrial dysfunction including ATP depletion, loss of mitochondrial membrane potential (MMP) and elevation of ROS, inducing pro-death autophagy and apoptosis simultaneously. Ir(III) derivatives as **4d**, containing a reactive chloromethyl group, were fixed on mitochondria through nucleophilic substitution with reactive thiols present in mitochondrial proteins [35]. The immobilization of **4d** on mitochondria resulted in a much higher cytotoxicity than the non-fixable complexes. They also selectively killed cancer cells over non-cancerous cells, and were utilized to monitor mitochondrial morphological changes. Thus, co-localization experiments with the mitochondrion-specific fluorescent commercial probe MitoTracker Deep Red (MTDR) showed that **4d**, **4e** and **4f** were specifically localized in mitochondria of human pulmonary carcinoma A549 cells [35, 36] (Fig. 4). In agreement with this result, the content of iridium in the mitochondria for **4d** was found to be much higher than in the cytosol and nuclei as indicated by inductively coupled plasma-mass spectrometry (ICP-MS) measurements [35]. The morphological changes in A549 cells exposed to **4e** and **4f** were studied by transmission electron microscopy (TEM). Compared with vehicle treatment, Ir(III) treatment increased the formation of autophagosomes and large vacuoles containing debris of mitochondria (which are characteristics of mitophagy) [36]. The authors demonstrated that 1,1'-dimethyl-2,2'-biimidazole Ir(III) complexes **4e** and **4f** induced mitophagy by depolarization of MMP, depletion of cellular ATP, perturbation in mitochondrial metabolic status, and induction of oxidative stress [36].

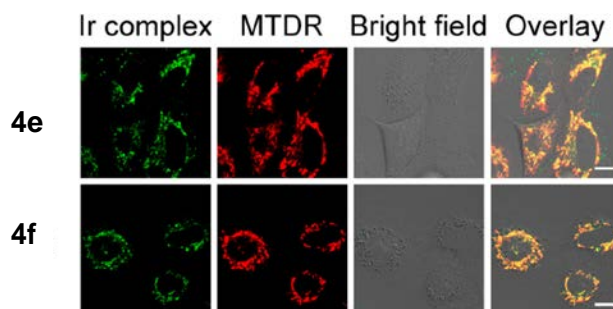
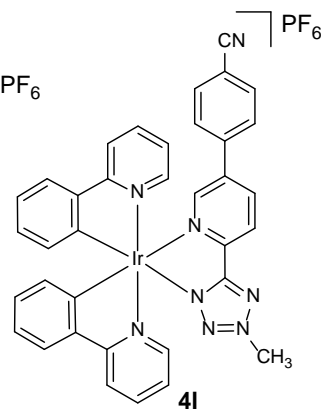
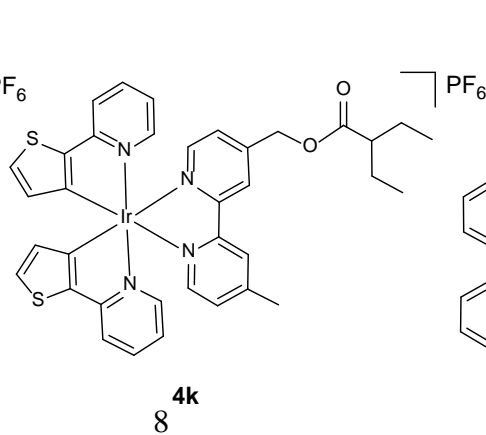
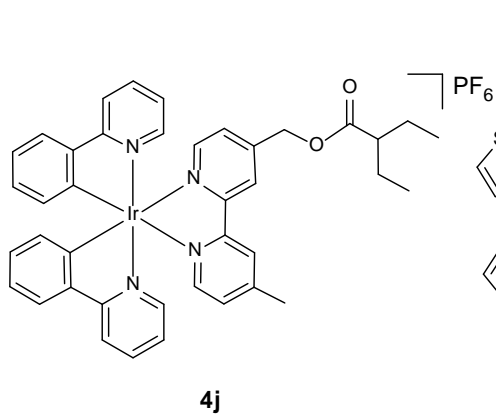
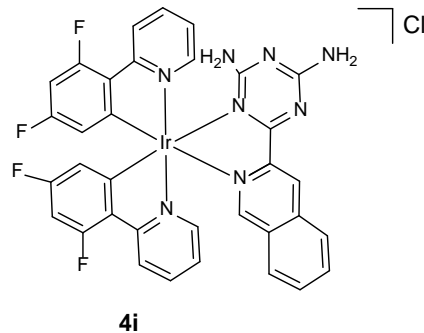
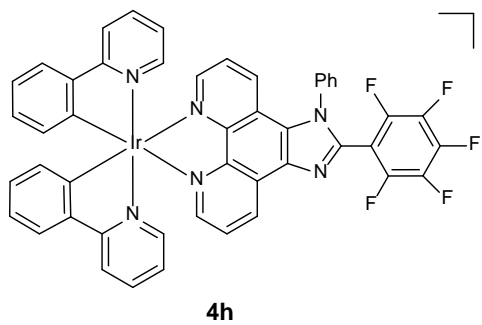
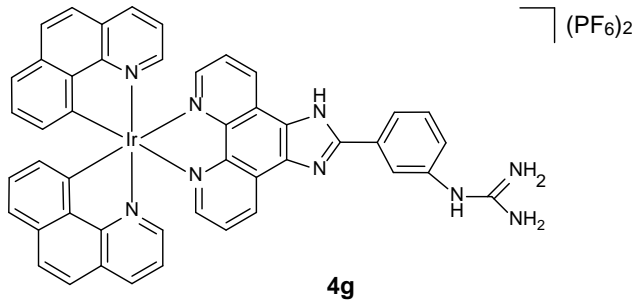
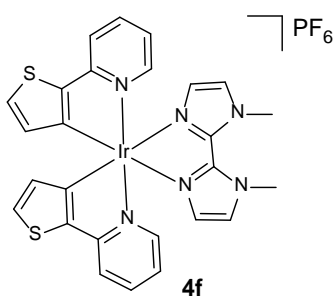
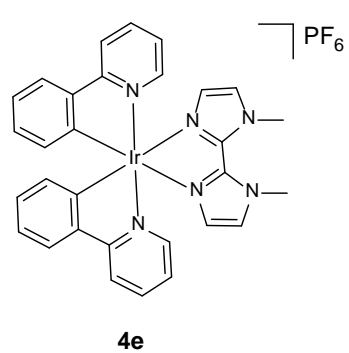
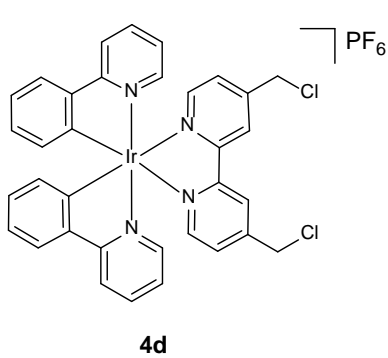
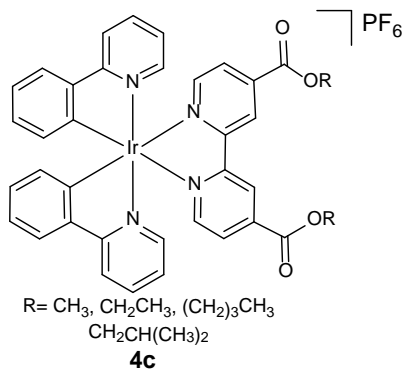
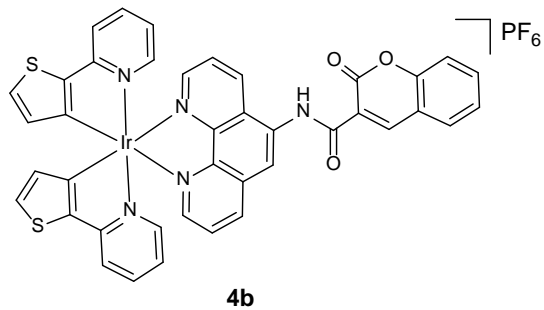
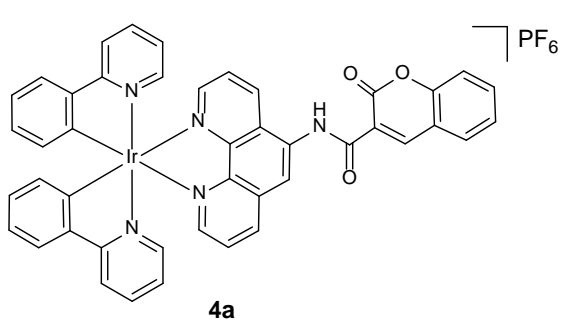


Fig. 4. Representative confocal images of A549 cells exposed to **4e/4f** (15 μ M, 1 h) and MTDR (100 nM, 30 min). Reproduced with permission from [36]. Copyright (2017) American Chemical Society.



Cyclometalated Ir(III) complexes containing guanidinium ligands as **4g** displayed moderate cytotoxicity by specifically targeting mitochondria and inducing a cascade of apoptotic events related to mitochondrial dysfunction [37]. Confocal microscopy showed that **4g** was located in the cytoplasm of HeLa cells after 3.5 h of incubation. Mechanism studies indicated that these complexes arrested the cell cycle in the G₀/G₁ phase and influence mitochondrial integrity, inducing cancer cell death through ROS-dependent pathways.

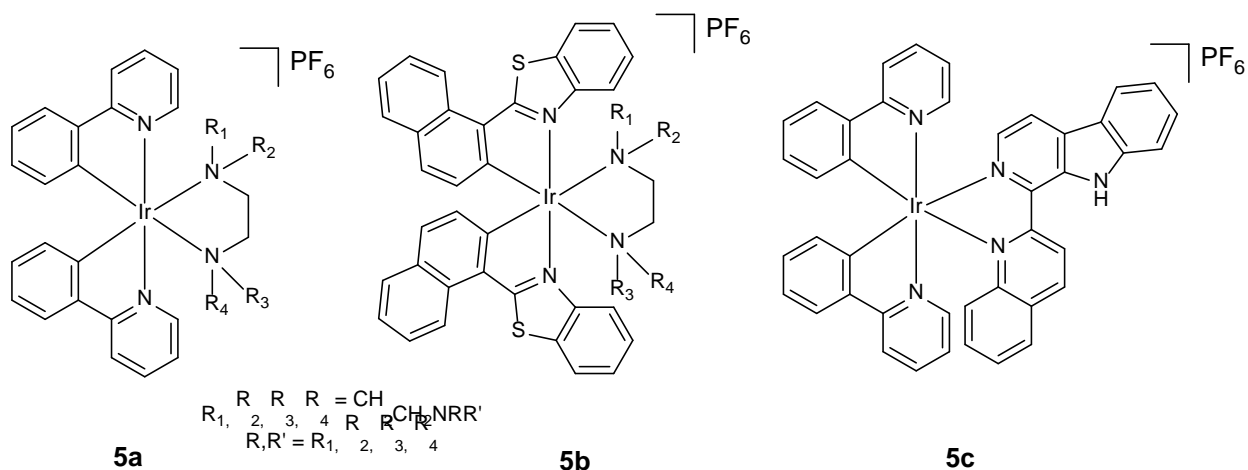
Chao *et al.* have described a series of cyclometalated Ir(III) complexes with different number of substituted fluorine atoms in the N^N ligand. **4h**, bearing the greatest number of fluorine atoms, showed the highest cytotoxicity and selectivity between tumor and normal cells and remarkable sensitivity to a cisplatin-resistant cell line (A549R) [38a]. By colocalization and ICP-MS, **4h** could penetrate cell membranes rapidly and preferentially targeted mitochondria. Further mechanism studies on **4h** including mitochondrial membrane potential depolarization and caspase 3/7 activation revealed that induced apoptosis via mitochondrial pathways. On the other hand, cyclometalated Ir(III) complexes with 2,4-diamino-1,3,5-triazine derivatives as **4i** exhibited also high selectivity between tumor cells and normal cells [38b]. ICP-MS results indicated that **4i** were taken up via an energy-independent pathway by normal liver LO2 cells while an energy-dependent pathway were found in the radiation-resistant A549 cell line. Treatment of these radiation-resistant cells with **4i** could result in generation of ROS, prominent depletion of $\Delta\Psi_m$ and activation of Caspase 9 and Caspase 3/7.

Mao and co-workers have recently prepared some valproic acid (VPA) Ir(III) conjugates such as **4j** and **4k** [39]. The ester bonds in **4j** and **4k** could be quickly hydrolysed by esterase so that the complexes displayed similar inhibition on the histone deacetylase (HDAC) activity to that of VPA. Furthermore, **4j** and **4k** showed much higher antiproliferative activities than cisplatin against various cancer cells including cisplatin-resistant A549 cells. Colocalization experiments of **4j** and **4k** with MTRD under one- and two-photon excitation demonstrated the specific mitochondria staining of the complexes in HeLa cells. In addition, these complexes induced a series of events associated with mitochondrial damage in HeLa cells including MMP depolarization, ROS production, cell cycle arrest, caspases activation and apoptosis.

Massi and co-workers have reported the synthesis of some cytotoxic cationic Ir(III) tetrazolato complexes **4l** that targeted mitochondria (co-located with MitoTracker® Red CMXRos), whereas the neutral analogues were mainly localized in the endoplasmic reticulum (ER) and showed lower cytotoxicity [40]. Energy dependent pathways are predominantly involved in the cellular uptake of these complexes as shown by comparing the emission from the Ir(III) complexes between cells incubated at 37 and 4 °C. **4l** appeared to induce apoptosis, characterized by the formation of cellular vacuoles and rounding of the mitochondria.

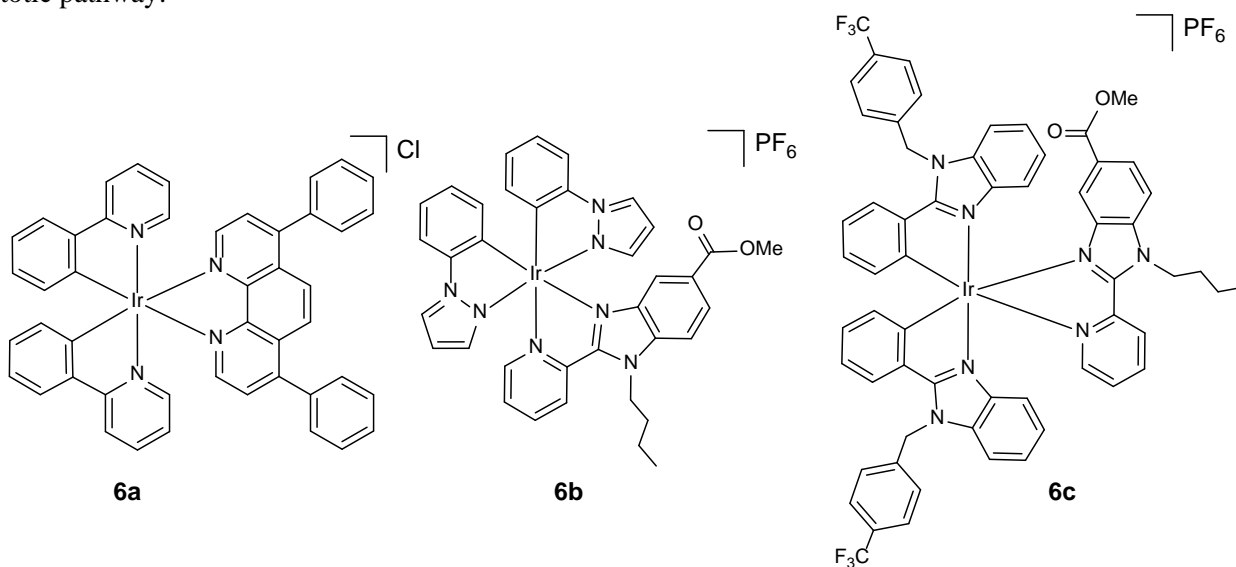
2.1.3. Localization in lysosomes

Lysosomes are the stomachs of the cells that degrade endocytosis and intracellular biomacromolecules and participate in various other cellular processes, such as apoptosis and cell migration. Lo and co-workers reported the synthesis of some luminescent cyclometalated Ir(III)–polyamine complexes **5a** and **5b** using branched poly(ethyleneimine) (bPEI) as ligands [41]. ICP-MS and confocal laser scanning microscopy data indicated that an energy-requiring process, such as endocytosis, was involved in the cellular uptake of these complexes. Both cyclometalating and polyamines ligands played a role in the photophysical properties, lipophilicity, cellular uptake, and cytotoxicity of the complexes towards HeLa and HEK293T (human embryonic kidney 293T) cell lines. On internalization, the bPEI complexes **5a** and **5b** were localized in the lysosomal compartments, whereas the etilendiamine (R¹= R²= R³= R⁴ = H) complexes were diffusely distributed throughout the cytoplasmic region. Ir(III) β -carboline complex **5c** caused about 35 % reduction in the viability of A549 cells (for 6 h, 10 μ M) and could specifically image lysosomes inducing an autophagic response [42]. The combination of these two properties makes **5c** an ideal theranostic agent to track lysosomal changes during autophagic processes. Additionally, **5c** displayed strong two-photon excited luminescence, which is favorable for live cell imaging and *in vivo* applications.



2.1.4. Localization in membrane

Fei and co-workers have studied the influence of the tuning the N^N ligand on the cellular behavior and toxicity effect of polypyridyl complexes as **6a**. Properties such as absorbance/emission efficiency, lipophilicity or cellular uptake increased as the size of the coordinated ligand did. Confocal microscopy revealed that after 1h incubation with HeLa cells, the highest amount of **6a** was in the cell membrane fraction, accounting for nearly 60%. Hence, the cytotoxic effect of **6a**, which was approximately 6-fold more potent than cisplatin in killing HeLa cells, may initiate from the membranous organelles in the cytoplasm [43]. In addition, compound **6a** induced ER stress, which promoted a fast cytosolic release of calcium. As a consequence, morphology and function of mitochondria were disturbed, initiating an intrinsic apoptotic pathway.



Brabec, Ruiz and co-workers have reported the synthesis and biological properties of **6b** and **6c**, which contain a 2-pyridyl-benzimidazole N^N ligand with an ester group as a handle for further functionalization [44]. These compounds exhibited IC₅₀ values in the high nanomolar range in some ovarian and breast cancer cell lines, becoming approximately 100× more cytotoxic than cisplatin in MDA-MB-231. As shown by confocal microscopy studies, **6c** was predominantly located in the actin cortex of A2780 cells (Fig. 5), which is a specialized layer of cytoplasmic protein (actin-rich network) on the inner face of the plasma membrane of the cell periphery, which functions as a modulator of plasma membrane behavior and cell surface properties. This particular feature was also supported by the origin of cellular blebs observed after the treatment with the Ir(III) compounds. Quantification by ICP-MS of metal levels on nuclear DNA and total cellular RNA in MCF-7 cells suggested that they exerted their toxic effects in tumor cell lines by a mechanism not involving coordinative binding to nucleic acids.

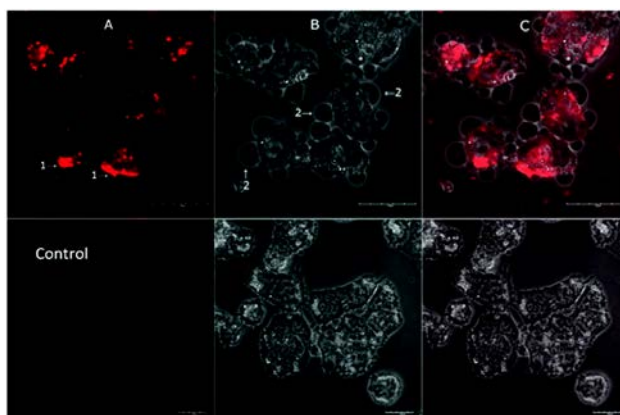
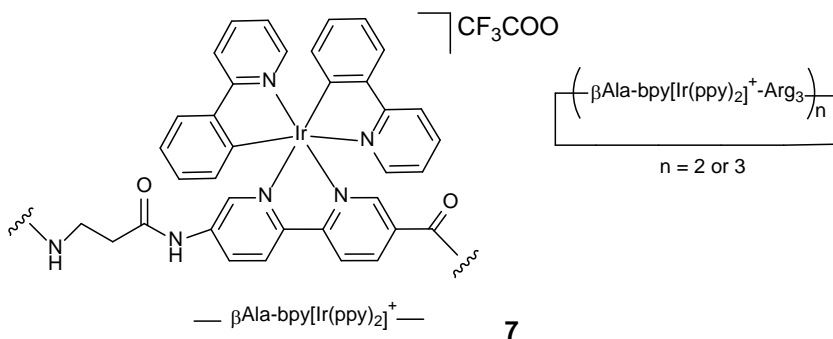
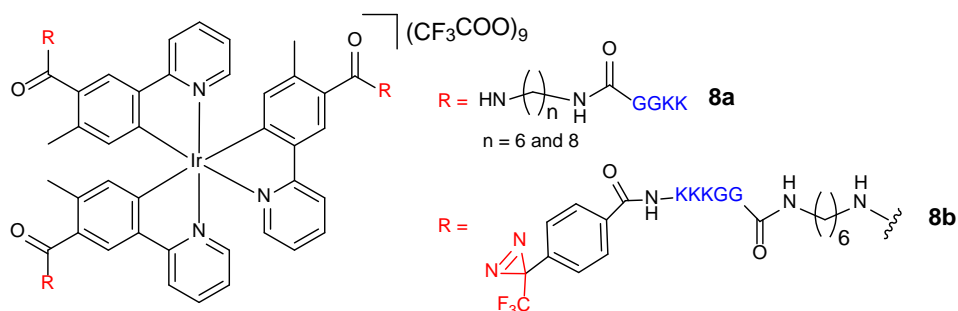


Fig. 5. Confocal microscopy studies of A2780 cells treated with **6c**. Cells were exposed to the Ir complex (5 μM) for 3 h (upper row); 1 in (A) designates accumulation in the actin cortex, 2 in (B) designates membrane protrusions (blebs). Controls (bottom row) were treated with the corresponding amount of DMSO (only one representative figure is shown). (A) Luminescence channel; (B) bright field channel; (C) merge of the luminescence and bright field channels). Reproduced from [44].

Vázquez *et al.* have reported a series of oligoarginine peptide derivatives **7**, which contain cyclometalated Ir(III) units and displayed remarkable cytotoxicity and lytic properties [45]. *In vitro* studies with unilamellar vesicles supported a membrane-disrupting mechanism of action. The luminescent properties of these peptides allowed to observe their aggregation on the cell membranes. Furthermore, the peptidic nature of these cytotoxic probes allows the straightforward modulation of their cytotoxicity through clever modification of the peptide sequence, or repositioning of the metal centers, so that their activity against non-tumoral cells could be reduced.



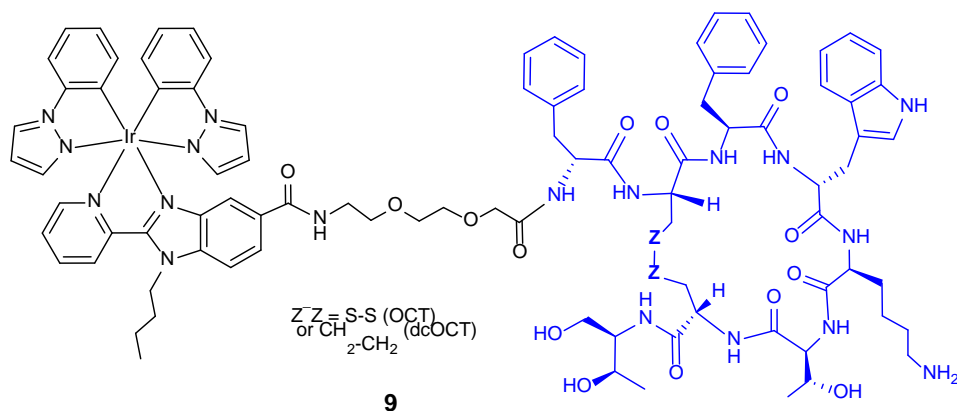
On the other hand, Aoki *et al.* have shown that amphiphilic tri-cyclometalated Ir(III) complexes **8a**, containing cationic peptides such as a KKGG sequence (K: lysine, G: glycine) and alkyl chain linkers of adequate length ($n = 6$ and $n = 8$), exhibited considerable cytotoxicity against cancer cells such as Jurkat, Molt-4, HeLa-S3, and A549. A strong green emission in Jurkat cells treated with these Ir complexes was observed by confocal microscopy [46]. Mechanistic studies suggested that **8a** interacted with anionic molecules on the cell surface and/or membrane receptors to trigger the Ca^{2+} dependent pathway and intracellular Ca^{2+} response, resulting in necrosis accompanied by membrane disruption. In addition, a series of cationic Ir complexes such as **8b** containing photoreactive 3-trifluoromethyl-3-phenyldiazirine groups were prepared in an attempt to identify the target molecules of **8a**. A proteomic analysis of the products obtained by the photoirradiation of **8b** with Jurkat cells indicated that the Ca^{2+} -binding protein “calmodulin (CaM)” was one of target proteins of these complexes [47].



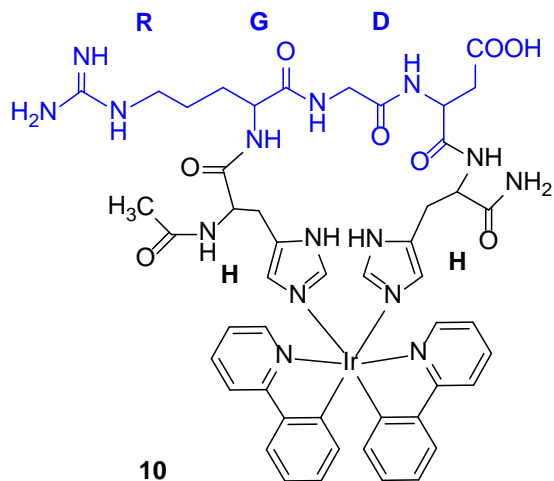
2.2. Protein-targeted inhibitors

2.2.1. Receptors-targeted

Targeted delivery approaches have emerged as a promising strategy to overcome many obstacles that often prevent a successful outcome of the disease, particularly those based on ligands whose receptors are overexpressed on the surface of malignant cells compared with healthy cells [48]. The conjugation of therapeutic agents to targeting vehicles based on small regulatory peptides offers several advantages including the disposal of efficient solid-phase procedures for synthesizing drug conjugates with improved pharmacological properties. Thus, Marchán, Brabec and co-workers hydrolyzed the ester bond of **6b** and conjugated the complex to octreotide-based peptides with the aim to selectively target cancer cells overexpressing somatostatin subtype-2 receptors (SSTR2) [49]. The authors demonstrated that Ir–octreotide conjugates **9** accumulated preferentially in SSTR2+ HeLa cells. ICP-MS measurements at 37 °C and 4 °C suggested that **9** internalized through an SSTR2-mediated energy-dependent endocytic mechanism, which was finally confirmed by competitive experiments with somatostatin. Interestingly, the peptide conjugation allowed the modification of the preferential cytotoxicity of the parent Ir complex **6b** without affecting its intracellular localization, as visualized by confocal microscopy. Furthermore, the cytotoxicity of the conjugates was increased in all cases upon visible light irradiation, which was attributed to an increase of the ROS production.



Integrins are a class of heterodimeric transmembrane receptors that mediate cell-cell communication and cell-extracellular matrix interactions. Particularly, $\alpha_v\beta_3$ and $\alpha_v\beta_5$ integrins are involved in tumor angiogenesis [50] so that they have been subject of selectively targeting angiogenic tumor cells over primary proliferating endothelial cells. The cyclo-RGD-dependent targeting (RGD = Arg-Gly-Asp) and cell killing effect in A549 cells of Ir-HRGDH **10**, an Ir-HH-cyclized peptide containing integrin targeting motif RGD, were shown by Fei *et al.* [51]. **10** showed better targeting affinity than its linear form and enhanced membrane permeability in comparison with fluorescein-labeled cyclic RGDyK peptide. Ir-HRGDH-guided KLA (Ir-HRGDH-KLA) had an LC_{50} (4.5 μ M) reduced by 2 orders of magnitude with respect to free KLA (cationic peptide KLA = (KLAKLAK)₂). Co-incubation of bovine serum albumin (BSA) with Ir(III)-peptides followed by SDS-PAGE indicated that BSA barely competed with peptide-Ir(III) at its cytoplasmic concentration (0.5 mM), and negligible BSA-Ir was produced.



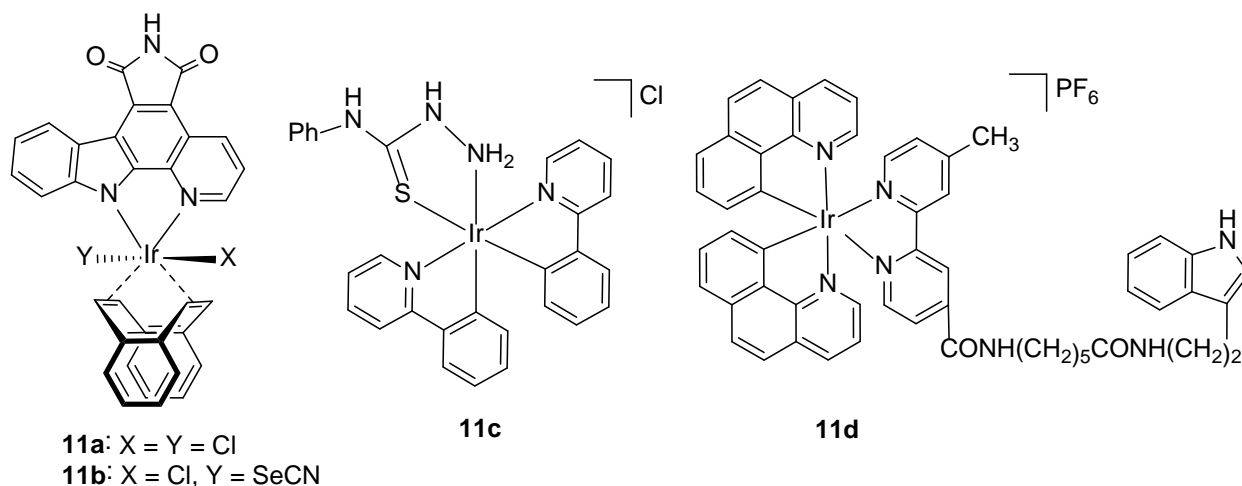
2.2.2. Protein binders and enzyme inhibitors

Octahedral metal coordination geometries in particular offer new gateways to design rigid, and globular molecules with defined shapes that can fill protein pockets such as enzyme active sites in a unique fashion. Meggers and co-workers have pioneered the development of kinetically-inert organometallic Ir(III) compounds as potent and specific inhibitors of enzyme activity despite using only reversible interactions [52a]. Thus the Ir(III) complex **11a** showed antiangiogenic properties *in vivo*, inhibiting angiogenesis in developing zebrafish embryos as well as tumor-cell-induced angiogenesis. The inhibition of protein kinases, most likely Flt4, is responsible for the *in vivo* bioactivity of **11b**. On the other hand, complex **11a** fulfills two independent functions: as a structural scaffold for the specific molecular recognition

of protein kinases, most likely VEGFR, resulting in light-independent antiangiogenic properties, together with a visible-light-induced photoreactivity triggering apoptosis in cancer cells [52b].

Other important enzymes implicated in cancer related events have been considered as alternatives targets for metal complexes. Cathepsin B, for example, is involved in immigration and invasion of numerous human and experimental tumors [53a] and therefore, is a possible therapeutic target for controlling tumor progression [53b]. Complexes containing a thiosemicarbazide N⁴S chelate ligands such as **11c** have demonstrated the capability to inhibit cathepsin B with IC₅₀ values in the order of magnitude than that of RAPTA-C [53c]. The loss of enzyme activity was explained in basis of a possible specific interaction of **11c** with the active site, since addition of 1 mM cysteine resulted in the full recovery of activity within 2 h. In addition, **11c** was probed to interact with the most common indole-binding protein and drug carriers in the circulatory system, serum albumin. Emission titrations with the complex showed a regularly decrease in the fluorescence intensity of human serum albumin (HSA) and the concomitant increase of a new peak. This was attributed to the emission of the complex when bound to the protein, and the binding was finally demonstrated to occur at the warfarin site I. In addition, **11c** was highly cytotoxic towards breast cancer cells although it was not demonstrated that either inhibition of cat B or the interaction with HSA were responsible for its antiproliferative activity.

On the other hand, Lo *et al.* prepared luminescent cyclometalated Ir(III) polypyridine indole complexes as **11d** to specifically bind to site II of bovine serum albumin (BSA) [54]. The emission intensities and lifetimes of the complexes increased in the presence of BSA, which was ascribed to the binding of the indole moiety of the complexes to a hydrophobic pocket of BSA. Flow cytometry and laser-scanning confocal microscopy studies revealed efficient uptake of a phenyl-quinoline complex analogous of **11d** by HeLa cells and subsequent localization in the perinuclear region. Temperature-dependence experiments suggested that the internalization of the complex was endocytic in nature, which was confirmed by cellular-uptake experiments involving the conjugate Ir-BSA. Additionally, the cytotoxicity of the complexes towards HeLa cells ranged from 1.1 to 6.3 μM, significantly smaller than that of cisplatin (30.7 μM).

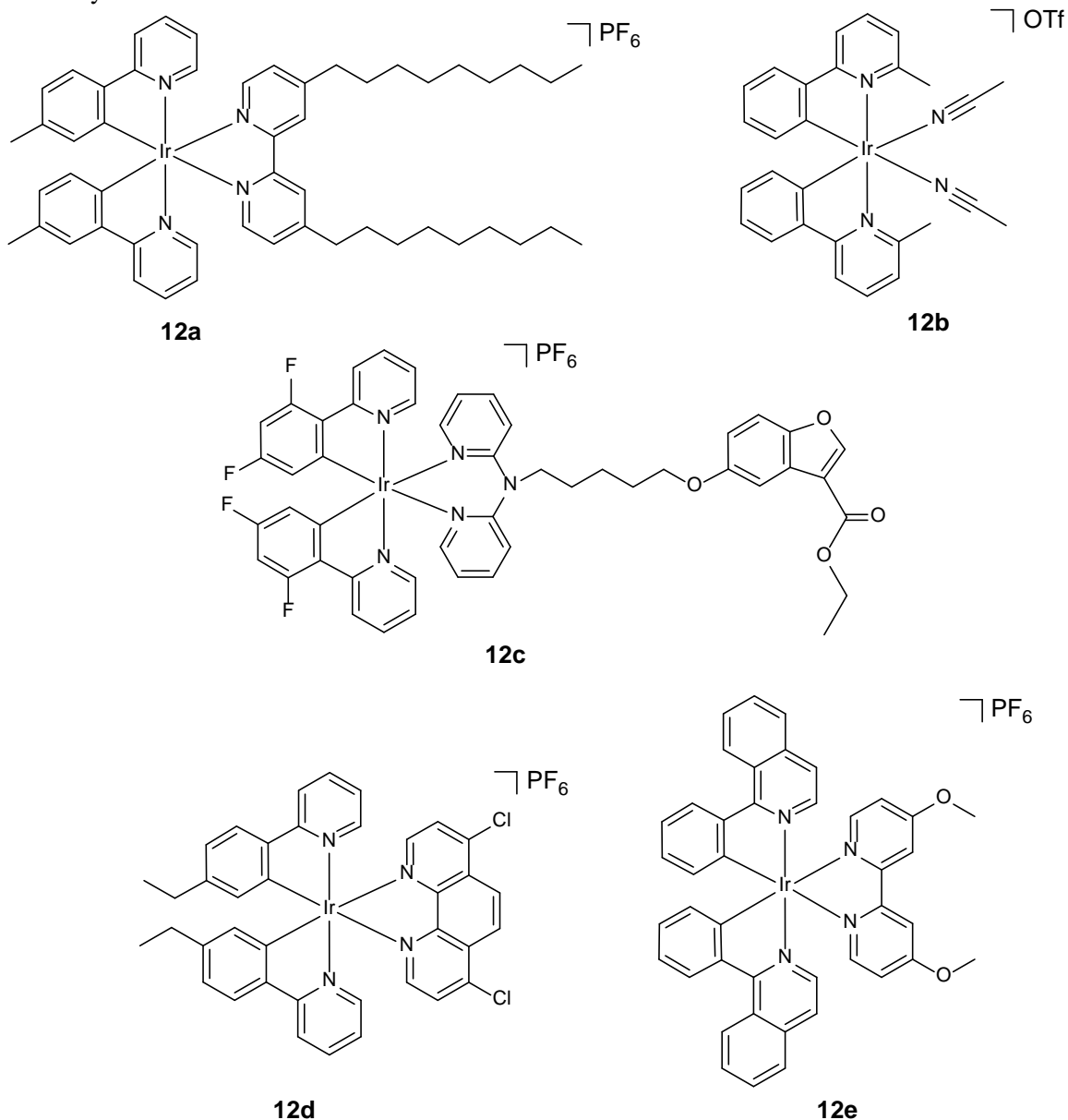


2.2.3. Protein-protein interactions inhibitors as anticancer agents

Protein-protein interactions (PPIs) represent a large class of therapeutic targets that play a crucial role in biological processes. Despite their importance, they were considered intractable due to their large and flat topology compared to classical small molecule binding sites [55]. Considerable progress on group 9 metal compounds targeting PPIs for the treatment of human diseases was achieved in the last decade. Ma and Leung, pioneers in the field, published a related review in late 2014 [8] and since then, very interesting papers in this fascinating area have been reported. Herein, we will review the main achievements on PPIs

disruptors as anticancer agents. In later sections, results focused on other important pathogenicities such as bacterial infections, inflammatory diseases, and neurological disorders will be reviewed.

Dysfunction of PPIs is implicated in oncogenesis as PPIs mediate the homo-/heterodimerization of receptor tyrosine kinases to initiate a relay of oncogenic signals to enable cancer progression [56]. For instance, abnormal activation of Ras/Raf/mitogen-activated protein kinase (MEK)/extracellular-signal-regulated kinase (ERK) signaling pathway enhances tumor initiation, progression, and metastasis and therefore, it is a frequent event in proliferative disorders such as renal cell carcinoma [56]. Ma, Leung and colleagues have recently identified [57] an Ir(III) complex containing the 4,4'-dinonyl-2,2'-bipyridine N^N ligand and two 2-(*p*-tolyl)pyridine C^N ligands, **12a**, as the lead compound for the inhibition of the H-Ras/Raf-1 interaction and its downstream pathways both *in vitro* and *in vivo*. Intriguingly, the Δ -enantiomer showed superior potency compared to the Λ -enantiomer or the racemic compound **12a**. Moreover, racemic **12a** and Δ -**12a** repressed tumor growth in a mouse xenograft model of human kidney cancer without causing weight loss or overt signs of toxicity to mice over 30 days. Compound **12a** also upregulated pro-apoptotic caspase activity *in vivo*.



The oncogenic mediator bromodomain-containing protein 4 (BRD4) has recently emerged as an attractive epigenetic target for anticancer therapy [58]. BRD4 is a transcriptional regulator that binds to acetylated lysine of histones in order to regulate the expression of target genes, such as *c-myc* and Bcl-2. Recently, Ma, Leung and colleagues developed metal-based inhibitors such as Ir(III) complex **12b** that targeted the epigenetic factor BRD4 and showed cytotoxicity against melanoma cell lines A375 and A2058 with IC₅₀ values between 3 and 13 μM. Significantly, **12b** inhibited tumor growth in a mouse model xenografted with A375 melanoma tumor by 40% compared to control group at the end of 16-day intraperitoneal treatment at a dosage of 100 mg/kg/d [59]. No significant weight loss was observed over the course of the treatment, indicating the low general toxicity of **12b** *in vivo* (Fig. 6). A mode of action involving covalent binding of **12b** to BRD4 was proposed according to an electrospray ionization mass spectrometry (ESI-MS) analysis, which reduces recruitment of BRD4 to *c-myc* and Bcl-2 promoter DNA. Downregulating the expression of *c-myc* also suppressed vascular endothelial growth factor (VEGF) signaling, resulting in the inhibition of angiogenesis.

NF-κB and STAT3 are ubiquitously expressed transcription factors and control numerous physiological processes [60], being frequently activated in advanced prostate cancer and sustain expansion of prostate cancer stem cells. The benzofuran-conjugated Ir(III) complex **12c** inhibited both IL-6-induced STAT3 activity and TNF-α-induced NF-κB activity in DU145 cells [61]. Moreover, **12c** inhibited both STAT3 and NF-κB translocation from the cytoplasm to nucleus. The ability of **12c** to block the DNA-binding activity of transcription factor STAT3 was confirmed in an ELISA. **12c** showed promising cytotoxicity against prostate cancer cells and suppressed tumor growth in a prostate cancer xenograft mouse model.

The p53 transcription factor is involved in the regulation of cell proliferation and apoptosis, DNA repair, angiogenesis, and innate immunity [62a]. Wild-type p53 functions as a tumor suppressor gene and promotes cell cycle arrest or apoptosis in cancer cells. However, inactivation of p53 by mutation or other mechanisms is a frequent event in tumorigenesis [62b]. One of the major endogenous negative regulators of p53 in humans is human double minute 2 protein (*hDM2*) [62c]. The cyclometalated Ir(III) compound **12d** has been described as the first metal-based disrupter of the p53/*hDM2* PPI in human amelanotic melanoma A375 cells without affecting the protein expression levels [63]. The authors demonstrated that **12d** reactivated p53 transcriptional transactivation *in cellulo*, induced apoptosis and suppressed the growth of cancer cells, which was attributed at least in part to the disruption of the p53/*hDM2* interaction.

Recently, the JmjC domain-containing (JMJD) family, which belongs to the Fe(II)/2-oxoglutarate dependent JMJC family of demethylases, has been found to possess histone-specific demethylase activities and to function as candidate oncogenes contributing to tumor formation [64a]. Their oncogenic potential may result from their ability to demethylate heterochromatic H3K9me_{3/2}, an important marker for the formation and maintenance of heterochromatin of genomic stability. In particular, JMJD2 proteins have been linked with mechanisms of epigenetic regulation of gene activation and silencing, cancer diagnostics and therapeutics, and the epigenetic control of herpesvirus infection and reactivation [64b]. Ma and Leung have identified the Ir(III) complex **12e** as the first metal-based inhibitor of JMJD2 activity with an IC₅₀ of around 15 μM in a fluorescence-based assay [65]. The inhibitory activity of **12e** against JMJD2 was selective (no inhibition JMJD3, JARID, and HDAC proteins was observed) and greater than that of N-oxalylglycine, a general JMJD inhibitor. Furthermore, **12e** suppressed the trimethylation of the p21 promoter on H3K9me₃ and decreased JMJD2D–H3K9me₃ interaction in human lung adenocarcinoma epithelial A549 cells, inhibiting also its proliferation at low micromolar concentrations.

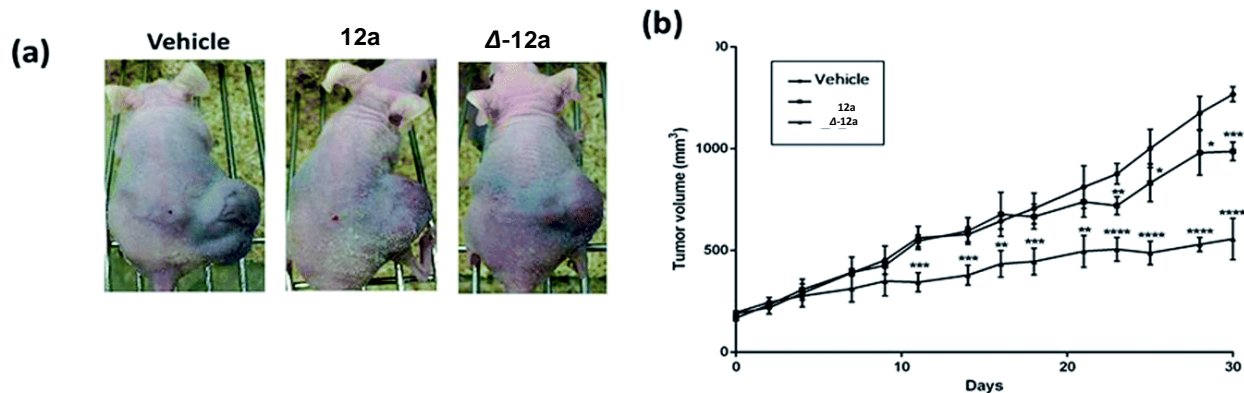


Fig. 6. The effects of racemic **12a** and Δ -**12a** in a kidney cancer xenograft model. Mice harboring A498 (human kidney cancer) tumors were injected with vehicle or with **12a** and Δ -**12a** (14 mg kg⁻¹) four times a week. (a) Photographs of control and treatment mice after 30 days. (b) Average tumor volumes of control group and treatment group over the measurement period. Reproduced from [57]. Licensed under CC-BY-3.0.

3. Cyclometalated Ir(III) complexes for phototherapy: from the visible to the NIR light activation

3.1. General

PDT is a non-invasive medical technique that relies on the use of light to control the drug activity along an adaptable time span at a specific space. It is based on the generation of toxic singlet oxygen (¹O₂) and/or reactive oxygen species (ROS) through the combination of a non-toxic molecule called a photosensitizer (PS), light and molecular oxygen (³O₂). PDT is generally divided, according to the mechanism of the photochemical reaction, into Type I and Type II (Fig. 7A). After light exposure, the PS is transformed from the ground singlet state (S₀) to the excited singlet state (S₁) and then undergo intersystem crossing (ISC) to the triplet excited state (T₁), where the photoreaction takes place. A Type I reaction consists of a hydrogen or electron transfer to the surrounding biological substrates, generating free radicals that can interact with molecular oxygen to finally form ROS (e.g. superoxide, hydroxyl radicals or peroxides). Instead, a Type II reaction is a direct energy transfer from the PS to ³O₂ what yields ¹O₂. Both ¹O₂ and ROS rapidly interact with adjacent biomolecules disrupting normal cell functions that finally drives to cell death [66].

In order to be clinically applicable, a PS must necessarily meet two requirements: on one hand, exhibit a strong phototoxicity. This behavior is described by the phototoxic index (PI), defined for a compound as the ratio of its toxicity in the dark and upon light irradiation (PI=[IC₅₀]_{dark}/[IC₅₀]_{light}). On the other hand, the PS should preferably have a strong absorption in the “phototherapeutic window” (within the range of 650–850 nm) to maximize light penetration through the human tissues [67] and to minimize both light toxicity and autofluorescence [68] (Fig. 7B).

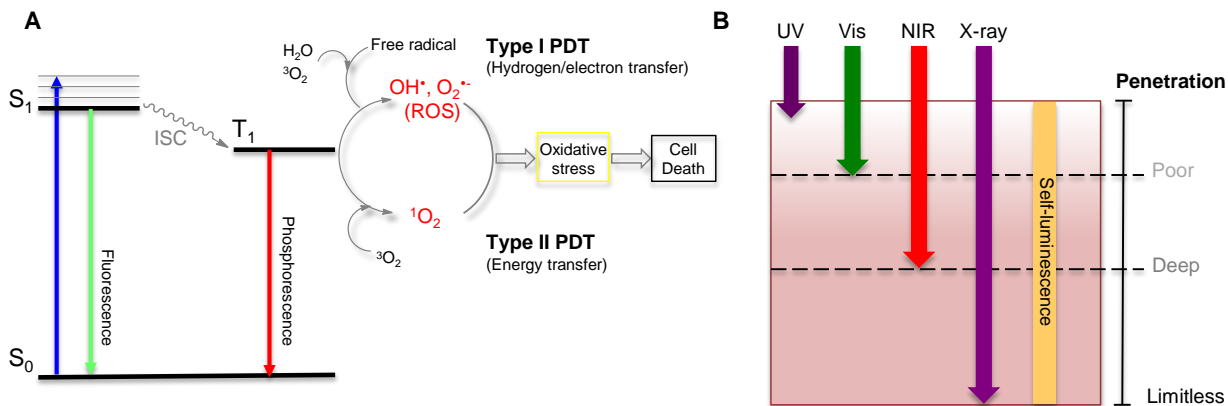


Fig. 7. (A) Scheme of the photochemical reactions for type I and type II PDT. (B) Comparison of tissue penetration of different excitation sources. Adapted from reference [66a].

To date, FDA-approved dye sensitizers for PDT treatment are mainly porphyrinoid compounds, including chlorins, bacteriochlorins, phthalocyanines, and related structures [69]. However, their clinical use is limited by the short lifetime of their excited-state and the low quantum yield of singlet oxygen production [70]. The later together with important side effects has promoted the development of new generations of PSs. A recent trend includes the use of metals due to the efficient intersystem crossing promoted by the metal, the favorable long lifetime of their triplet MLCT excited state and the bathochromic shift in the absorption spectra. Thus, the first metallic PSs were also porphyrin-based compounds where the metal was introduced in the porphyrin core [71] as well as on the periphery [72]. The success of these type of metallic PSs is well exemplified in the palladium bacteriopheophorbide (TOOKAD[®], Fig. 8) which has successfully completed Phase III clinical trials for the treatment of prostate cancer and has submitted marketing authorization to the European Medicine Agency [73].

Beyond this cyclic tetrapyrrolic type of PSs, transition metal complexes represent an emerging class of PSs, and have become a highly valued and productive field of study regarding PDT. The vast majority of the metal complexes screened as PSs are octahedral polypyridine Ru(II) complexes [74], being the Ru(II) complex TLD-1433 (a Ru(II) dyad derived from α -terthienyl appended to imidazo[4,5-*f*][1,10]phenanthroline) approved to enter phase Ib clinical trials in Canada (ClinicalTrials.gov Identifier NCT03053635) for the treatment of non-muscle invasive bladder cancer [75] (Fig. 8).

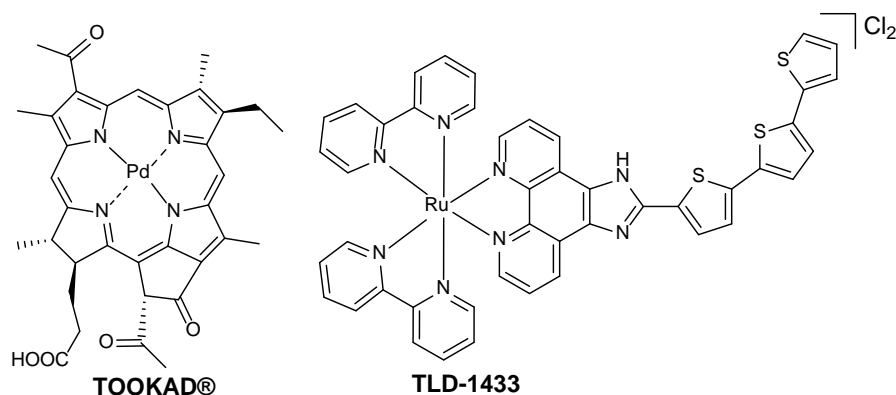


Fig. 8. Chemical structure of metal-based PSs TOOKAD[®] and TLD-1433.

Ir(III) complexes have arisen as potential alternatives to the isoelectronic Ru(II)-based PSs. Unlike most promising Ru(II) PDT agents, Ir(III)-based PSs usually contain cyclometalated ligands. Moreover,

the use of ‘half-sandwich’ cyclopentadienyl Ir(III) complexes as PSs is rare [76]. They have limited water-solubility and chemical stability respect to cyclometalated octahedral Ir(III) complexes. In addition, they later enable broader tuning of the intrinsic photophysical properties [77], increase ligand-field stabilization energy and pronounce decoupling of the ³MLCT excited states respect to those that are metal-centered [78]. Thus, these complexes possess multiple advantages: (1) tunable emission spectra that extend to the near-infrared (NIR), (2) energy-level control, (3) long lifetime (~ μs) and (4) ROS generation under hypoxic conditions via electron or energy transfer [79]. In this section, we present the recent achievements in the use of Ir(III) complexes as novel PSs.

3.2. One photon PDT

The introduction of the aforementioned anticancer potencies into phosphorescent cyclometalated Ir(III) complexes have provided an opportunity not only for the construction of theranostic materials but also for developing specific organelle-targeted PDT agents. These are highly effective PSs since they rapidly disrupt specific biological cell functions under photoactivation. Thus, the PDT effect of the majority of Ir(III) PSs have been designed and evaluated to target a specific organelle.

3.2.1. Mitochondria and lysosome-targeted PS

As mentioned before, targeting mitochondria represents a promising tactic to improve the cancer treatment efficacy [80]. Moreover, mitochondria are considered the primary target for PDT treatment since they produce the majority of the ATP and play important roles in cell proliferation and apoptosis [81]. The prevailing chemistry-based strategies to approach mitochondria include coupling lipophilic cation scaffold or peptides [82]. In this sense, several biscyclometalated Ir(III) compounds have been developed to target and exhibit an efficient PDT effect in this organelle. Lo *et al.* synthesized phosphorescent water-soluble Ir(III) complexes **13a-13e** and demonstrated that both photophysical and photochemical properties can be tuned by varying the cyclometalated ligand [83]. The complexes exhibit intense green to orange-red emission but the nature of the excited state varies from mixed ³MLCT and ³LLCT for **13a-13c** to essentially ³IL for **13d-13e**. Accordingly, the quantum yield for ¹O₂ production (Φ_Δ) increases in the order **13a** < **13b** < **13c** < **13e** < **13d** (i.e. longer-lived ³IL excited states allow more efficient energy and/or electron transfer from the complexes to ³O₂). Their *in vitro* PDT activity was evaluated on HeLa cells by MTT assay. All the PEG complexes present no dark toxicity (IC₅₀ > 300 μM) but upon 30 min of blue light irradiation (365 nm), these values dropped (3.4-23.2 μM) close to those of their PEG-free counterparts without irradiation (0.12-21.1 μM). The mitochondrial localization of the complexes facilitates the oxidative damage in the organelle causing necrotic cell-death after irradiation. Therefore, PEGylation reduces significantly the dark toxicity and can be used for the construction of efficient PSs. Furthermore, *in vivo* studies using zebrafish as an animal model evidenced the application of **13c** as visualizing reagents (Fig. 9).

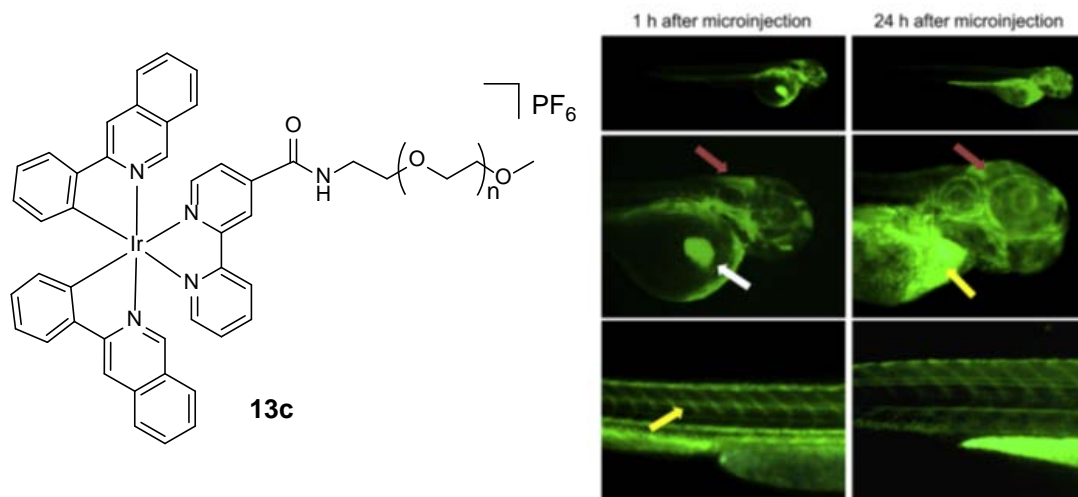
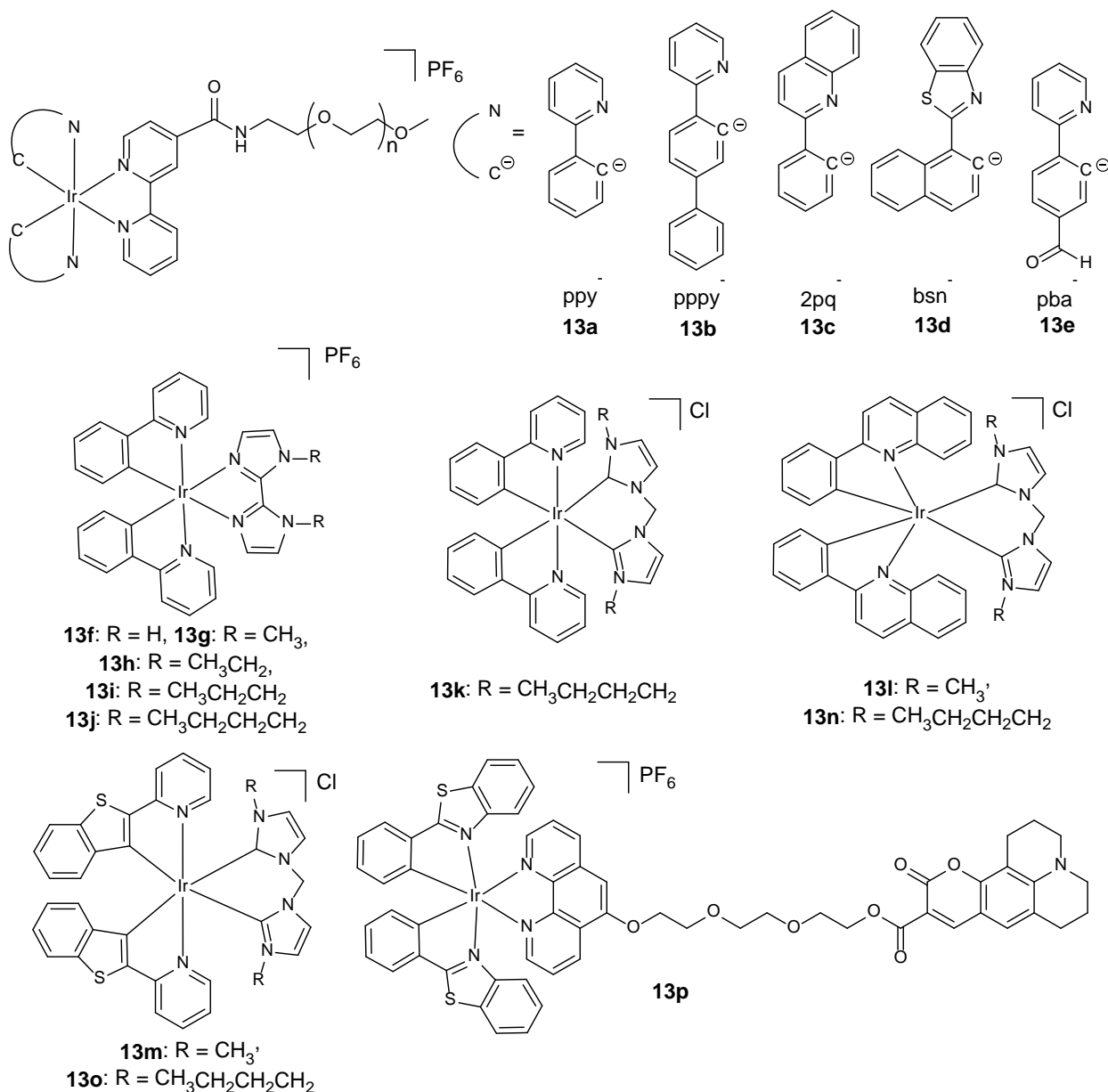


Fig. 9. *In vivo* biodistribution of complex **13c** in zebrafish larva. Left column: the intravascular loaded complex moved from the point of injection (white arrow) to notochord, spinal cord (yellow arrow), and brain ventricle (red arrow) via blood vessels. Right column: the loaded complex gradually accumulated at the spaces around the yolk sac and cardiac cavity (yellow) and the head space (red arrow) 24 h after loading. Image reproduced with permission from [83]. Copyright (2013) Elsevier.

The effect of tuning the lipophilicity to improve the PDT activity of the PS has recently been studied by Chao *et al* [84]. They prepared five cyclometalated Ir(III) complexes based on 2,2'-biimidazole with different substitutions (hydrogen **13f**, methyl **13g**, ethyl **13h**, propyl **13i**, and butyl **13j**). The complexes showed high cytotoxicity towards four different cell lines (HeLa, A549, A549R and LO2) when exposed to 405 nm light irradiation for 5 min. **13j** exhibited the highest photoinduced activity in HeLa cells (PI = 150) and good selectivity between normal and cancer cells (i.e. $PI_{LO2} = 5.8$). Moreover, the complexes may overcome platinum resistance as indicated by the higher phototoxicity against cisplatin-resistant A549R cancer cells rather than A549 cells. Complex **13j** possesses the highest lipophilicity and the strongest ability to produce singlet oxygen ($\Phi_{\Delta} = 0.59$) of the complexes of the series. Thus, the light-induced toxicity could be attributed to its excellent targeting of mitochondria and the generation of ROS under light exposure.

Ir(III) complexes bearing bis(NHC) ligands such as **13k** display up to 3 orders of magnitude higher cytotoxicity in HeLa and A549R cells upon 10 min irradiation at 365 nm [85]. Co-localization analysis with the organelle-specific stain for mitochondria showed high Pearson's correlation coefficients for Ir(III) and MitoTracker Red (MTR) in both cell lines. Mechanism studies showed that the most lipophilic **13k** exerted its anticancer efficacy by initiating a cascade of events related to mitochondrial dysfunction including ROS production, cytochrome *c* release, caspase 3/7 activation and apoptosis. Subsequently, the cyclometalating ligand was modified to explore the PDT activity under visible light irradiation [86]. Complexes **13l-13o** were able to generate 1O_2 and kill cancer cells more effectively than cisplatin under 450 LED illumination. On the whole, the *in vitro* antiproliferative activity of these complexes was in accordance with their relative lipophilicity and cellular uptake, which follow the order: **13n** > **13l** > **13o** > **13m** > cisplatin. In general, it was observed that complexes containing the quinoline ligand **13l** and **13n** displayed higher antiproliferative and photo-toxicity activity than the complexes containing the thionaphthene ligand **13m** and **13o**. Hence, modification of the C^N ligand allowed the tuning of the photophysical and photochemical properties of the complexes, while the N-heterocyclic carbene ligand preserved the mechanism of action of the complexes.

You *et al.* reported the synthesis of a bichromophoric dyad **13p**, consisting on the fluorescent coumarin 314 (C314) and a luminescent Ir(III) complex [87]. The dyad produces $^1\text{O}_2$ with high quantum yields ($\Phi_{\Delta} = 0.98$) and demonstrated its utility to visualize the $^1\text{O}_2$ endogenously produced in macrophages. The occurrence of α -dehydrogenative oxidation by $^1\text{O}_2$ in the julolidine moiety of C314 was responsible for the photoluminescence response. In addition, **13p** was cytotoxic to HeLa (PI = 110), A549 (PI = 217) and MCF-7 (PI = 51) cancer cells under photoirradiation with blue light. The induction of apoptosis and necrosis was correlated with the accumulated levels of $^1\text{O}_2$.



Very importantly, Zhao and Huang demonstrated that mitochondria-targeted Ir(III) PSs are more practicable in cancer therapy. To do so, they designed and synthesized two photosensitizers, **14a** and **14b** that specifically targeted the mitochondria and lysosomes in living cells, respectively (Fig. 10) [88]. The complexes have similar photophysical properties and singlet oxygen quantum yields (0.17 and 0.21) owing to the same C^N ligand. Since the PDT performance is usually limited for the low oxygen concentration in solid tumors (~ 4%) [89], the authors evaluated the phototoxicity of **14a** and **14b** under normoxic and

hypoxic conditions. HeLa cells incubated with **14a** for 12 h maintained 87% cell viability, which dramatically decreased to 7.6% right after 475 nm light irradiation, and further to 2.3% in 4 h under normoxia. When the irradiation was performed under hypoxia, 3.3% cell viability was obtained, indicating a high PDT efficiency. In contrast, the cell viability in presence of **14b** remained at a high percentage (> 66%) under hypoxic or normoxic conditions. The authors attributed this result to the fact that mitochondria-targeted PSs inhibited mitochondrial respiration, resulting in higher intramitochondrial oxygen content, especially under hypoxia conditions, which is advantageous for PDT in hypoxic tumor cells.

Even so, lysosomes are emerging as attractive pharmacological targets for selective killing of cancer cells with pH-sensitive PSs. The pH in the tumor (pH 6.5-6.8) is more acidic than in blood and normal tissues (pH 7.4), whereas in lysosomes it is still more acidic (pH 4.5-5.5). This pH-sensitive PSs could target tumor tissues and further be activated by the significantly increased acidity in the lysosomes of cancer cells [90]. With this idea in mind, Mao *et al.* described cyclometalated Ir(III)- β -carboline complexes as **14c** [91] and a series of mixed-ligand phosphorescent Ir(III) complexes as **14d** [92]. Both exhibited pH-responsive orange phosphorescent emission and the Φ_{Δ} increased from pH 7.4 to pH 3.0. The pH sensitive emission of **14c** could be contributed by the protonation/deprotonation processes of the benzimidazolyl-NH and the indolyl-NH on the β -carboline ligand. In **14d** this phenomenon can be ascribed to the deprotonation of N-H groups of the imidazole rings on the tridentate ligand, which may cause pH-dependent switching from the ^3LC state to the highly emissive $^3\text{LLCT}$ and $^3\text{MLCT}$ excited states [93]. **14c** displayed negligible cytotoxicity in the dark in A549 cells ($\text{IC}_{50} \geq 100 \mu\text{M}$) and high phototoxicity upon visible light irradiation (425 nm, 36 J cm^{-2}). Instead, **14d** displayed moderate phototoxicities against different cancer cell lines with the highest phototoxicity index value in A549 cells ($\text{PI} > 54.1$). Interestingly, **14d** also showed a remarkable phototoxicity in A549R cells ($\text{PI} = 46$), which indicate that the PDT strategy is able to bypass cisplatin resistance. Mechanism studies showed that both mediated PDT mainly induced caspase- and ROS-dependent apoptotic cell death through lysosomal damage.

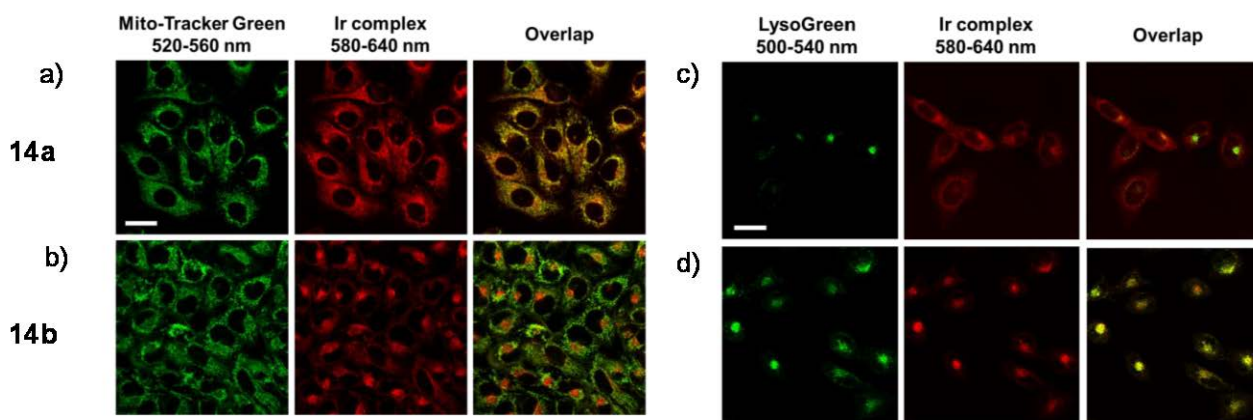
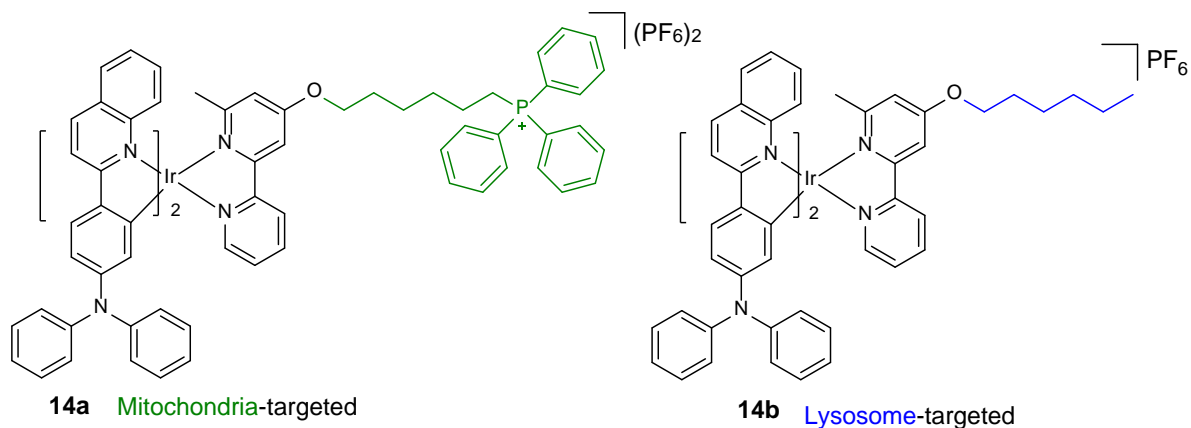
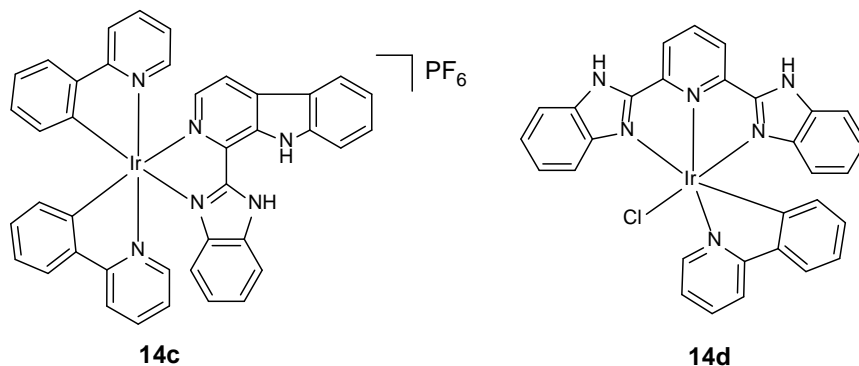


Fig. 10. Confocal microscopy images of HeLa cells and corresponding colocalization of green and red channel. The cells were incubated with a) **14a** (5 μ M, up row) and b) **14b** (5 μ M, down row) at 37 $^{\circ}$ C for 12 h and then incubated with Mito-Tracker Green (200 nM) at 37 $^{\circ}$ C for 30 min. c) **14a** (5 μ M, up row) and d) **14b** (5 μ M, down row) at 37 $^{\circ}$ C for 12 h and then incubated with LysoGreen (200 nM) at 37 $^{\circ}$ C for 5 min. Image reproduced with permission from [88]. Copyright (2016) John Wiley & Sons.



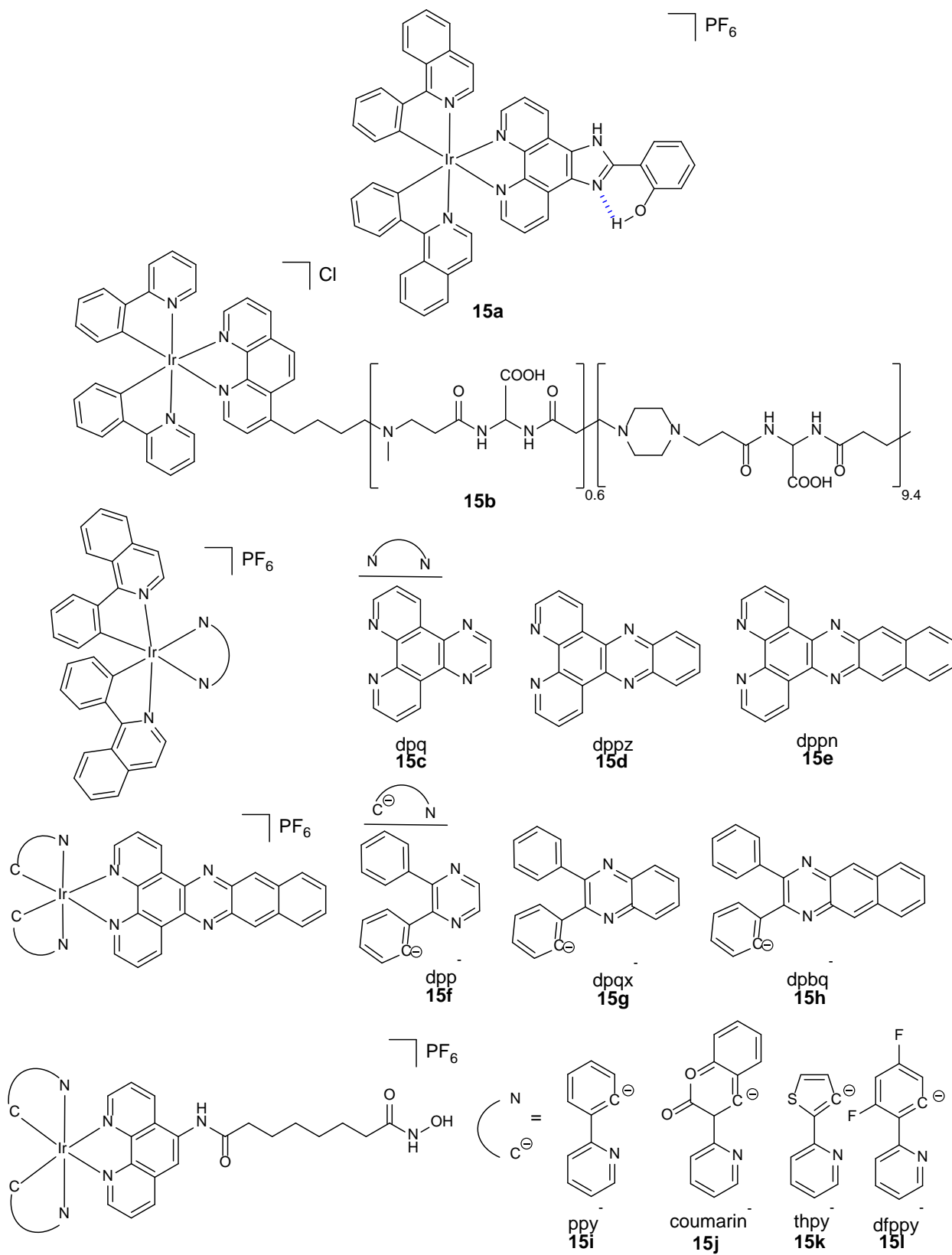
Lysosome-targeted pH-sensitive PSs

3.2.2. ER and nucleus-targeted PS

Other developed complexes have been located in the endoplasmic reticulum (ER), perinuclear region and even in the nucleus. The ER plays a major role in the synthesis, maturation and folding of proteins and is the main storage for intracellular Ca^{2+} [94]. When under pressure, ER responds through coordinated signaling mechanism known as the unfolded protein response (UPR) to protect the cell from stress [95]. In the stressful tumor microenvironment, the UPR maintains ER homeostasis and enables tumor survival. On the other hand, the nucleus is more sensitive to $^1\text{O}_2$ damage than other organelles. Considering that DNA double strand breaks are the most direct and serious lesion type for cytotoxicity and that ROS can afford this via oxidative damage [96], nuclear-targeted generation of multiple ROS can greatly improve the therapeutic effects [97]. Thus, other kind of strategies for cancer therapeutics consist to overcome activated ER stress by triggering pro-apoptotic pathways of the UPR or develop nuclear-targeted agents which could generate multiple ROS under irradiation.

Gupta *et al.* developed a series of Ir(III) complexes of the type of **15a** with imidazolyl-phenanthroline backbone as the polypyridyl ligand [98]. The systematic substitutions of the appended phenyl ring and alkylation of the imidazolic N demonstrated that the strong intramolecular hydrogen bonding interaction (O–H \cdots N) in **15a** is responsible for the specific localization and fluorescence emission in the ER of cells. In addition, MCF-7 cells treated with this complex and exposed to light at 405 nm showed progressive membrane blebbing, contraction of cells and generation of cellular processes, leading to nearly complete cell death after 1 h of exposure. Phenanthroline Ir(III) fragments have also been conjugate to artificial carriers such as poly(amidaamine) copolymer PhenISA [99]. The water-soluble metallopolymer Ir-PhenISA **15b** forms nanoaggregates with a hydrodynamic diameter of ~30 nm in aqueous media and exhibits improved photophysical properties in comparison with the free Ir emitter. The rigid environment provided by the polymer prevents self-quenching and annihilation effects, so that **15b** presents a 9 nm blue-shifted emission, longer lifetime and higher quantum yield. However, this also prevents a direct contact between the Ir(III) pendants and molecular oxygen so that generation of $^1\text{O}_2$ is reduced to half of the PhenISA-free complex. In HeLa cells studies, **15b** penetrates the cellular membrane and is located in the perinuclear region as visualized by two-photon excitation (TPE) microscopy at 840 nm. Moreover, the complex induces apoptosis cell-death upon Xe lamp irradiation without any sign of necrosis observed for the free complex.

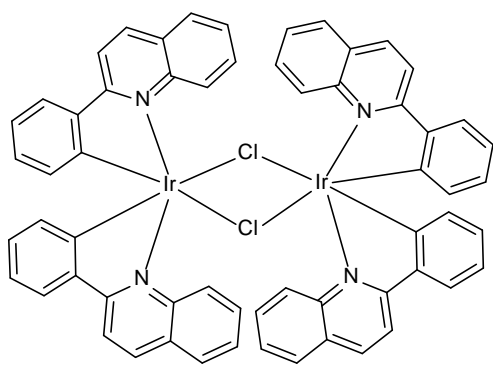
Sun and McFarland studied the effects of extending the π -conjugation of the diimine ligand **15c–15e** versus the cyclometalating ligand **15f–15h** in the luminescent properties and applications of Ir(III) complexes as PSs for PDT. [100]. Extending the π -conjugation on both the diimine and the cyclometalating ligands influenced ground-state absorption, while the nature of the emitting triplet excited states was only affected when varying the C \wedge N ligand. Localization in the membrane was evident for complexes **15c–15e** without light activation, but relocation to the cytosol and mitochondria was observed after visible light treatment of 50 J cm^{-2} . In contrast, **15f–15h** accumulated throughout the cell with some preference for the nucleus prior to light treatment. Localization trends of **15f** and **15g** was difficult due to changes in cell shape upon light activation, but **15h** was relocated from nucleus to the cytoplasm. **15h** presented submicromolar visible light EC_{50} values (350–600 nM) and the largest PI of the series in SK-MEL-28 (PI > 400) and HL60 (PI > 140) cell lines. Its PDT effect was attenuated approximately 10-fold with red light activation. The authors suggested that the strong PDT effect of this complex could be mainly ascribed to the extremely high photosensitization efficiency of the $^3\pi,\pi^*$ configuration as well as the strong and broad absorption in the visible to the NIR region.



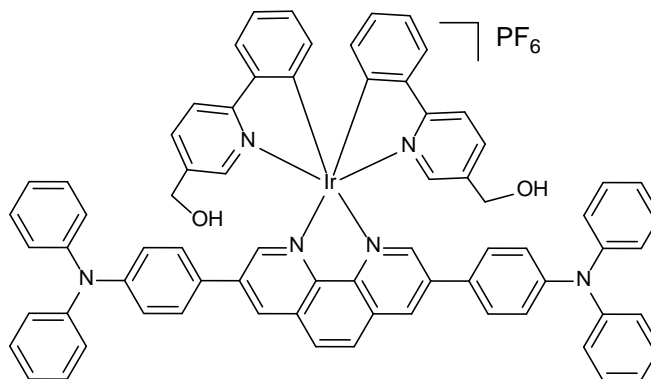
HDACs are a group of enzymes that catalyze the removal of the acetyl groups of the amino-terminal ϵ -group of lysines on histones. HDACs modulate most key cellular processes, including apoptosis, transcriptional regulation, DNA damage repair, cell cycle control, autophagy, metabolism, senescence and chaperone function. Because HDACs have been found to function incorrectly in cancer, the development of HDAC inhibitors (HDACis) are being investigated to act as cancer chemotherapeutics [101]. Mao and co-workers synthesized four phosphorescent Ir(III) complexes **15i-15l** with synergistic inhibitory effects on cancer cells due to their histone deacetylase HDAC inhibitory potency and PDT activity [102]. All Ir(III) complexes show a markedly increased cytotoxicity when irradiated with UV (365 nm) or visible (425 nm) light towards the screened cancer cells, including cisplatin-resistant A549R cells. They also display much lower phototoxicity against LO2 human normal cells. Mechanistic studies showed that **15i** induced apoptotic cell death mainly through inhibition of HDACs, ROS production and mitochondrial damage.

3.2.3. Cytoplasm-targeted PS

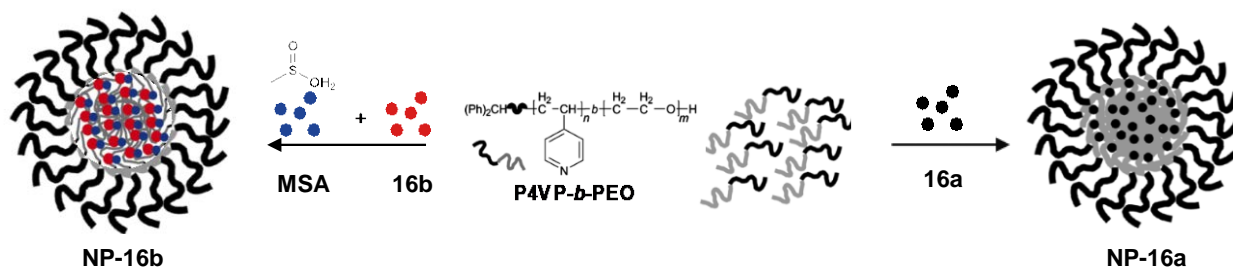
Polymeric nanoparticles have been studied extensively over the past few decades for the fabrication of drug delivery systems. Considerable research is being directed towards developing biodegradable nanoparticles (NPs) for drug delivery and tissue engineering, encapsulating a variety of diagnostic and therapeutic agents [103]. Further, these NPs enhance the water solubility of some metal complexes and have shown good biocompatibility [104]. Taking into account the above, Yang *et al.* developed coordination cross-linking method to prepare core-stabilized NPs of complex **16a** using pyridine blocks in poly(4-vinyl pyridine-*b*-ethylene oxide) (P4VP-*b*-PEO) [105] and a three component self-assembly of the same polymer, an monomer Ir(III) complex **16b** and methane sulfonic acid (MSA) [106]. In the first case, the molar ratio of the Ir(III) chloride-bridged dimer to the pyridyl unit in the block copolymer to be cross-linked was ~1:2 and **NP-16a** showed average hydrodynamic diameter of 193.6 nm. In the second case, PEO-*b*-P4VP/MSA was treated with **16b** to form hydrogen bonds between the sulfonate groups of PEO-*b*-P4VP-MSA and the hydroxyl groups of the Ir complex. The diameter of **NP-16b** was approximately 334 nm. The confocal fluorescence microscopy images suggested that **NP-16a** and **NP-16b** are mainly located inside the cytoplasm. MTT assay confirmed the PDT effect of **NP-16a**. The cell viability of HeLa cancer cells decreased from ~80% in the dark to ~10% when irradiated with visible light ($\lambda > 400$ nm) for 10 min. Similar results were obtained for **NP-16b**.



16a



16b



NP-16b

NP-16a

The combination of chemotherapy and PDT in a single delivery system has been investigated by the group of Zhao for enhancing anticancer therapeutic efficacy. To do so, they prepared two GSH-responsive cyclometalated Ir(III) complexes and encapsulated them in amphiphilic micelles with the surfactant Pluronic F127-FA containing folic acid (FA) as targeting moiety [107] (Fig 11). The chemotherapeutic activity was obtained from the well-known drug camptothecin, which was conjugated to both complexes through GSH responsive disulfide bond linkages. The micelles **NP-16c** showed excellent real-time imaging capability, release of the free anticancer drug camptothecin (CPT) in tumor cells and generation of $^1\text{O}_2$ for PDT upon visible light irradiation. On account of having folic acid targeting ligand, the micelles displayed greater accumulation and selective cancer cell killing in folate receptor (FR) overexpressed HeLa cells than FR low-expressed MCF-7 cells.

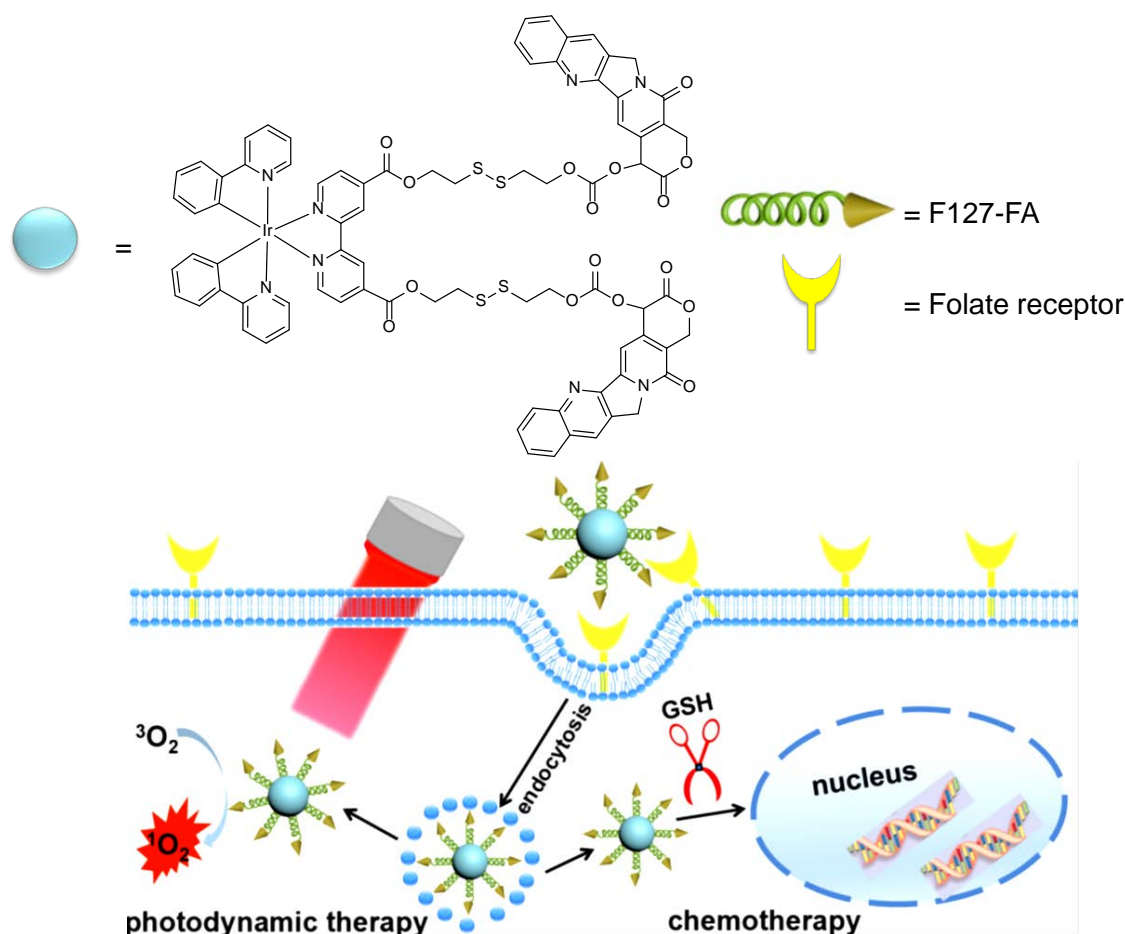
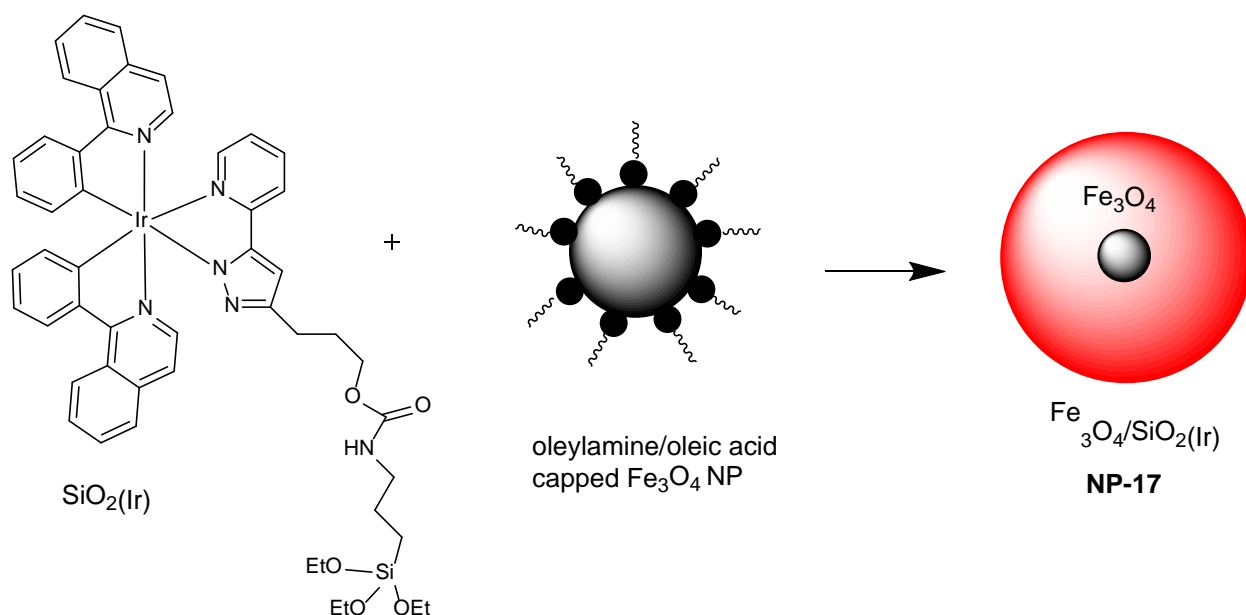


Fig. 11. Schematic Illustration of the ROS generation upon visible light illumination for PDT and anticancer drug release in **NP-16c** triggered by GSH for chemotherapy in tumor cells. Image modified with permission from reference [107]. Copyright (2017) American Chemical Society.

On the other hand, magnetic nanomaterials can be modified by incorporation of a PS that has been proved to be capable of generating $^1\text{O}_2$ [108]. Unfortunately, when magnetic nanoparticles are conjugated with dye molecules or quantum dots, a significant luminescence quenching occurs [109] and as a consequence the $^1\text{O}_2$ production decreases [110]. In order to overcome these disadvantages, Hsiao, Chi and Chou reported the synthesis of a multifunctional nanomaterial for MRI, luminescence imaging and therapeutic efficiency [111]. The system **NP-17** consists of highly magnetized $\text{Fe}_3\text{O}_4/\text{SiO}_2$ core/shell nanocomposite functionalized with an Ir(III) complex. While the superparamagnetic iron oxide nanoparticles (SPION) were capable of generating *in vitro* MRI signals, the complex serves as a dual luminescent and PS moiety. **NP-17** showed an emission band centered at 595 nm, a quantum yield of 0.62 and sensitized $^1\text{O}_2$ with a ~85% efficiency. The remaining quantum yield was checked to be useful for optical imaging. Evidence of $^1\text{O}_2$ -induced apoptosis was observed in HeLa cells when exposed to light (200 mW) for 5 min and incubated for 480 min. No sign of cell death was observed by microscopy and MTT assay when cells were irradiated in absence of **NP-17** or when treated for up to 100 mg mL^{-1} without exposure to light for 480 min.



Ir(III) tris-C^N-cyclometalated complexes have also been developed as PDT agents [112] in spite of their neutral nature, which is known to limit the cellular uptake and consequently its biological activity. Different approaches have been explored to improve the water-solubility and ensure biocompatibility of these PSs. On one hand, Aoki *et al.* introduced protonable groups in the structure of the C^N ligand (Fig. 12A), resulting in pH-dependent generation of ¹O₂ by photoirradiation. The authors demonstrated that complex **18a** was delocalized in the cytosol and induced necrotic cell-death in HeLa-S3 cells under 377 and 470 nm photoirradiation. On the other hand, Zhao *et al.* have prepared for the first time an Ir(III) complex cored hyper-branched phosphorescent conjugated polymer dots **18b/PSMA** for hypoxia imaging and PDT [113]. The red phosphorescent Ir(III) complex in the core serves as oxygen-sensitive dye, the 9,9-dioctylfluorene as the conjugated backbones of the hyper-branched conjugated polymer while the poly(styrene-co-maleic anhydride) polymer (PSMA) provide the negative charges to ensure both water-solubility and biocompatibility. The authors illustrated the potential applications in image-guided PDT by real-time luminescence imaging and MTT assay (Fig. 12B).

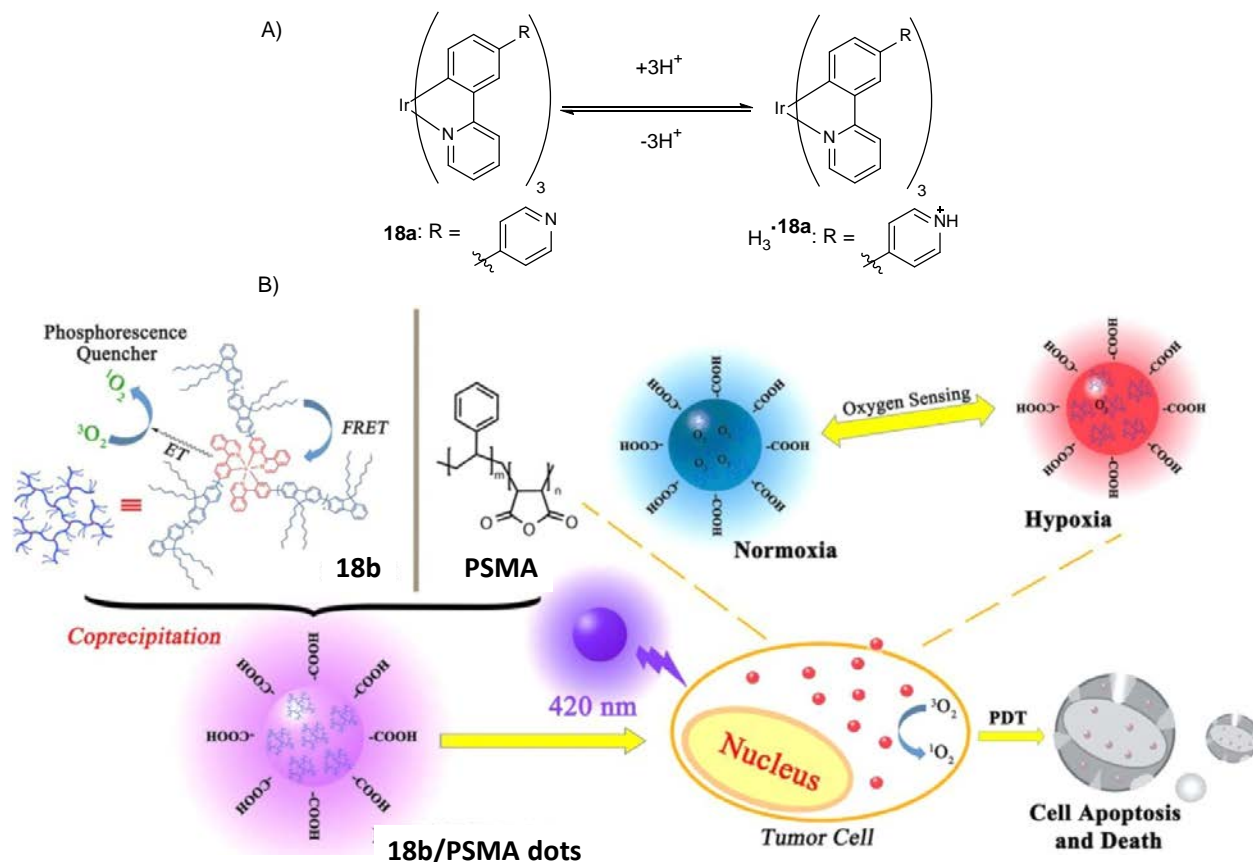


Fig. 12. A) Protonation reaction of **18a**. B) Chemical structures and design strategy of the phosphorescent polymer dots **18b/PSMA** for ratiometric hypoxia imaging and the mechanisms of Ir-HPC/PSMA dots in photodynamic therapy. Image reproduced with permission from [113]. Copyright (2017) American Chemical Society.

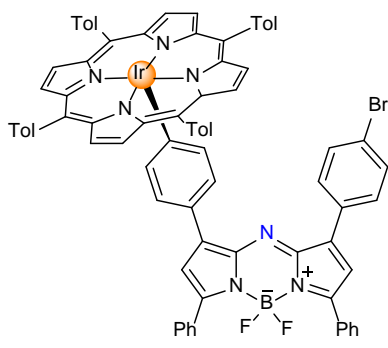
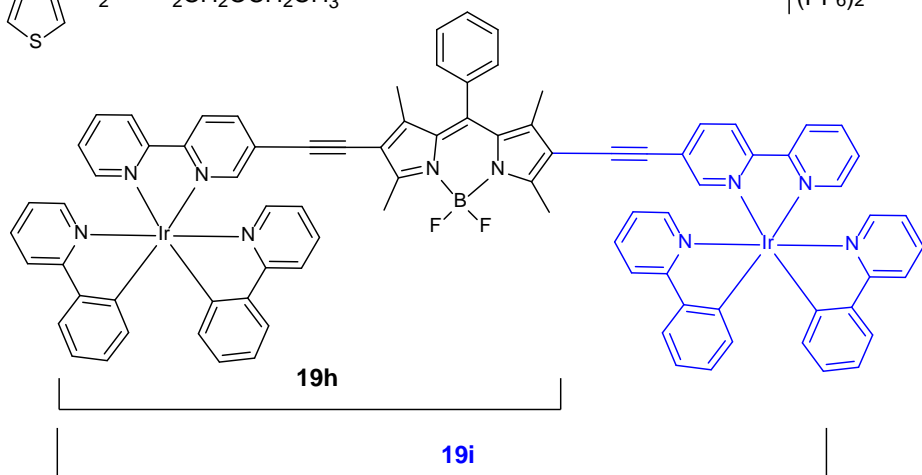
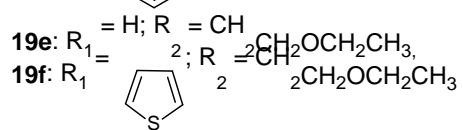
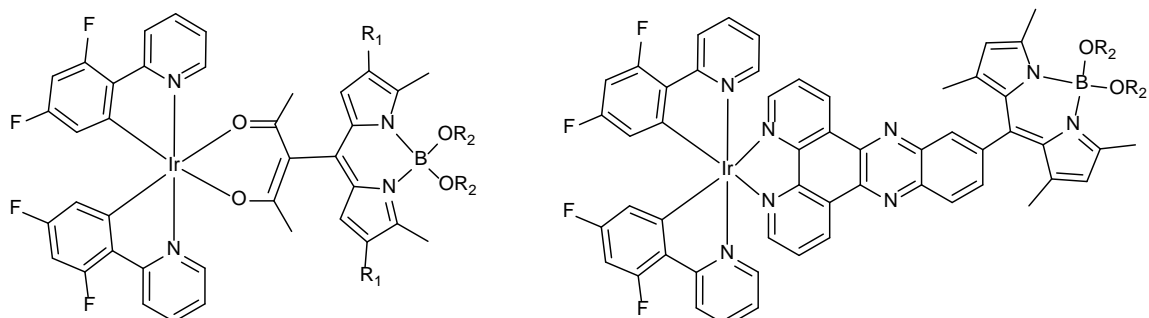
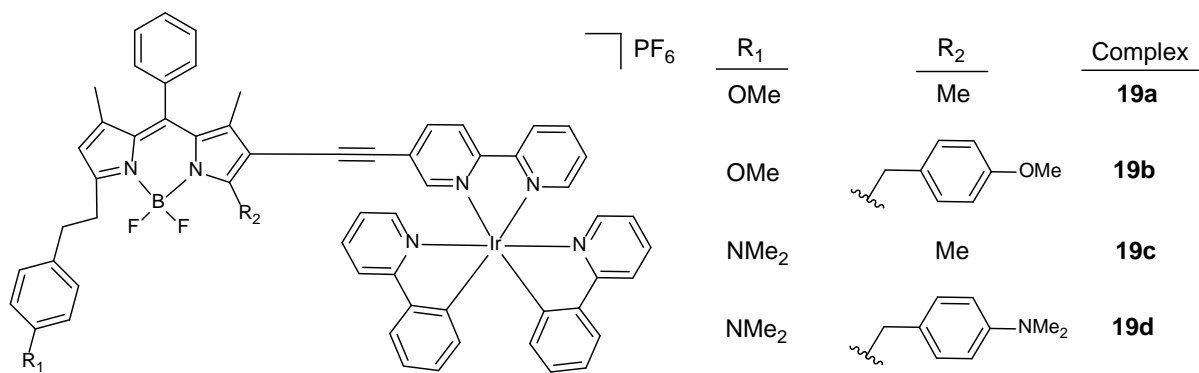
3.2.4. Towards NIR activation

The main drawback of transition-metal based PSs is that they are usually excited by short-wavelength UV/Vis light in conventional one-photon PDT. Hence, the mismatch between their absorption spectra and the wavelength for an adequate tissue penetration still hinders the treatment of larger or thicker solid tumors. One approach to improve the clinical effectiveness of PDT *in vivo* is to develop new PSs that can be activated at NIR wavelengths [114]. Concerning this aspect, a considerable body of work has been focused in red-shifting the excitation and emission spectra of Ir(III) complexes by the conjugation of bulky organic fluorophores or the use of π -expansive C^N cyclometalating and/or N^N ligands. The attachment of up-conversion nanoparticles as well as the use of two-photon absorption (see section 3.3) has also been explored.

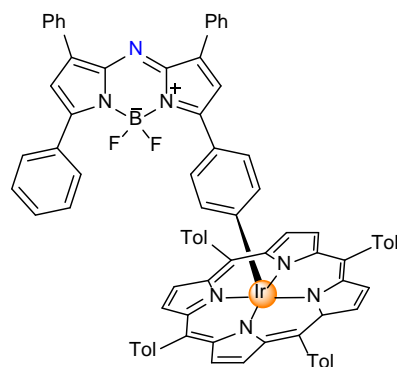
(a) Conjugation of bulky organic fluorophores

The development of fluorescent-PDT agents is currently undergoing intensive investigation for the construction of promising theranostic biomaterials. Conceptually, a light-harvesting chromophore is conjugated to a transition metal complex so that the effective ISC promoted by the metal allow the $^1\text{O}_2$ generation in detriment of the fluorescent emission efficiency of the organic dye. In this regard, different research groups have functionalized biscyclometalated Ir(III) complexes with the BODIPY unit to access strong NIR absorptions. Zhao *et al.* have designed mono **19a**, **19b**, **19c** and **19d** [115] and dinuclear **19i** [116] BODIPY-complexes via π -conjugation linkers, whereas Ortiz and Martínez-Martínez used meso-

acetylacetonated BODIPY ancillary ligands **19e** and **19f** [117]. In spite of the coupling strategy and the structural modifications of the BODIPY moiety, all the complexes exhibit similar photophysical properties. No significant shift of the absorption bands but a remarkable quenching of the fluorescence emission is observed after Ir(III) complexation. The metal, therefore, induces an efficient ISC from the singlet to the triplet excited states upon visible light irradiation. The long-lived T_1 states are BODIPY-localized 3LC states as evidenced by nanosecond time-resolved transient difference absorption spectra and DFT calculations. This phenomenon enables the complexes to photosensitize 1O_2 with different efficiencies (Table 1). Complex **19f** presented the highest 1O_2 quantum yield ($\Phi_{\Delta} = 0.86$) and outstanding theranostic behavior; it internalized in HeLa cells with minimal dark-toxicity, while triggering a strong phototoxicity ($IC_{50} = 50$ nM) after green light irradiation (6.8 J cm^{-2}). In contrast, the styryl-BODIPY complexes **19a-19b** exhibited phototoxicity in LLC lung cancer cells with moderate PI values whereas the PDT performance of **19g** and **19i** was not demonstrated.



19j



19k

	λ_{ex} (nm)	ϵ (10 ⁻⁵ M ⁻¹ cm ⁻¹)	λ_{em} (nm)	Φ_{F} (%)	Φ_{Δ} (%)	Ref.
19a	593/552 (593/558)	1.133/0.420 (1.029/0.348)	616 (616)	11.7 (34.4)	53 ^b	[115]
19b	646/596 (650/604)	0.896/0.394 (0.948/0.345)	674/611 (678)	13.8 (18.2)	81 ^b	[115]
19c	632 (628)	0.895 (1.035)	736 (714)	0.4 (1.3)	6 ^b	[115]
19d	714 (712)	0.788 (0.558)	800 (792)	0.18 (1.0)	2 ^b	[115]
19e	517 (515)	0.446 (0.099)	528 (526)	8.0 (90)	86 ^c	[117]
19f	597 (600)	0.338 (0.041)	652 (677)	22.0 (9.0)	60 ^d	[117]
19g	502	0.260	546		51 ^e	[117]
19h	527	0.83	543/742	0.30 ^a	-	[116]
19i	394/567	0.37/1.06	591/740	0.24 ^a	74.9 ^f	[116]

^aWith 2,6-diiodo-BODIPY as a standard ($\Phi_{\text{F}} = 2.7\%$ in CH₃CN). ^bUsing methylene blue ($\Phi_{\Delta} = 0.57$ in CH₂Cl₂) as reference and $\lambda_{\text{ex}} = 611, 652, 642$ and 664 nm, respectively. ^cUsing Rose Bengal as reference and $\lambda_{\text{ex}} = 530$ nm. ^dUsing New methylene blue as reference and $\lambda_{\text{ex}} = 605$ nm. ^eUsing Phenalenone as reference and $\lambda_{\text{ex}} = 370$ nm. ^fUsing 2,6-diiodo-BODIPY as a standard ($\Phi_{\text{F}} = 0.83\%$ in CH₃CN) and $\lambda_{\text{ex}} = 540$ nm.

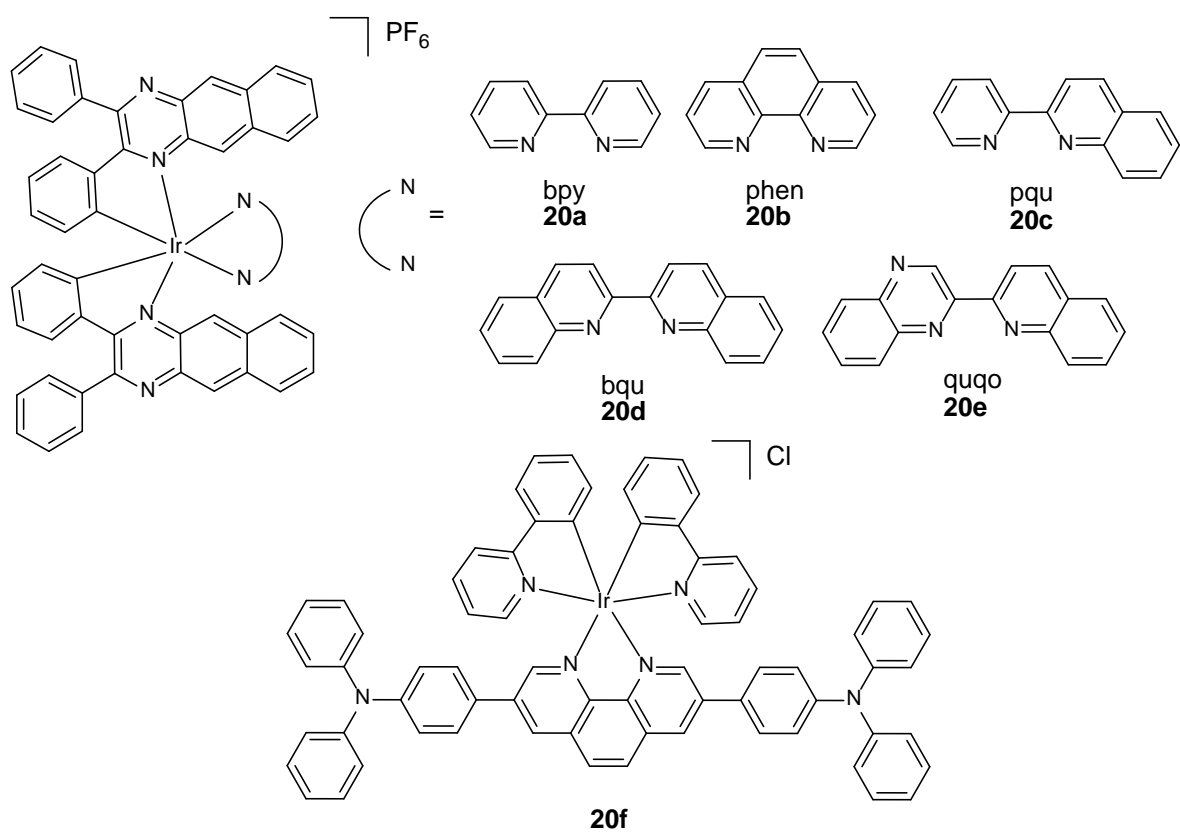
In addition, Ir-C bonded porphyrin-aza-BODIPY conjugates **19j** and **19k** have also demonstrated the ability to combine the features of NIR absorption of the aza-BODIPY dye (> 700 nm) with the remarkable ¹O₂ production of the Ir(III)-porphyrin ($\Phi_{\Delta} = 85$ and 79% , respectively) [118]. Aside from BODIPY, others organic chromophores such as coumarin [119] and naphthalimide [120] have been used to prepare triplet PS with strong visible-light absorption and long-lived excited states. However, their application as singlet-oxygen generators in cells has not been demonstrated yet.

(b) Use of π -expansive ligands

One of the common strategies to achieve red-to-NIR emission of the complexes include the introduction of π -conjugated systems either on one or both C^N and N^N ligands [121]. Similarly, to the previous approach, the resulting complexes present very long triplet lifetimes, which increase the reactivity of the triplet state and presumably produce potent *in vitro* PDT effects. In this regard, Sun and McFarland have prepared five heteroleptic Ir(III) complexes with a π -expansive cyclometalating 2,3-diphenylbenzo[g]quinoxaline (dpcbq) ligand and diimine ligands with varying degrees of π -conjugation (N^N = bpy **20a**, phen **20b**, pqu **20c**, bqu **20d** and quqo **20e**) [122]. Their UV-vis absorption spectra are characterized by intense absorption bands below 500 nm, and spin-forbidden bands between 600 and 800 nm ($\epsilon < 200$ M⁻¹ cm⁻¹), whose intensity increased with the π -conjugation of the diimine ligands. All complexes displayed weak and structured NIR phosphorescence, with maximal emission output spanning 700–1400 nm and quantum yields on the order of 10⁻³. The emitting triplet excited state was attributed to dpbb ligand centered ³ π, π^* state with mixed ³ILCT/³MLCT/³LLCT character. Despite the small quantum yield, their luminescence was probed to be useful for monitoring the cellular uptake and localization of **20a-20e** in melanoma cells at sub-lethal conditions. While the photophysics properties of the complexes differ slightly, their theranostic PDT effects varied drastically. Complexes **20b**, **20c**, and **20e** became very potent cytotoxins in melanoma SK-MEL-28 cells under visible (EC₅₀ of the order of 12-18 nM) or red light

activation (EC_{50} of the order of 150-200 nM). This potent nanomolar light-triggered activity combined with a lower dark toxicity resulted in **20e** having a selectivity factor over cancer cells as large as 40 and a PI of 273. However, it was not possible to verify the correlation between the distinct PDT profiles of the complexes with their 1O_2 quantum yields in cell-free experiments, cellular uptake or DNA aggregation capabilities.

Similarly, Yang and co-workers prepared a cationic Ir(III) complex **20f** containing a donor- π -donor type unit as N^N ligand [123]. **20f** exhibits an intense absorption peak centered at about 450 nm and displays highly efficient orange-red phosphorescence at 620 nm with a quantum yield of ~3% in PBS buffer. This together with the good biocompatibility with HeLa cells allow the luminescence imaging of **20f**, which mainly accumulated in the cytoplasm. More importantly, 1O_2 generation was observed under 730 nm continuous wave (CW) laser irradiation, owing to its reverse saturable absorption property. The PDT effect was assessed on the xenograft HeLa tumor model and although evidenced of apoptosis was demonstrated, no changes in tumor size was observed after the treatment by 730 CW laser for two weeks. To get a more efficient photo-ablation of cancer cells, the authors loaded the complex into polypyrrole nanoparticles (Ir-PPy NPs) [124]. These polymer nanoparticles are able to absorb in the NIR region and transform the light energy into heat. Thus, the Ir-PPy NPs combined photothermal and PDT driven effects by 730 nm CW laser irradiation. SEM and TEM images showed monodispersed nanospheres of ~60 nm and a zeta potential of ~16 mV in aqueous solution. When Ir-PPy NPs (200 $\mu\text{g mL}^{-1}$ in aqueous solution) were exposed to a 730 nm laser with a power density of 0.5 W cm^{-2} for 10 min, the temperature raised 6.1 $^{\circ}\text{C}$. The photothermal efficacy of Ir-PPy NPs (35.5%) and the PPy NPs (33.5%) were comparable and evidenced that the photothermal properties resulted from the PPy component. In parallel, the Ir(III) complex could generate 1O_2 as confirmed by the consumption of the 1O_2 scavenger 1,3-diphenylbenzo[c]furan (DPBF). Unfortunately, the PDT performance of the NPs has not been demonstrated *in vivo* yet.



(c) Conjugation to UCNPs

Lanthanide-doped upconverting nanoparticles (UCNPs) have the ability to convert low energy NIR photons (typically 800 or 980 nm) into high energy UV, visible and shorter NIR emission via multiphoton upconversion processes [125]. Therefore, conjugation of PSs to UCNPs is presented as an alternative to achieve NIR triggered generation of ROS. With this idea in mind, Vetrone and co-workers synthesized $\text{LiYF}_4:\text{Tm}^{3+}, \text{Yb}^{3+}@\text{SiO}_2$ UCNPs capable to convert NIR light to very intense UV light, and decorated the surface with a hydrophilic organoiridium complex [126]. Following 980 nm excitation, the upconverted UV light corresponding to the $^1\text{I}_6 \rightarrow ^3\text{F}_4$ and $^1\text{D}_2 \rightarrow \text{H}_6$ transitions is absorbed by the Ir(III) complex (Fig. 13). The ROS release was demonstrated indirectly through the photo-oxidation of the DPBF probe molecule in the presence of UCNP@SiO₂@Ir nanostructures after the irradiation with a 980 nm laser (185 W cm⁻²). Although the presence of the Ir(III) complex was required for the efficient production of ROS, its PDT effect was not tested *in vitro*. Even so, the development of hybrid platforms based on UCNPs could open up the door for the construction of highly selective anticancer reagents thanks to combination of the NIR activation of the drug and the EPR effect of the nanostructures.

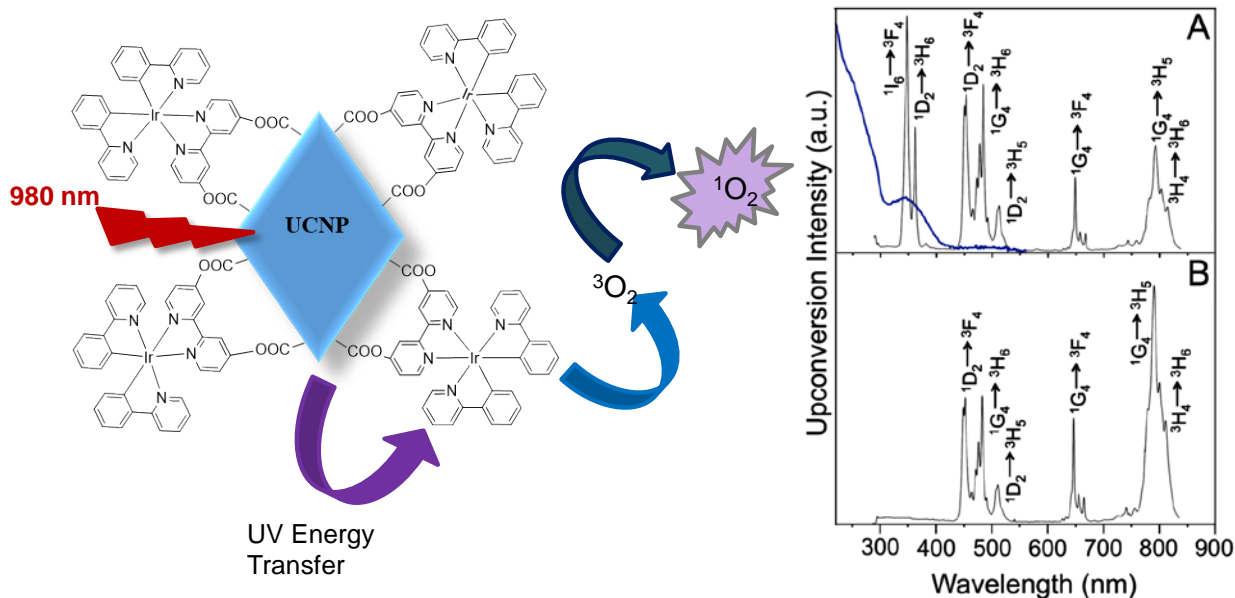


Fig. 13. A) Absorption spectrum of the synthesized organoiridium complex (blue line) and upconversion luminescence spectrum of the $\text{LiYF}_4:\text{Tm}^{3+}, \text{Yb}^{3+}@\text{SiO}_2$ UCNPs (black line) and (B) upconversion luminescence spectrum of the UCNPs following functionalization with the cyclometalated Ir complex. $\lambda_{\text{exc}} = 980 \text{ nm}$. Image reproduced with permission from [126]. Copyright (2017) The Royal Chemical Society.

Besides NIR light, X-ray radiation is suitable for activating PDT against deep-seated tumors. In the last years, a group of researchers have developed new PDT derivatives called X-ray induced PDT, or X-PDT [127] to achieve even greater light penetration [128]. Very recently, Lin and co-workers have designed tunable and functionalizable metal-organic layers (MOLs) that have been able to be excited with X-rays to induce PDT by generating reactive oxygen species [129]. These MOLs were built from $[\text{Hf}_6\text{O}_4(\text{OH})_4(\text{HCO}_2)_6]$ secondary building units (SBUs) and $\text{Ir}[\text{bpy}(\text{ppy})_2]^+$ derived tricarboxylate ligands (Fig. 14). Upon X-ray irradiation, Hf atoms in the SBUs absorbed X-rays and transferred energy to $\text{Ir}[\text{bpy}(\text{ppy})_2]^+$ in the ligands to generate $^1\text{O}_2$. The IC₅₀ values for Hf-BPY-Ir against two types of murine colon adenocarcinoma cells, CT26 and MC38, were calculated to be 3.82 ± 1.80 and $11.66 \pm 1.84 \mu\text{M}$,

respectively. *In vivo* anticancer efficacy experiments on subcutaneous flank tumor-bearing mouse models of CT26 and MC38 showed up to 90% reduction in tumor volumes.

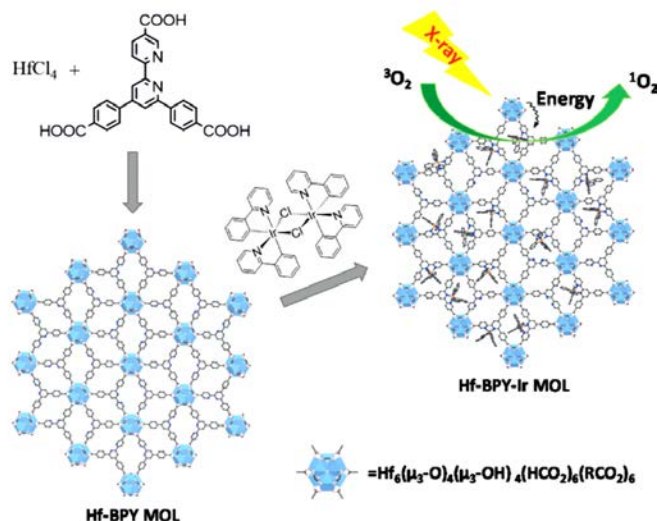


Fig. 14. Synthesis of Hf-based MOFs and MOF-enabled X-PDT to generate singlet oxygen. Image reproduced with permission from [129]. Copyright (2017) John Wiley and Sons.

3.3. Two photon PDT

The two-photon absorption (TPA) has attracted a great deal of attention in PDT since multiphoton excitation could be harnessed to extend the wavelength of excitation of a metal complex. TPA is a non-linear optical phenomenon in which a molecule is promoted to an excited state by the simultaneous absorption of two photons, each of which contributes one half of the total energy required to induced emission. Accordingly, two lower-energy NIR-photons populate the same PS-active excited state as one higher-energy photon but the re-emitted light is shorter in wavelength than the exciting light for the two-photon emission (Fig. 15) [130].

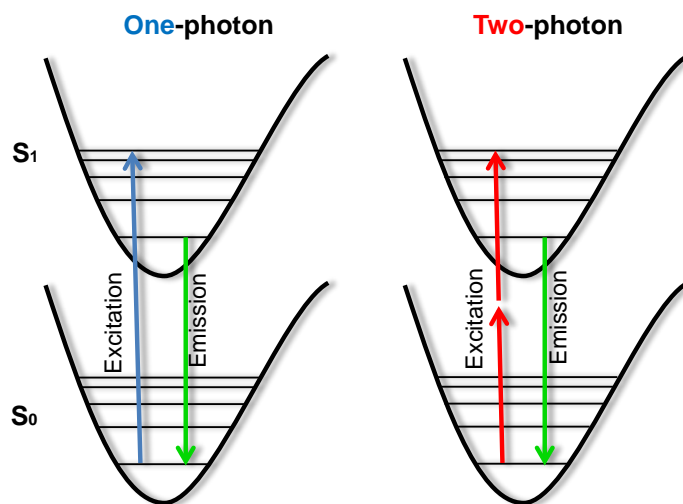


Fig. 15. Jablonski diagrams of the difference between one-photon and two-photon excitation. One-photon excitation occurs through the absorption of a single photon. Two-photon excitation occurs through the absorption of two lower-energy photons via short-lived intermediate states. The subsequent fluorescence emission process for both relaxation modes is the same. Adapted from ref. [70]

TPA has been successfully applied in confocal fluorescence microscopy for more than two decades, and is currently being explored in various research areas such as 3D data storage, up-converted lasing, optical power limiting, material micro-fabrication and PDT [70]. Two-photon PDT has potential advantages over conventional one-photon PDT using (quasi) continuous-wave (CW) illumination. Thus, selective closure of blood vessels has been demonstrated via TPE-PDT *in vivo*, evidencing greater tissue penetration with improved 3D spatial control. In addition, NIR light activation allows the administration of higher light doses and minimizes the side effects thanks to the reduced interaction between the NIR light and the tissue [131].

Two-photon PDT requires high TPA cross-section δ , which can be calculated from Equation (1).

$$\delta = \frac{h\nu}{N_0} = \frac{10^3 h\nu\beta}{N_A C}$$

where δ is typically reported in Goepfert-Mayer units (GM, 1 GM = 10^{-50} cm⁴ s photons⁻¹ molecule⁻¹), N_0 is the number density of absorption centers, N_A is the Avogadro constant, C represents the solute molar concentration, and β is the value of the TPA coefficient, which is determined by fitting the experimental results with self-compiled programs [132]. Photo-stability, which is not considered in the TPA action cross-section, is another of the most important criteria for developing fluorescent imaging agents, and can be estimated by the figure of merit (F_M) as described by Belfield and co-workers [133].

The utilization of luminescent cyclometalated Ir(III) complexes with TPA behavior has awakened a great interest for the development of potential clinically applicable PS. You and Nam synthesized the first molecular dyad capable of lysosomal staining and ¹O₂ sensitization for potential application in image-guided PDT [134]. The dyad (Irbtp-RhB, **21**) consists of a biscyclometalated Ir(III) complex (Irbtp) and rhodamine B (RhB) bonded through a thiourea linkage. The authors demonstrated that whereas the RhB moiety is responsible of the strong fluorescence ($\lambda_{ex} = 550$ nm, $\lambda_{em} = 570$ nm, photoluminescence lifetime (τ_{obs}) = 1.84 ns, photoluminescence quantum yield ($\Phi_F = 2.3 \pm 0.2\%$), the Irbtp entity possess high ability for photosensitization of ¹O₂, with a quantum yield Φ_Δ of 43% when excited at 365 nm. In addition, they proposed a mechanism for the photophysical processes that explains the independent actions of fluorescence and ¹O₂ sensitization of the Irbtp-RhB (Fig. 16). Finally, its two-photon PDT potential was also evaluated *in vitro*. The 800 nm (two-photon absorption of Irbtp) photoirradiation of HeLa cells attenuated the cell viability < 30% with a phototoxicity efficacy of 2.72 after 15 min of photoirradiation.

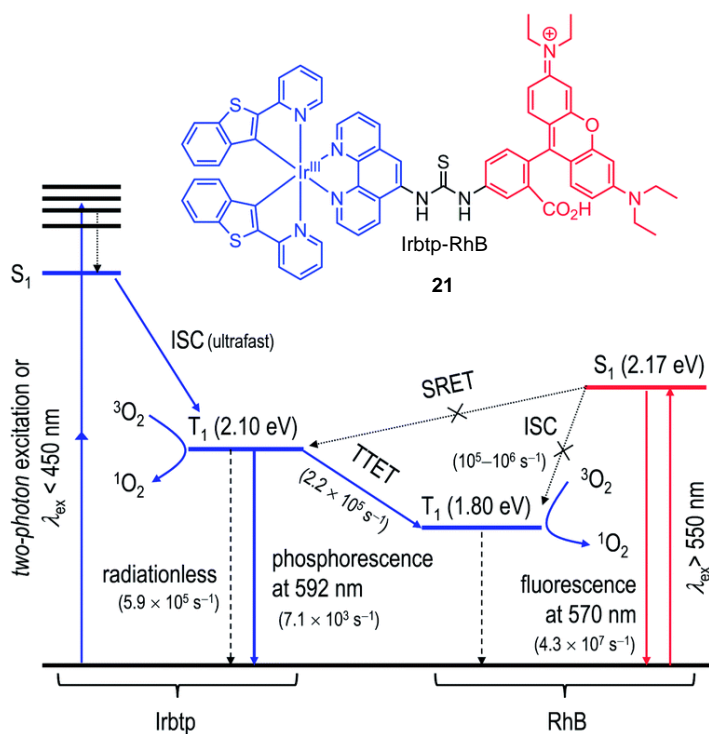
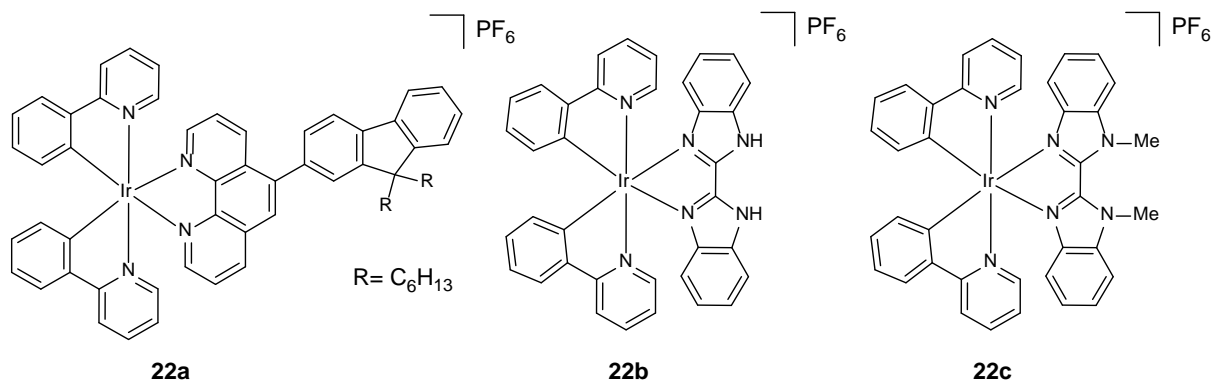


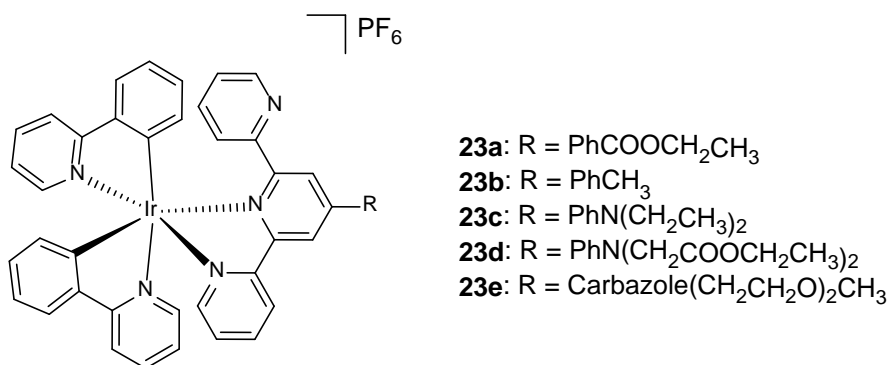
Fig. 16. Proposed mechanism for the photophysical processes of **21**: ISC, intersystem crossing; SRET, spin-restricted energy transfer; TTET, triplet–triplet energy transfer. Copyright (2017) The Royal Chemical Society.

In a similar manner, Natrajan and Lemerrier synthesized an heteroleptic Ir(III) complex, **22a**, based on the [Ir(ppy)₂] scaffold and 5-fluorene-1,10-phenantroline as diimine chelating ligand [135]. The emission profile of **22a** following non-resonant two-photon excitation with 150 fs NIR laser pulses (700–1000 nm) was identical to the one-photon emission spectrum. The TPA cross-section at 740 nm was 45 GM, comparable to those obtained for its lighter Ru(II) analogue (10 GM at 900 nm and 50 GM at 750 nm). The complex was probed to be a good candidate as TPE PDT photosensitizer *in vitro* with C6 Glioma cells. Cells treated with **22a** (1 or 10 μM) and irradiated for 5 min under two-photon conditions with 740 nm fs pulsed light underwent a morphology change from an elongated to a round shape. The mechanism of cell damage is currently under investigation.

On the other hand, Bryant and Weinstein prepared two Ir(III) complexes with the same [Ir(ppy)₂] scaffold featuring a bisbenzimidazol **22b** or its *N,N*-dimethylated derivative **22c** [136]. The compounds phosphoresce intensely under NIR TPE and demonstrated a time-dependent cytoplasmic localization *in live* U2OS cells. Both complexes **22b** and **22c** were efficient PS under one photon irradiation (405 nm) resulting in apoptotic cell death in several cancer cell lines at low light doses (3.6 J cm⁻²). In HeLa cells the LD₅₀ values were as low as 0.3 and 0.5 μM, respectively. However, only **22b** showed low dark cytotoxicity (LD₅₀ > 100 μM) and therefore a very convenient PI value > 333. The high dark toxicity of **22c** (LD₅₀ = 6.2 μM, PI = 12.4) was attributed to the presence of NMe groups, which may prevent H-bonding affecting intermolecular interactions within the cells. Remarkably, **22b** has an appreciable two-photon cross-section of 112 GM at 760 nm, and also displays high PS activity killing cancer cells under NIR two-photon excitation as evidenced by Annexin V/Propidium iodide dual-staining assay.



Variations in the ligand structures have enabled the organelle-specific accumulation of Ir(III) complexes [137]. Thus, Tian and co-workers adjust the bio-affinity of five terpyridine-based cyclometalated Ir(III) complexes by the introduction of different R-substituents (R = PhCOOCH₂CH₃ **23a**, PhCH₃ **23b**, PhN(CH₂CH₃)₂ **23c**, PhN(CH₂COOCH₂CH₃)₂ **23d**, Carbazole(CH₂CH₂O)₂CH₃ **23e**) [138]. As expected, the complexes displayed ¹MLCT and ³MLCT bands ranging from 350 to 520 nm, and emission band located between 570-600 nm with varied luminescent lifetimes and quantum yields. The largest TPA cross-sections were located around 800 ± 30 nm with δ values between 60 and 110 GM. Their antitumor potencies were first evaluated by MTT assay in human liver cancer cells HepG2 and non-cancerous human embryo liver fibroblast HELF. The results revealed low cytotoxicity of **23a** in the dark and high cell damage under UV light irradiation. Interestingly, **23a** presented higher phototoxic effects (~ 4% viability) than **23b** (~ 35% viability) although no difference in their ¹O₂ generation was observed, being **23b** a representative of the other four complexes. The authors speculated that the variations in activity could be product of their different subcellular localization; **23a** targeted the intracellular nucleus whereas the others overlap with mitochondria. In addition, **23a** was capable of migrating sequentially from the nucleus to mitochondria and inducing ‘double’ damage under two-photon irradiation. Finally, using two-photon laser excitation (800 nm, 600 mW) this complex was also able to inhibit tumor growth in mouse model with an antitumor rate (ATR) of 41.55%, comparable to the commercial PDT agent Ce6 (ATR: 40.76%) (Fig. 17).



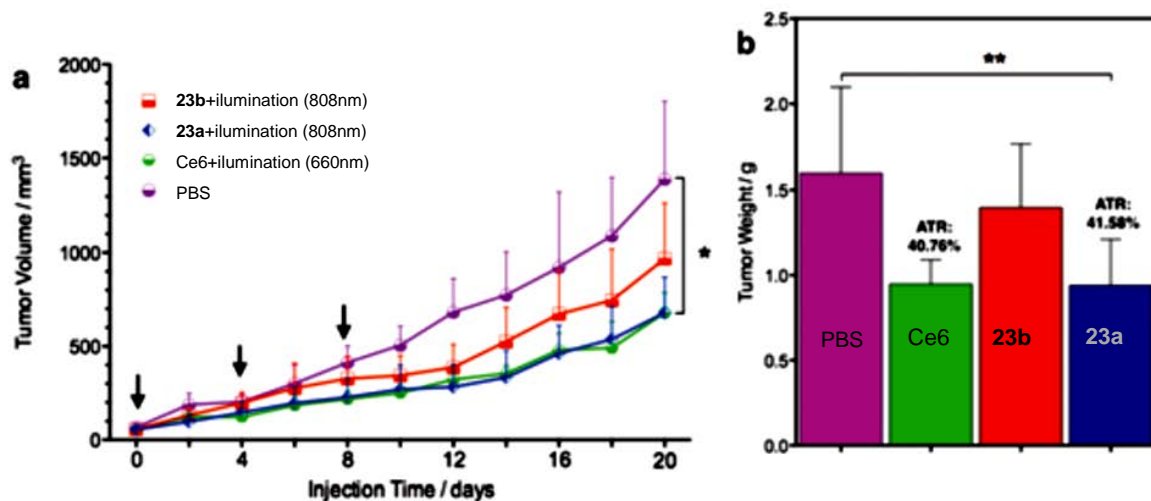
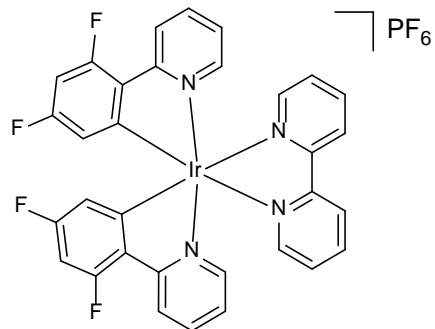
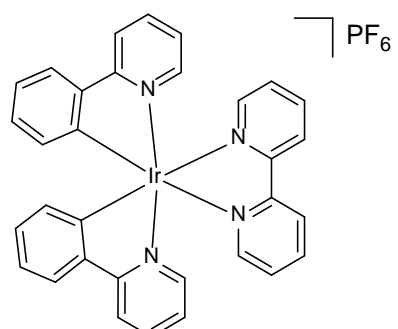


Fig. 17. (a) Growth curve of solid tumour model treated with PBS, Ce6, **23a** and **23b** growth curve and (b) growth inhibition rate 3 in the mice over 21 days under different treatments, the arrow indicates the injection (local) time point. Image reproduced with permission from [138]. Copyright (2017) The Royal Chemical Society.

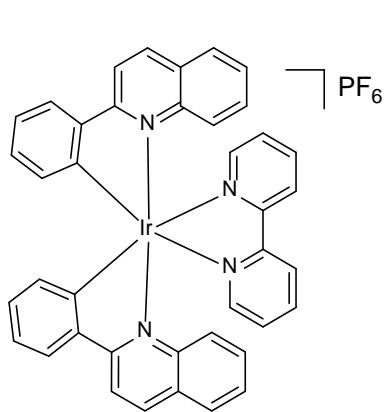
Kwon, Rhee and Lim synthesized ER-targeted Ir(III) PSs [139]. To enhance ROS production, the energy levels of the PSs were controlled by the introduction of different ligands (difluorophenylpyridine (dfppy) **24a**, 2-phenyl-pyridine (ppy) **24b**, 2-phenylquinoline (2pq) **24c** and 1-phenylquinoline (1pq) **24d**, whereas bipyridine ligand was employed to afford overall cationic Ir(III) complexes. All of them present TPA properties, which allow their visualization in the ER vicinity of HeLa cells by two-photon laser scanning microscopy. Furthermore, fluorescence lifetime imaging microscopy (FLIM) analysis confirmed the localization of **24c** in the ER (phosphorescence lifetime of ca. 500 ns in the ER and only ca. 5 ns in the nucleus). **24c** and **24d** effectively triggered cell death via ROS generation ($\Phi_{\Delta} = 0.95$ and 0.78 , respectively) upon 10 sec of sun light irradiation (100 mW cm^{-2} ; 1 J cm^{-2}) in SK-OV-3 ovarian and MCF-7 breast cancer cells in comparison to **24a** and **24b**, cisplatin and the photoactivatable $[\text{Ru}(\text{bpy})_3]^{2+}$, which shown not noticeable differences in their IC_{50} regardless of the light control. It is to be noted that **24c** and **24d** requires much lower energy than previously reported Ir(III) complexes ($12\text{-}36 \text{ J cm}^{-2}$) to be activated. The use of **24c** as a two-photon-based PDT agent was further confirmed by visualizing the morphological changes of SK-OV-3 cells upon co-incubation at 5, 30, and 60 min and 860 nm irradiation. Through matrix-assisted laser desorption ionization mass spectrometry (MALDI-MS), the authors demonstrated that their mechanism of action was based on protein cross-linking and protein oxidation (Fig. 18). Furthermore, in living cells the damaged proteins were found to be near the ER and mitochondria.



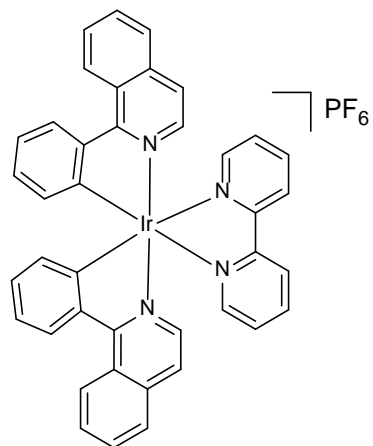
24a



24b



24c



24d

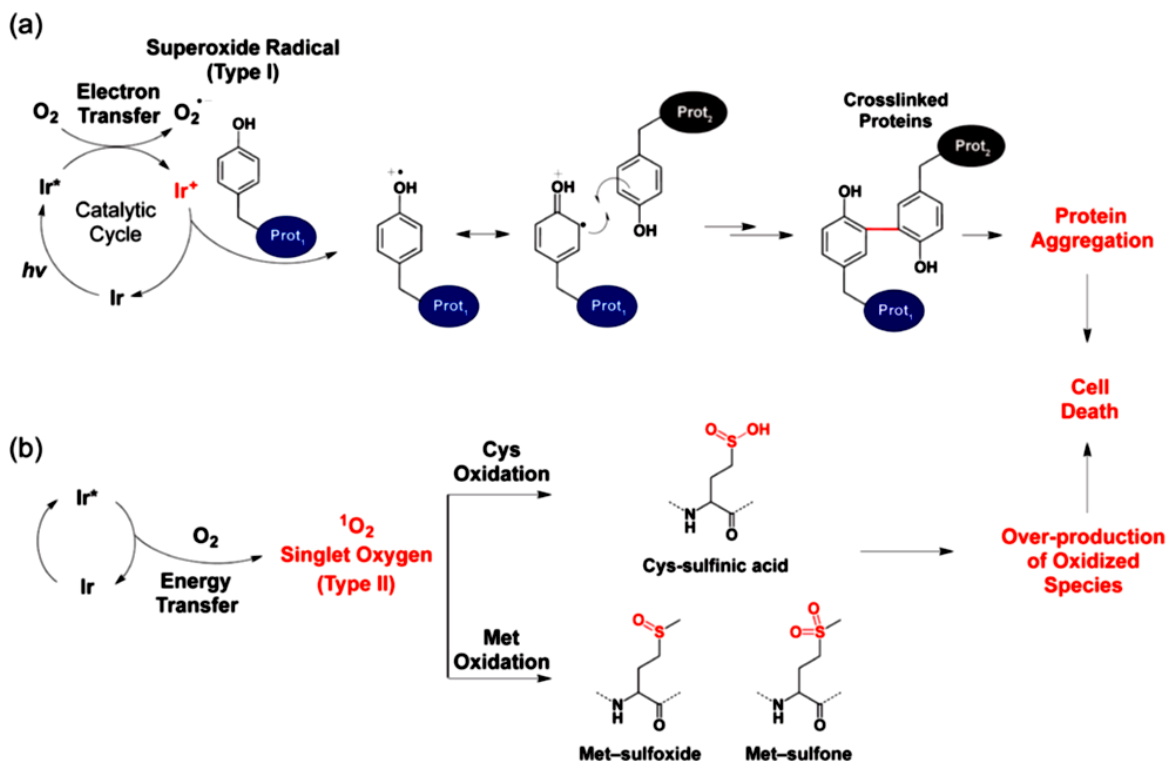
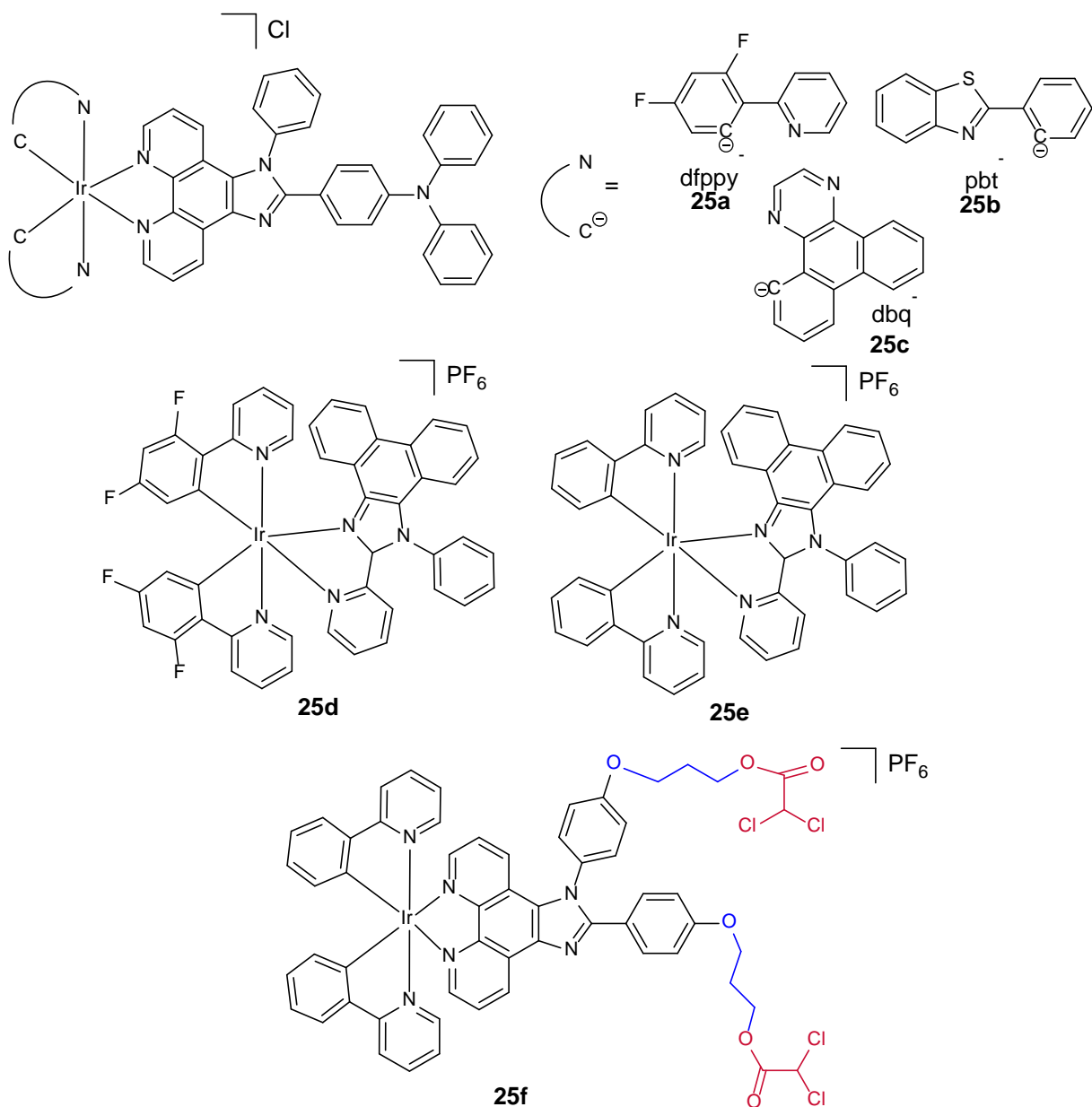


Fig. 18. Proposed modes of action of Ir(III) complexes **24a-24d** for PDT. (a) Photo-cross-linking pathway through a catalytic cycle initiated by a one-electron process from the Ir(III) complex to O₂, which can result in cell death via protein aggregation. (b) Protein oxidation pathway from ¹O₂ by triplet-triplet energy transfer of the excited state of the Ir(III) complex. Overexpression of oxidized proteins also induces cell death. Image reproduced with permission from [139]. Copyright (2016) American Chemical Society.

However, organelle-targeted PSs generally suffer from aggregation induced fluorescence quenching and reduced photocytotoxicity, resulting in inferior imaging and PDT efficacy [140]. Fortunately, the discovery of aggregation-induced emission (AIE) paves the way to reverse the situation [141]. In this sense, Chao *et al.* designed a series of mitochondria-targeted AIE-active Ir(III) complexes [142]. The complexes shared the diimine ligand containing a triphenylamine moiety, which is known to be an AIE fluorogen and a potential TPA cross-section enhancer [143], and differed on the C^N cyclometalating ligand (dfppy **25a**, pbt **25b**, dbq **25c**). **25a-25c**, but especially **25a**, showed a large enhancement in emission when increasing the water content, being the maximum luminiscence for the 90% (v/v) water-DMSO mixture. The dynamic light scattering (DLS) measurements revealed nanoparticles formation of 88.99-250.09 nm in the same mixture, evidencing that the complexes are AIE-active. Noteworthy, both ¹O₂ and ROS generation were maximum at 90% water, and selective accumulation in mitochondria (over 80%) was demonstrated by confocal laser scanning microscopy and ICP-MS in HeLa cells. **25a** presented the largest TPA cross-section (214 GM at 730 nm excitation) reported to date for TPA bioactive organometallic molecular probes. Their aggregation-induced PDT activity was tested *in vitro* in cancerous HeLa and non-cancerous L02 cell lines, as well as 3D multicellular spheroids (MCTSs). Compared to monolayer cells, all Ir complexes showed less one-photon PDT efficacy in MCTSs. Importantly, TPA PDT of **25a** showed impressive lethality (0.35 μM, PI = 110) towards MCTSs, lower than half of its IC₅₀ in one-photon PDT and even lower than in 2D monolayer cells. In contrast, **25b**, **25c** and the phorphyrin derivatives H₂TPP showed a better therapeutic outcome by OPA rather than TPA mainly caused by their poor TPA cross-section values. With the same idea in mind, the authors prepared related

mitochondria-targeted complexes, **25d** and **25e** [144]. The N^N ancillary ligand was design so that it possesses properties of TPA as well as AIE. To get so, an imidazole ring and a free rotational phenyl substituent were introduced. The combination of lipophilicity (log P of 1.98 for **25d** and 1.55 for **25e**) with the positive charge promoted the nanoaggregation in water. In the aggregate state, properties such as phosphorescence, $^1\text{O}_2$ yields, and photostability were significantly higher than in the monomeric states, indicating their potential as PSs in the aggregate state. In addition, the maximum TPA cross-sections were 114.4 GM for **25d** and 97.1 for **25e** at 740 nm. Similarly, to the previous results obtained for **25a**, **25b** and **25c** demonstrated outstanding therapeutical efficacy for the treatment of HeLa MCTSs under two-photon PDT condition (Table 2). The uptake levels of the compounds in multicellular spheroids (MCTSs) were monitored in real-time by two-photon imaging technology of confocal laser scanning microscopy (CLMS), which elegantly demonstrated that the effectiveness of the two-photon PDT treatment was due to the in-depth penetration of TPE ($\sim 114 \mu\text{m}$) in comparison with OPE ($\sim 42 \mu\text{m}$) (Fig. 19).



Complexes	2D monolayer cells			3D multicellular tumor spheroids		
	Dark ^a	Light ^b	PI ^c	Dark	OP ^d (PI)	TP ^e (PI)
25d	9.54 ± 0.35	0.16 ± 0.01	59.6	14.62 ± 0.58	1.07 ± 0.13 (13.7)	0.42 ± 0.06 (34.8)
25e	10.63 ± 0.42	0.24 ± 0.02	44.3	17.09 ± 0.46	1.30 ± 0.10 (13.1)	0.51 ± 0.04 (33.4)
Cisplatin	18.10 ± 0.73	17.82 ± 0.67	1.0	30.60 ± 0.82	28.45 ± 0.91 (1.1)	30.32 ± 0.87 (1.0)

^aThe IC₅₀ values in the dark. ^bThe IC₅₀ values under one-photon light irradiation. ^cPI is the phototoxicity index, which is the ratio of the IC₅₀ values in the dark to those upon light irradiation. ^dOP: one-photon light irradiation. ^eTP: two-photon light irradiation

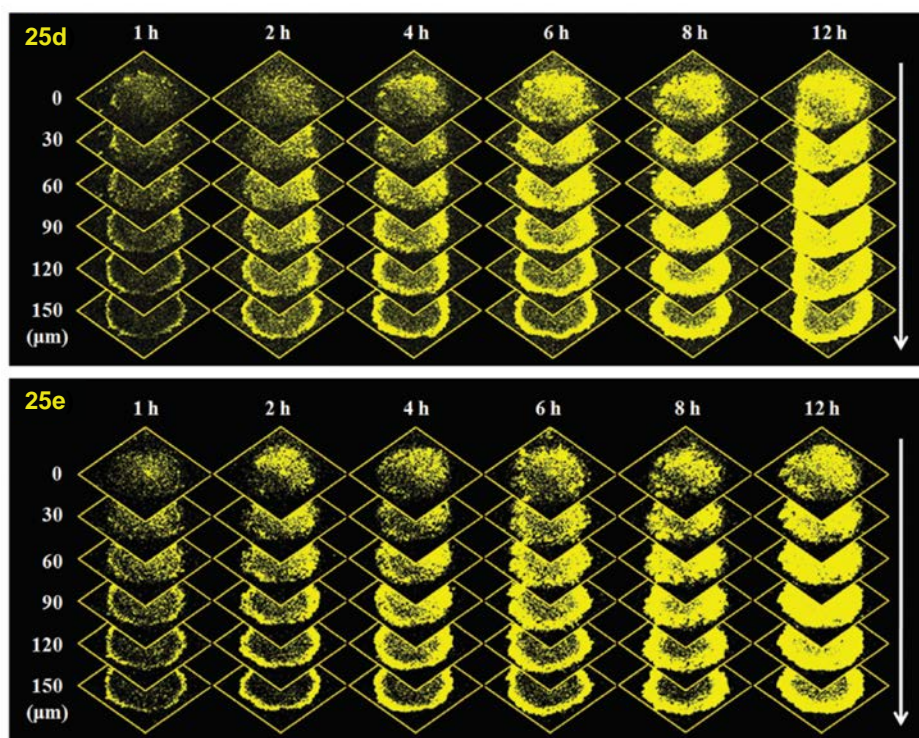


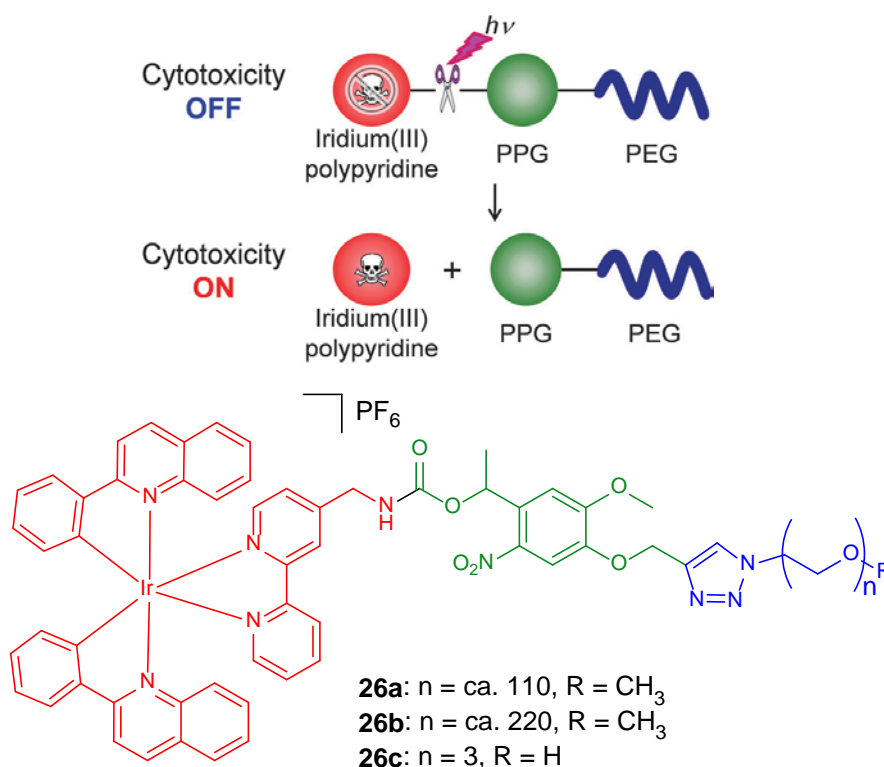
Fig. 19. Cellular uptake investigation of **25d** and **25e** (1 mM, $\lambda_{\text{ex}} = 740$ nm, $\lambda_{\text{em}} = 550 \pm 20$ nm) in HeLa MCTSs with incubation times of 1–12 h. Image reproduced with permission from [144]. Copyright (2017) The Royal Chemical Society.

Using similar N^N ligands that in **25a**, **25b** and **25c**, the authors have recently designed a series of dichloroacetate (DCA) DCA-Ir(III) co-drugs such as **25f** [145]. The conjugation of the mitochondrial targeted DCA to the Ir(III) complex was more efficient in the treatment of cancerous cell lines, implying that these two moieties indeed work in synergy to kill cancer cells. **25f** showed the maximum TPA-cross sections (159 GM) and a singlet oxygen quantum yields of 0.68. In one photon PDT, the IC₅₀ value of free-DCA complex in MCTSs increased by 147% with respect to monolayer cells, whereas that of **25f** only increased by 50%. This result indicates that following incorporation with DCA chemotherapy, the cells within MCTSs become more sensitive to PDT. In addition, **25f** showed enhanced toxicity after two photon irradiation due to the deeper penetration and the MCTSs treated shrank dramatically.

3.4 Photoactivated chemotherapy (PACT)

Photoactivated chemotherapy (PACT) exploits different mechanisms of drug photo-activation in an oxygen-independent fashion. Thus, PACT represents an important approach to target oxygen-deprived tumors where the efficacy of PDT agents is reduced. The photoactivation of Ru(II) complexes have been studied in detail and among the different mechanisms, redox processes [146] and ligand dissociation [147] are a highlight. The nature of the photochemical process is intimately related to the nature of the excited state, the energy and nature of closely-lying states as well as the availability of the dynamic process [148]. So for example, Ru(II) complexes can populate metal centered (3MC) [149] or ligand field (3LF) [150] states, which favor ligand substitution, and therefore have been proved to be suitable cages for molecules bearing nitrogen atoms. On the contrary, Ir(III) complexes tend to emit from mixed 3MLCT and 3LC states because of the large spin orbit coupling constant (SOC) [151]. That is why Ir(III) complexes are highly photostable and their use in PACT remains undeveloped.

Even so, Lo *et al.* have reported the only known example of a photoactivatable Ir(III) complex [152a]. Similarly, to the photocaged Re(I)-peptide conjugate [152b] and the Ru(II) complex [153] previously designed by Gasser, the authors used the photocaging technology to prevent the activity of the Ir(III) complex before irradiation. Thus, the active $[Ir(2pq)_2(bpy-CH_2NH_2)]$ ($bpy-CH_2NH_2 = 4$ -aminomethyl-4'-methyl-2,2'-bipyridine) was PEGylated through the incorporation of a nitrobenzyl photolabile protecting group (PPG). The resulting complexes **26a**, **26b** and **26c** showed good biocompatibility with HeLa cells in the dark with IC_{50} ranging from 10.4 to 65.9 μM , whereas 5, 10 or 20 min of continuous UV-A irradiation led to a remarkable decrease of their IC_{50} . Complex **26a** exhibited an IC_{50} as low as 1.4 μM and the largest PI of 25.9 for $t = 20$ min. The authors demonstrated that the complexes target the mitochondria (Pearson's colocalization coefficient = 0.98) and that their phototoxicity was due to the photorelease of the polypyridine Ir(III) complex rather than ROS generation.



4. Cyclometalated Ir(III) complexes in bacterial infections, inflammatory diseases, and neurological disorders

4.1. Antibacterial agents

The great problem of antibiotic resistance is the large mortality worldwide, in addition to the economic costs involved. Among the most current pathogens are included: *Enterococcus faecium*, *Staphylococcus aureus*, *Escherichia coli*, *Klebsiella pneumoniae*, *Acinetobacter baumannii*, *Pseudomonas aeruginosa*, *Mycobacterium tuberculosis* and *Enterobacter* species [154].

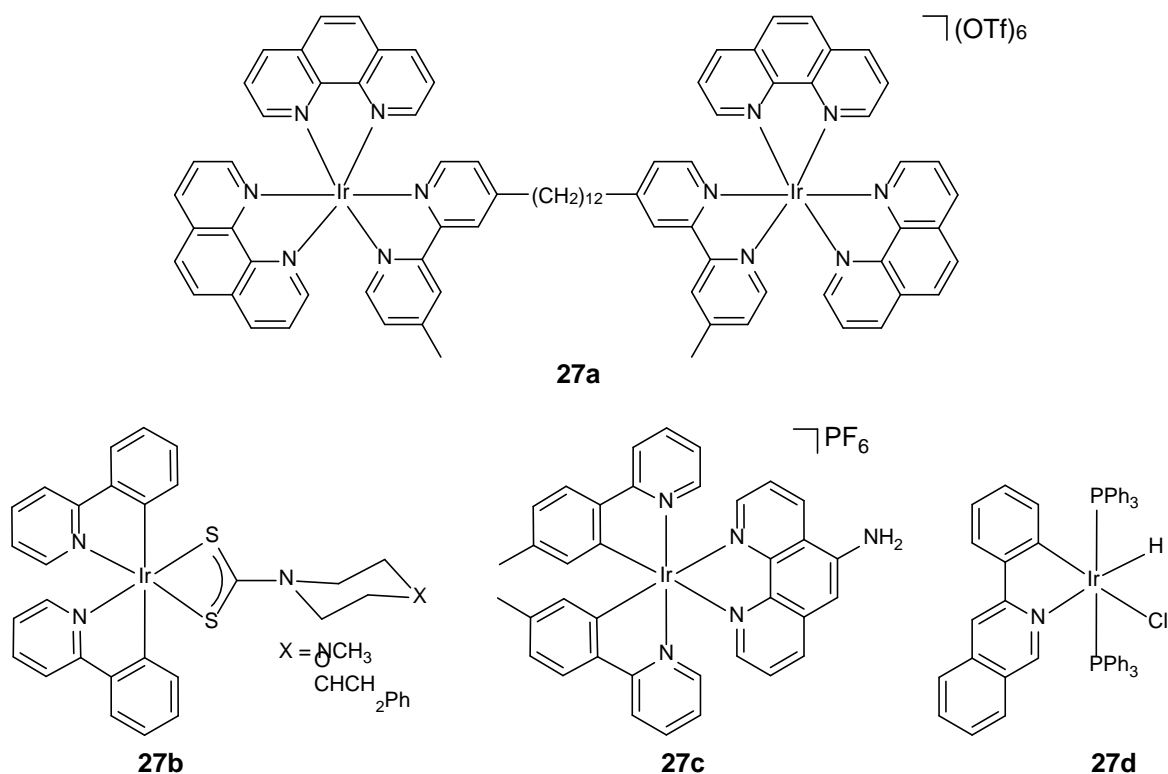
Given the increasing resistance of bacteria to drugs currently in clinical use, in combination with decreased effectiveness and increased toxicity of current antibiotics, there is a growing interest in the development of new classes of antibacterial agents [155,156].

The development of drugs containing metal ions in their molecular structure offers a great structural diversity and the variation of the oxidation states of the metal. Moreover, it also allows the possibility of ameliorating the activity of an organic drug in clinical by its coordination to the metal center [157,158]. Recently, the term ‘metalloantibiotic’ has been applied in a general manner to metal complexes exhibiting antibacterial capability [155]. Metal complexes of copper(II), silver(I), iron(II) and ruthenium(II) among others, have been studied for antibacterial activity [155,159,160]. Recent studies on Ir(III) complexes showed that they also exhibit antibacterial properties [161]. Most of the Ir(III) compounds reported as antibacterial agents are ‘half-sandwich’ type complexes, including mononuclear [161-168] and polynuclear [169-171] examples. Among them, excel the studies carried out by Rao Kollipara *et al.* However, only limited examples of kinetically inert Ir(III) complexes with antibacterial properties have been reported [172-175].

Probably, one of the earliest studies on the antibacterial activity of a kinetically inert Ir(III) polypyridyl complex was carried out by Collins and co-workers [172]. They prepared the dinuclear complex **27a** and studied its antimicrobial activity against four strains of bacteria Gram positive *Staphylococcus aureus* and methicillin-resistant *S. aureus*, and Gram negative *Escherichia coli* and *Pseudomonas aeruginosa*. They found that complex **27a** was inactive, maybe due to a high charge (+3) on each metal center. They also prepared a similar dinuclear Ir(III) complex with a lower charge (+2) and a chloride ligand on each metal. For this last complex, the minimum bactericidal concentration (MBC) to minimum inhibitory concentration (MIC) ratios was mostly > 2, concluding that it was bacteriostatic rather than bactericidal.

Recently, three mononuclear C^N cyclometalated Ir(III) complexes of the type **27b** bearing dithiocarbamate derivatives have been reported to have antibacterial activity against four pathogenic bacteria (*E. coli*, *V. cholerae*, *S. pneumoniae*, and *B. cereus*) [173]. The complex bearing the morpholine derivative (X = O) was the most active. The delocalization of the π -electrons over the chelate ring was proposed to increase the lipophilicity of the complexes and facilitate their penetration ability into the cell membrane of bacteria, thereby producing inhibition of bacterial growth.

Ma, Leung and co-workers have reported the antibacterial activity of four Ir(III) kinetically-inert organometallic complexes **27c** against four different bacterial strains (*Staphylococcus aureus*, *Escherichia coli*, *Enterococcus faecalis* and *Klebsiella pneumoniae*) using a disk diffusion assay [174]. Complex **27c**, which contains the relatively smaller C^N ligand and one amino group in the N^N ligand, exhibited a selective antibacterial activity towards *S. aureus*, with a MIC of 3.60 μ M and a MBC/MIC ratio of approximately 2. This suggested that a small C^N ligand improves the antibacterial activity, and the amino group could confer to the complex the adequate lipophilicity to penetrate the cell wall of *S. aureus* bacteria. Complex **27c** is the first example of a substitutionally-inert group 9 organometallic compound utilized as a direct inhibitor of *S. aureus*.



A recent study by Panwar *et al.* demonstrated that the use of ‘aggregation induced phosphorescence (AIP)’ activates cyclometalated Ir(III) complexes such as **27d** for sensing and inhibition of bacterial growth in aqueous solution [175]. The antibacterial activity of **27d** was tested against the representative bacterial strains Gram positive (*B. subtilis*) and Gram negative (*E. coli*), with MIC values of 4 and 8 $\mu\text{g mL}^{-1}$, respectively. Complex **27d** showed AIP after binding to bacterial cells in aqueous solution, in fact luminescence was observed only in stained *E. coli* cells, suggesting that the Ir(III) complex can penetrate into the cells, causing cell death. Preliminary DNA binding and cleavage studies suggested that the antibacterial activity was due to the DNA binding ability of the Ir(III) complexes. This ‘dual’ role observed in detection as well as inhibition of bacterial growth, encourages research of other less costly metal complexes to monitor and control bacterial levels in drinking water and seawater at a commercial level.

4.2. Alzheimer's disease

The number of people living with Alzheimer's disease (AD) is growing rapidly. For example, it has been estimated that 5.5 million Americans of all ages have AD. This is the most expensive disease in America and costs more than cancer and heart diseases. In 2017, the direct costs to American society of caring for those with Alzheimer's and other dementias might amount to about 259 billion dollars [176a]. It is currently accepted that AD progression is related to the presence of aggregates form of beta-amyloid ($\text{A}\beta$) peptides in brain, which trigger the formation of amyloid plaques and neurofibrillary tangles [176b]. Therefore, the design of small molecules that can target the aggregation of amylogenic peptides as potential therapeutic agents for AD is an area of study that has attracted a lot of attention recently [177]. In addition, the early diagnosis of the disease may slow down its progression or allow a palliative treatment to alleviate the symptoms [176b].

The research groups of Ma and Li reported the first application of Group 9 metal complexes as inhibitors of amyloid fibrillogenesis and as luminescent probes for $\text{A}\beta_{1-40}$ peptide [178]. They synthesized three novel cyclometalated Ir(III) solvato complexes with different aromatic C^N ligands such as **28a**. The presence of aromatic co-ligand ppy allows the complex to interact with the hydrophobic residues around

the N-terminal domain of the A β ₁₋₄₀, and the labile co-ligands H₂O can be displaced by the imidazole N-donor moiety of the histidine residues. They demonstrated that **28a** inhibits A β ₁₋₄₀ peptide aggregation *in vitro* with a higher potency than others metal-based inhibitors previously reported. In addition, it was observed that the luminescence of **28a** in the presence of aggregated A β ₁₋₄₀ was three times higher than in an equivalent mass concentration of monomeric A β ₁₋₄₀ peptides. This fact suggests that complex **28a** could be used to distinguish between aggregated and monomeric A β ₁₋₄₀ or monitor its fibrillogenesis.

More recently, Ma, Leung *et al.* have synthesized other luminescent Ir(III) complexes capable of inhibiting and monitoring A β fibrillation [176b]. When A β ₁₋₄₀ peptides were incubated in the presence of C[^]C[^]C Ir(III) complex **28b** (50 μ M) the images obtained by TEM showed a significant reduction in fibrils length compared to the negative control. The luminescent enhancement of **28b** at $\lambda_{\text{max}} = 484$ nm was higher when it was treated with A β ₁₋₄₀ fibrils than a comparable mass concentrations of A β ₁₋₄₀ monomers, probably due to the binding of **28b** within the hydrophobic interior of the fibrils. The same group has also investigated a series of luminescent Ir(III) complexes containing various C[^]N and N[^]N ligands such as **28c** [179], which showed a considerably enhanced luminescence response in the presence of the A β ₁₋₄₀ monomers or fibrils (Fig. 20). ESI-TOF mass spectrometry experiments revealed that complex **28c** was not covalently bound to the A β ₁₋₄₀ peptide. It showed an IC₅₀ value >100 μ M at 24 h toward human neuroblastoma cells (SH-SY5Y). This value was higher than the concentration of **28c** required for complete inhibition of A β ₁₋₄₀ peptide aggregation. This suggested a therapeutic window whereby A β ₁₋₄₀ peptide aggregation could be controlled without causing significant damage to brain cells. In addition, complex **28c** exerted a neuroprotective effect against the cytotoxicity induced by all three forms of A β ₁₋₄₀ peptide for SH-SY5Y cells or mouse primary cortical cells.

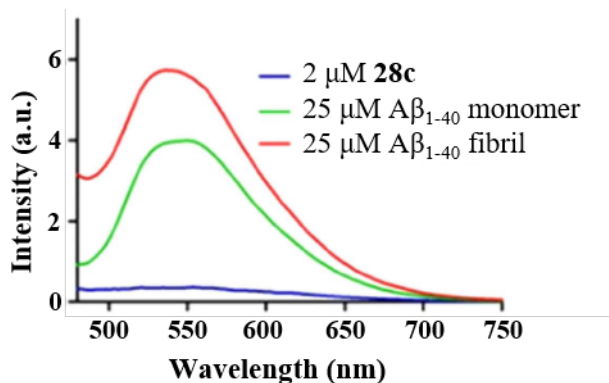
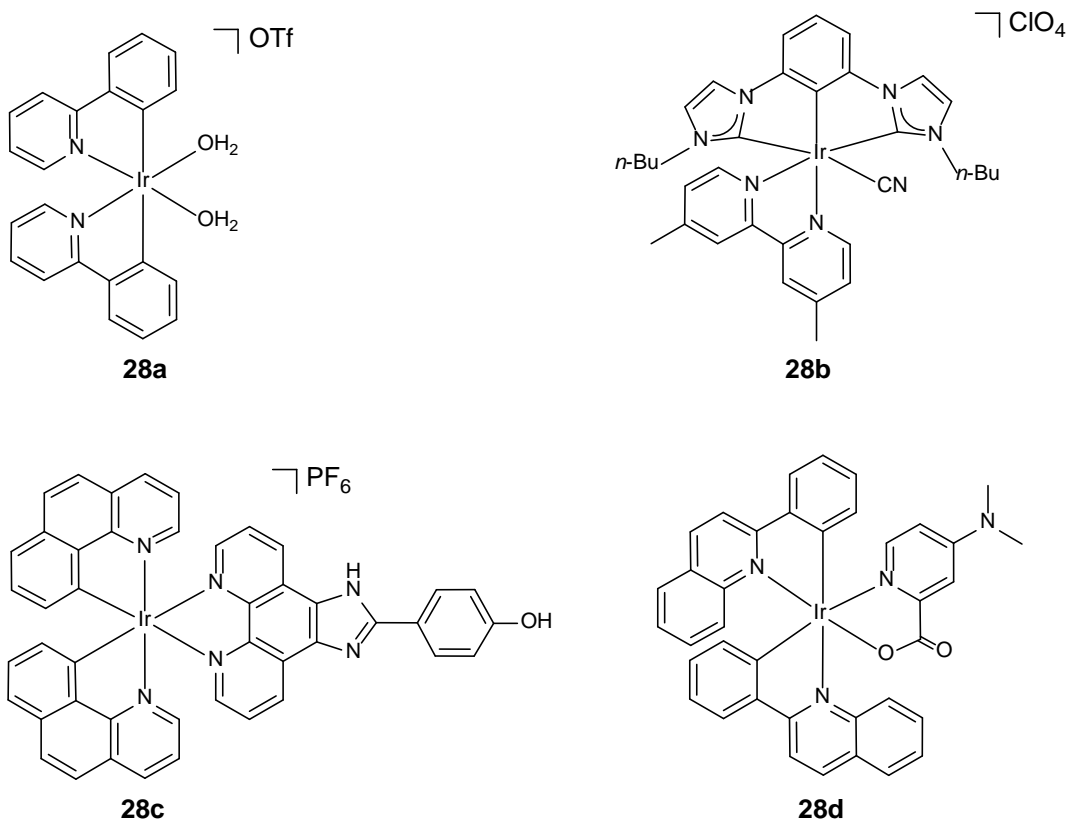


Fig. 20. Luminescence response of 2 μ M of **28c** in the absence or presence of 25 μ M A β ₁₋₄₀ monomers or fibrils. $\lambda_{\text{Ex}} = 360$ nm. Reproduced from [179]. Licensed under CC-BY-4.0.

Lim and co-workers have just reported a new Ir(III) complex **28d** as a chemical tool for oxidizing amyloidogenic peptides upon photoactivation and control of their aggregation pathways under mild conditions (presence of O₂ and visible light) [180]. The rational desing of **28d** was based on several characteristics such as excitation by low energy radiation, formation of ROS upon photoactivation, and a stable octahedral geometry, with a ligand that promotes the interaction with amylogenic peptides. Thus, the dimethylamino group was suggested to be essential for interactions with amylogenic peptides. Complex **28d** was easily photactivated with visible light [ϵ (463 nm) = 5.78 (\pm 0.12) $\times 10^3$ M⁻¹cm⁻¹]. The quantum yield of ¹O₂ [$\Phi_{\Delta} = 0.25$ (\pm 0.03)] confirmed the ability of **28d** to generate ¹O₂ from triplet dioxygen. The oxidative modifications and identification of oxidation sites in three representative amylogenic peptides (A β found in AD, α -Syn found in Parkinson's disease and hIAPP found in diabetes) were studied by MS and NMR. This study supports that A β ₄₀ is oxidized at specific sites (potentially methionine 35, histidine 13 and histidine 14) after light stimulation in the presence of oxygen. TEM images analysis demonstrated that the treatment of A β ₄₀ with complex **28d** in the presence of both light and O₂, induces the formation of short and thin fibrils instead of large aggregates produced in the absence of **28d**. Therefore, complex **28d**

was demonstrated to be a promising tool for the oxidative modifications of amyloidogenic peptides and the consequent control of their aggregation.

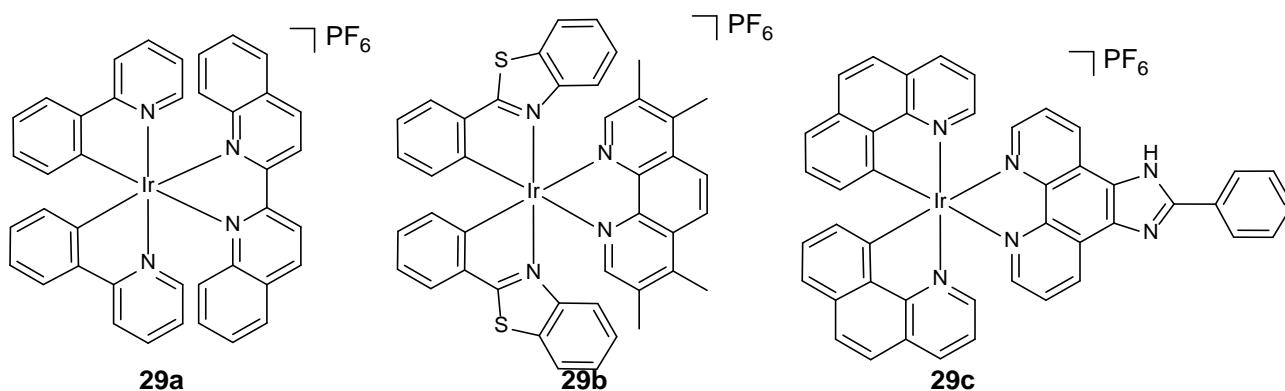


4.3. Chronic inflammatory diseases

TNF- α is a homotrimeric pro-inflammatory cytokine of the immune system whose overproduction has been associated with several chronic inflammatory diseases such as rheumatoid arthritis, Crohn's disease or psoriasis. [181] Direct targeting of TNF- α by protein biotherapies has been an undeniable success for the treatment of such diseases. Clinically approved inhibitors of TNF- α include monoclonal antibodies (infliximab, adalimumab) and soluble receptors of TNF- α (etanercept). These biotherapies display several drawbacks including opportunistic infections [182] and treatment resistance due to autoimmune reactions [183]. Furthermore, despite many efforts, no orally active drug targeting TNF- α has been identified so far [184]. PPIs represent a large class of therapeutic targets that play a crucial role in biological processes. Considerable progress was achieved in the last decade since 27 PPIs have now been tackled by small molecules including Ir(III) organometallic compounds that act as potent inhibitors of the TNF- α -TNFR (TNF receptor) PPI by suppressing the expression of TNF- α [8, 24a, 185]. The octahedral geometry of Ir(III) complexes provides a large structural complexity and conformational flexibility, which may make access to the TNF- α binding site easier. Indeed, Leung, Ma *et al.* reported in 2012 [24a] the first Ir(III)-based inhibitor of TNF- α , the Ir(III) biquinoline complex **29a**. Molecular docking showed that the **29a** binds to the same binding pocket as chromone SPD304. In a cell-free assay, complexes **29a** and **29a** inhibited the TNF- α -TNFR interaction with potency comparable to SPD304, a potent small-molecule inhibitor of TNF- α . Furthermore, complexes **29a** and **29a** inhibited TNF- α -induced NF- κ B luciferase activity in human hepatocellular carcinoma (HepG2) cells with superior potency to SPD304 [24a]. Interestingly, Ir(III) complex **29b** was verified as a potent inhibitor of the TNF- α -TNFR (TNF receptor) PPI *in vitro* and *in cellulo* [186]. Thus, in a cell-based luciferase assay, **29b** showed superior ability to inhibit TNF- α induced

NF- κ B activity *in cellulo* compared to the positive control compound SPD304 and **29a**. Complex **29b** inhibited the TNF- α -TNFR protein-protein interaction as revealed by an ELISA test. Moreover, **29b** inhibited I κ B α phosphorylation in a dose-dependent fashion in cells. To gain additional mechanistic understanding into the activity of **29b**, they further synthesized enantiopure *A*-**29b** and *B*-**29b** and discovered that while both complexes could inhibit TNF- α -TNFR binding, *A*-**29b** (IC₅₀ ~ 30 μ M) was more potent than *B*-**29b** (IC₅₀ ~ 57 μ M). This result was corroborated by an AlphaScreen assay measuring the strength of the TNF- α -TNFR interaction in the presence of compounds.

TNF- α converting enzyme (TACE) is a specific zinc dependent metalloprotease that is involved in the formation of the biologically active form of TNF- α . TACE is also considered an attractive therapeutic target in inflammatory diseases. So that, Ma and co-workers have proposed the inhibition of TACE as an interesting alternative to reduce TNF- α activity [187]. They reported complex **29c** as the first metal able to inhibit TACE enzymatic activity. **29c** was also able to lessen the phosphorylation of p38 MAP kinase (MAPK), which directly activates TACE.



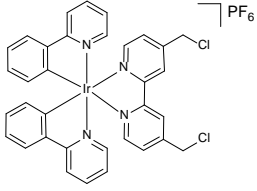
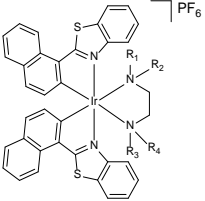
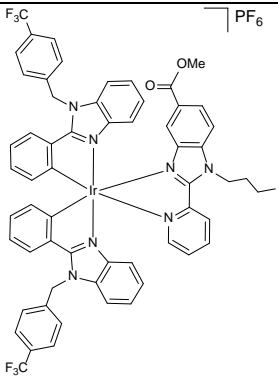
5. Overall structure activity relationships of some representative complexes

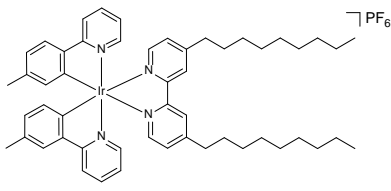
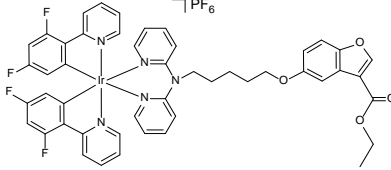
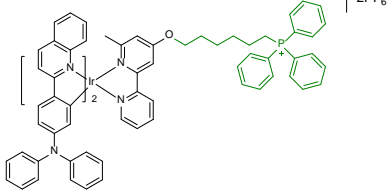
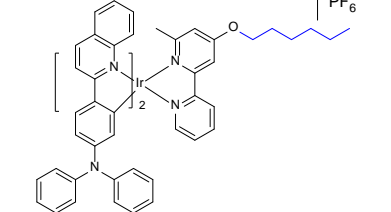
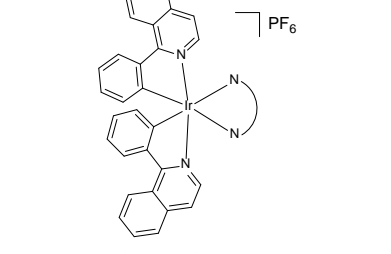
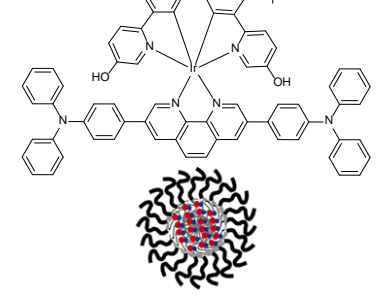
This review outlines recent progress of the development of luminescent Ir(III) complexes bearing cyclometalated ligands both in therapy and phototherapy of some major diseases such as cancer, bacterial infections, Alzheimer's, and autoinflammatory diseases. A summary table (Table 3) of some representative compounds has been collected with characters such as structure of the complexes, emission maximum, targeting organelles, (photo)cytotoxicity, relevant disease and reference. Moreover, Table 3 includes all the compounds that have shown efficacy in *in vivo* models (**12a**, **12c**, Hf-BPY-Ir-MOL and **23a**). In cells, the compounds can be located in various subcellular organelles such as the mitochondria (in about one-third of cases) or the lysosomes, and in the membrane. The number of compounds located in ER and nucleus is rather low. **12a** is the lead compound for the inhibition of the H-Ras/Raf-1 interaction whereas the benzofuran-conjugated Ir(III) complex **12c** inhibits both IL-6-induced STAT3 activity and TNF- α -induced NF- κ B activity in DU145 cells. As mitochondria play important roles in cell proliferation and apoptosis, they are a primary target for PDT treatment. In fact, in some cases the location changes to the mitochondria after irradiation (complexes **15c-15e** and **23a**). Unfortunately, there is no a clear relationship between the structure and the localization of compounds. However, the photosensitizers **14a** (containing a (C₆H₅)₃P group) and **14b** (containing an alkyl group) specifically targeted the mitochondria and lysosomes in HeLa cells, respectively. When the irradiation for **14a** was performed under hypoxia, 3.3% cell viability was obtained, indicating a high PDT efficiency. In contrast, the cell viability in presence of **14b** remained at a high percentage (> 66%) under hypoxic or normoxic conditions. Extending the π -conjugation of the PSs for PDT **15a-e** on both the diimine and the cyclometalating ligands influenced ground-state absorption, while the nature of the emitting triplet excited states was only affected when varying the C^N ligand.

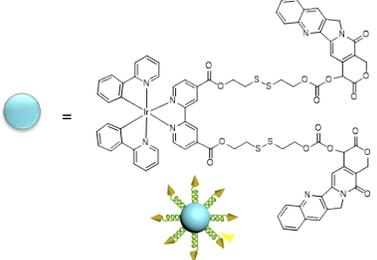
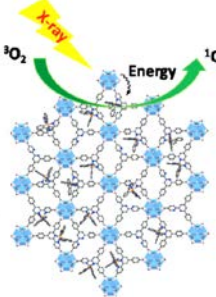
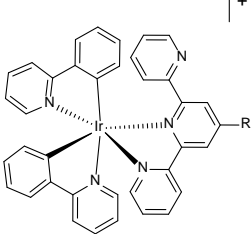
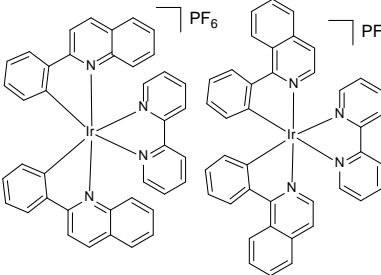
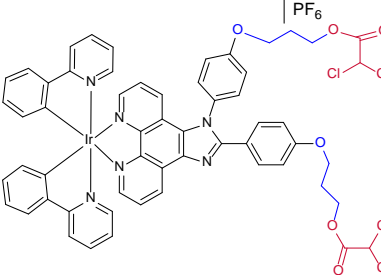
Relocalization in SK-MEL-28 cells from cytosol to mitochondria after light irradiation was observed after visible light treatment.

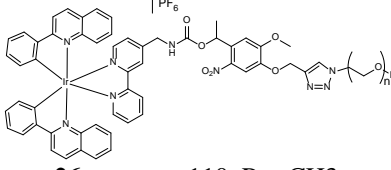
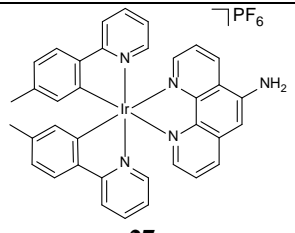
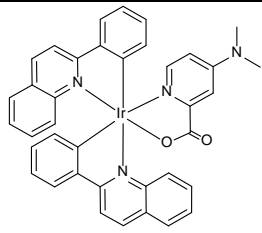
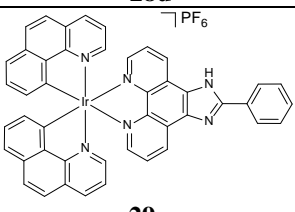
Smart nanoplateforms decorated with or containing Ir(III) drugs are currently been used to improve properties such as solubility or targeting. Thus, PDT effect in HeLa cancer cells was observed for **NP-16b** when irradiated with visible light ($\lambda > 400$ nm), being mainly located at the cytoplasm. Likewise, amphiphilic micelles decorated with FA as targeting moiety, **NP-16c**, containing a camptothecin Ir(III) conjugate and GSH responsive disulfide bond linkages have shown ROS generation upon visible light illumination ($\lambda > 400$ nm) for PDT. Remarkably, the nanoscale metal-organic layers **Hf -BPY-Ir-MOL**, containing Ir(III), have been probed useful for deeply penetrating X-ray-induced PDT, showing *in vivo* anticancer efficacy experiments on subcutaneous flank tumor-bearing mouse models of CT26 and MC38 showed up to 90% reduction in tumor volumes.

Other applications in bacterial infections, inflammatory diseases, and neurological disorders are briefly covered in this review including the direct inhibitor of *S. aureus* **27c** (which contains one amino group in the N^N ligand), the TACE inhibitor **29c** (an enzyme involved in the formation of the biologically active form of TNF- α), and the photosensitizer **28d** which is able to induce oxidation of amyloidogenic peptides, controlling their aggregation pathways under mild conditions.

Table 3. Some representative examples of Ir(III) luminescent complexes in therapy and phototherapy						
Structure	λ_{em} (nm)	Organelle/ target	Disease	IC ₅₀ (μ M)/ viability	IC ₅₀ (μ M) Light/ viability	Ref.
 <p>4d</p>	630	Mitochondria	Cancer MDB-MA-231	0.33	-	[35]
 <p>5b</p> <p>R₁, R₂, R₃, R₄ = CH₂, NRR'</p>	598-603	Lysosomes	Cancer HEK293T	0.12-2.3	-	[41]
 <p>6c</p>	580	Membrane	Cancer A2780	0.197	-	[44]

 <p>12a</p>	-	Protein H-Ras/Raf-1	Cancer H1299 In vivo Kidney model mouse xenograft model	6.3	-	[57]
 <p>12c</p>	-	Protein STAT3 NF-kB	Cancer DU145 In vivo prostate cancer xenograft mouse model	4.34	-	[61]
 <p>14a</p>	590	Mitochondria	Cancer (HeLa)	87%	475 nm Normoxia 2.3% Hypoxia 3.3%	[88]
 <p>14b</p>	600	Lysosome	Cancer (HeLa)	>66%	475 nm >66%	[88]
 <p>15c-15e</p> <p>c= dpq d= dppz e= dppn</p>	588- 590	Relocalization from cytosol to mitochondria after light irradiation	Cancer (SK- MEL-28)	0.27-1.53	Vis 0.003-0.019 Red 0.034-0.25	[100]
 <p>NP-16b</p>	621	Cytoplasm	Cancer (4T1 cells)	80%	>400 nm 10%	[106]

 <p>NP-16c</p>	615	-	Cancer (HeLa)	36.1%	>400 nm 13.07%	[107]
 <p>Hf-BPY-Ir-MOL</p>	-	-	Cancer Mouse models of CT26 and MC38 (colon adenocarcinoma)	-	X Ray 83.6-90% reduction tumor volumen	[129]
 <p>23a: R = PhCOOCH2CH3</p>	596	From nucleus to mitochondria under two photon irradiation	Cancer (mouse model)	-	Two photon 800 nm ATR (antitumor rate) = 41.55%	[138]
 <p>24c and 24d</p>	562-592	ER	Cancer (SK-OV-3 cells)	4.01-3.67	Sun light 1.58-0.65 860 nm Morphological changes	[139]
 <p>25f</p>	590	Mitochondria	Cancer (HeLa MCTSs)	1.92	730-750 nm 0.11	[145]

 <p>26a: n = ca. 110, R = CH₃</p>	560	Mitochondria	Cancer (HeLa)	36.2	UV-A Led 1.4	[152a]
 <p>27c</p>	555	-	Antibacterial Cancer A2058	1.24	-	[174]
 <p>28d</p>	600	-	Alzheimer	-	-	[180]
 <p>29c</p>	585	-	Inflammatory	-	-	[187]

6. Conclusions

This review outlines a number of different mechanisms where cyclometalated Ir(III) complexes have efficacy in certain important diseases. As shown, small structural changes, as the modification of ancillary ligands with a rational choice of functional groups and linkers can strongly tune their lipophilicity, biological activity, cellular uptake efficiency and subcellular distribution. Covalent conjugation of vectorization moieties indeed seems quite promising for drug delivery purposes. Thus, many Ir(III) anticancer agents act *via* targeting non-nucleic acid biomolecules, thereby perturbing cell function, which in many cases can be visualized thanks to the intrinsic luminescence of the complexes, many of them being located in mitochondria (in about one-third of cases). In addition, an increasing number of academic researchers are focusing their investigations on the peculiar interactions that Ir(III) compounds have with visible light, trying to exploit them in photodynamic therapy. Cyclometalated Ir(III) complexes have arisen as potential alternatives to the isoelectronic Ru(II) based PSs, due to the fact that they enable broader tuning of the intrinsic photophysical properties, increase ligand-field stabilization energy and pronounce decoupling of the ³MLCT excited states respect to those that are metal-centered. Thus, these complexes possess multiple advantages among which stand out their emission spectra ranging from the visible to the NIR, longer lifetimes (~ μs) and ROS generation capabilities under hypoxic conditions. Three different strategies have been commonly exploited to achieved red-to-NIR emission: the introduction of extending π-conjugated systems either on one or both C^N and N^N ligands and the conjugation of light-harvesting chromophores or upconvertible nanoparticles. Furthermore, improved outcomes of PDT treatments of

tumors have been demonstrated *in vivo* with two photon absorption Ir(III) based photosensitizers. Overall, these coordinatively saturated and substitutionally inert Ir(III) complexes show improved stability compared to most of known metallodrugs. Some major issues remain such as the small number of Ir(III) complexes that have shown efficacy in *in vivo* models, rendering it difficult to assess the full potential of this class of compounds. A remarkable complex is **12a**, as lead compound for the inhibition of the H-Ras/Raf-1 interaction and its downstream pathways both *in vitro* and *in vivo*. On the other hand, PDT has been established as an effective cancer treatment but has yet to become mainstream, being the lack of selectivity one of the main concerns. In addition, many Ir(III) PSs show low absorption in the biological optical window, a two-photon absorption strategy being impractical for deep-tissue applications. One advantage of upconversion-assisted photochemistry is that it does not require high-intensity pulsed lasers. Antimicrobial Ir(III)-based PSs are still unknown.

Abbreviations

A2058	human metastatic melanoma cell
A2780	human ovarian carcinoma cell
A2780cisR	cisplatin-resistant A2780
A375	human melanoma cell
A549	human lung adenocarcinoma epithelial cell
A549R	cisplatin-resistant A549 cell
A β	beta-amyloid
acac	acetylacetonate
AFM	atomic force microscopy
AD	Alzheimer's disease
AIE	aggregation-induced emission
AIP	aggregation-induced phosphorescence
ATP	adenosine-5'-triphosphate
ATR	antitumor rate
Bcl-2	B-cell lymphoma 2
BODIPY	boron-dipyromethene
bPEI	branched poly(ethyleneimine)
bpy	2,2'-bipyridine
bqu	2,2'-bisquinoline
bsn	2-(1-naphthyl)benzothiazol
BRD4	epigenetic factor bromodomain-containing protein 4
BSA	bovine serum albumin
CaM	calmodulin
CD44	glycoprotein involved in cell-cell interactions
cisplatin	<i>cis</i> -diamminedichloridoplatinum(II)
CLMS	confocal laser scanning microscopy
<i>c-myc</i>	gene regulator of cellular metabolism and proliferation
Cp*	ligand 1,2,3,4,5-pentamethylcyclopentadienyl
CPT	Camptothecin
CW	continuous wave
dbq	dibenzo[f,h]quinoxaline
dfppy	difluorophenylpyridine
dpbq	2,3-diphenylbenzo[g]quinoxaline
dpp	2,3-diphenylpyrazine
dpq	dipyrido[3,2-f:2',3'-h]quinoxaline
dpqx	2,3-diphenylpyrazine

dppz	dipyrido[3,2-a:2',3'-c]phenazine
dppn	benzo[I]dipyrido[3,2-a:2',3'-c]phenazine
DLS	dynamic light scattering
DMSO	dimethyl sulfoxide
DPBF	1,3-diphenylbenzo[c]furan
EC ₅₀	half maximal effective concentration
ELISA	Enzyme-Linked ImmunoSorbent Assay
ER	endoplasmic reticulum
ERK	extracellular signal-regulated kinase
ESI-MS	electrospray ionization mass spectrometry
ESI-TOF	electrospray ionization time-of-flight mass spectrometry
FDA	food and drug administration
FR	folate receptor
FRET	fluorescence resonance energy transfer
GSH	glutathione
HA	hyaluronan
HDAC	histone deacetylase
<i>hDM2</i>	human double minute 2 protein
HeLA	human cervical adenocarcinoma cells
HepG2	human hepatocellular carcinoma cells
HEK293T	human embryonic kidney 293T cells
hIAPP	amylogenic peptides in diabetes
HL60	human promyelocytic leukemia cells
pppy	2-((1,10-biphenyl)-4-yl)pyridine
ppy	2-phenylpyridine
pq	phenylquinoline
HSA	human serum albumin
HT-29	human colon carcinoma cell
IC ₅₀	half-maximal inhibiting concentration
ICP-MS	inductively coupled plasma-mass
IL	intra-ligand
ISC	intersystem crossing
JMJD2	Jumonji domain 2 histone demethylase
Jurkat	human leukaemic T cell lymphoblast
KLA	pro-apoptotic peptide (KLAKLAK)
LC ₅₀	median lethal concentration
LD ₅₀	lethal dose which causes the death of 50% of test cells
LLCT	ligand-to-ligand charge transfer
LMMCT	ligand-to-metal-metal charge transfer
LO2	human hepatic cell
MBC	minimum bactericidal concentration
MCF-7	human breast adenocarcinoma cells
MCTS	multicellular spheroids
MDA-MB-231	human breast adenocarcinoma cells
MEK	mitogen-activated protein kinase
MIC	minimum inhibitory concentration
MLCT	metal-to-ligand charge transfer
MAPK	mitogen-activated protein kinase
MLLCT	metal-to-ligand-ligand charge transfer
MMLCT	metal-metal-to-ligand charge transfer
MMP	mitochondrial membrane potential

MMT	3-(4,5-dimethyl-2-thiazolyl)-2,5-diphenyltetrazolium bromide
MOLs	metal-organic layers
Molt-4	human acute T lymphoblastic leukaemia
MS	mass spectrometry
MSA	methane sulfonic acid
mSiO ₂	mesoporous silica
MTDR	mitotracker deep red
mTOR	mammalian target of rapamycin
MTR	mitotracker red
NADH	dihydronicotinamide adenine dinucleotide
NF-κB	nuclear factor κB
NHC	<i>N</i> -heterocyclic carbene
NIR	near-infrared region
NMR	Nuclear magnetic resonance
NP	nanoparticle
OCT	octreotide
OPA	one photon absorption
pbt	2-phenylbenzo[d]thiazole
P4VP- <i>b</i> -PEO	poly(4-vinylpyridine- <i>b</i> -ethyleneoxide)
PACT	photoactivated chemotherapy
PDT	photodynamic therapy
PEG	poly(ethyleneglycol)
PET	photoinduced electron transfer
phen	1,10-phenanthroline
PhenISA	phenanthroline pendants of a poly(amidoamine) copolymer
PI	phototoxicity index
PPG	photolabile protecting group
PPI	protein-protein interactions
ppy	2-phenylpyridine
PPy	polypyrrole
pqu	2-(2-pyridinyl)quinoline
PS	photosensitizer
PSMA	poly(styrene-co-maleic anhydride) polymer
py	pyridine
quqo	2-(quinolin-2-yl)quinoxaline
RAF	rapidly accelerated fibrosarcoma family kinases
RGD	Arg-Gly-Asp
ROS	reactive oxygen species
SARs	structure-activity relationships
SBU	secondary building units
SDS-PAGE	sodium dodecyl sulfate polyacrylamide gel electrophoresis
SK-MEL-28	human melanoma cells
SK-OV-3	human ovarian cancer cells
SK-SY5Y	human neuroblastoma cells
SPION	Superparamagnetic iron oxide nanoparticles
SSTR2	somatostatin subtype-2 receptors
STAT3	signal transducer and activator of transcription 3
T47D	human breast adenocarcinoma cells
TACE- TNF-α	converting enzyme tumor necrosis factor-alpha
TEM	transmission electron microscopy
thpy	2-(2-thienyl)pyridine

TNF- α	tumor necrosis factor- α
TPA	two-photon absorption
TPE	two-photon excitation
UCNP	upconverting nanoparticle
UPR	unfolded protein response
VPA	valproic acid
VEGF	vascular endothelial growth factor
α -Sym	amylogenic peptides in Parkinson's disease

Acknowledgements

This work was supported by the Spanish Ministry of Economy and Competitiveness and FEDER funds (Project CTQ2015-64319-R). The MetDrugs network (CTQ2015-70371-REDT) is acknowledged for providing opportunities for discussion. A. Z. and G. V. thanks Fundacion Séneca-CARM (Exp. 19020/FPI/13) and the University of Murcia (R-1034/2016), respectively, for a grant.

References

- [1] a) D.-L. Ma, H.-Z. He, K.-H. Leung, D. S.-H. Chan, C.-H. Leung, *Angew. Chem. Int. Ed.* 52 (2013) 7666. b) D. Ma, T. Tsuboi, Y. Qiu, L. Duan, *Adv. Mater.* 29 (2017) 1603253. c) M. Martínez-Alonso, J. Cerdá, C. Momblona, A. Pertegas, J. M. Junquera-Hernández, A. Heras, A.M. Rodríguez, G. Espino, H. Bolink, E. Ortí, *Inorg. Chem.* 56 (2017) 10298.
- [2] *Iridium Catalysis (Topics in Organometallic Chemistry)* P. G. Andersson, Ed. Springer-Verlag: Berlin 2011 Vol. 34.
- [3] A. Lightfoot, P. Schnider, A. Pfaltz, *Angew. Chem., Int. Ed.* 37 (1998) 2897.
- [4] a) A. Savini, G. Bellachioma, G. Ciancaleoni, C. Zuccaccia, D. Zuccaccia, A. Macchioni, *Chem. Commun.* 46 (2010) 9218. b) T.P. Brewster, J.D. Blakemore, N.D. Schley, C.D. Incarvito, N. Hazari, G.W. Brudvig, R.H. Crabtree, *Organometallics* 30 (2011) 965.
- [5] A.S. Goldman, A.H. Roy, Z. Huang, R. Ahuja, W. Schinski, M. Brookhart, *Science* 312 (2006) 257.
- [6] a) R. Crabtree, *Acc. Chem. Res.* 12 (1979) 331. b) *Iridium Complexes in Organic Synthesis.* Edited by L.A. Oro and C. Claver. Wiley-VCH, Weinheim 2008.
- [7] a) D.-L. Ma, S. Lin, W. Wang, C. Yang, C.-H. Leung, *Chem. Sci.* 8 (2017) 878. b) Y. Chi, T.-K. Chang, P. Ganesan, P. Rajakannu, *Coord. Chem. Rev.* 346 (2017) 91.
- [8] D.-L. Ma, D. S.-H. Chan, C.-H. Leung, *Acc. Chem. Res.* 47 (2014) 3614.
- [9] T. Giraldi, G. Sava, G. Mestroni, G. Zassinovich, D. Stolfa, *Chem.-Biol. Interact.* 22 (1978) 231.
- [10] Z. Liu, P. J. Sadler, *Acc. Chem. Res.* 47 (2014) 1174.
- [11] a) Z. Liu, A. Habtemariam, A.M. Pizarro, S.A. Fletcher, A. Kisova, O. Vrana, L. Salassa, P.C. A. Bruijninx, G.J. Clarkson, V. Brabec, P.J. Sadler, *J. Med. Chem.* 54 (2011) 3011. b) Z. Liu, L. Salassa, A. Habtemariam, A.M. Pizarro, G. J. Clarkson, P.J. Sadler, *Inorg. Chem.* 50 (2011) 5777. c) Z. Liu, A. Habtemariam, A. M. Pizarro, G. J. Clarkson, P. J. Sadler, *Organometallics* 30 (2011) 4702. d) A. J. Millett, A. Habtemariam, I. Romero-Canelon, G. J. Clarkson, P. J. Sadler, *Organometallics* 34 (2015) 2683. e) Z. Liu, I. Romero-Canelón, A. Habtemariam, G.J. Clarkson, P.J. Sadler, *Organometallics* 33 (2014) 5324.
- [12] J. M. Hearn, I. Romero-Canelón, B. Qamar, Z. Liu, I. Hands-Portman, P.J. Sadler, *ACS Chem. Biol.* 8 (2013) 1335.

- [13] a) Z. Liu, I. Romero-Canelón, B. Qamar, J.M. Hearn, A. Habtemariam, N. P. E. Barry, A. M. Pizarro, G. J. Clarkson, P. J. Sadler, *Angew. Chem., Int. Ed.* 53 (2014) 3941. b) S. Betanzos-Lara, Z. Liu, A.M. Pizarro, B. Qamar, A. Habtemariam, P.J. Sadler, *Angew. Chem. Int. Ed.* 51 (2012) 3897. c) Z. Liu, R.J. Deeth, J.S. Butler, A. Habtemariam, M.E. Newton, P.J. Sadler, *Angew. Chem. Int. Ed.* 52 (2013) 4194.
- [14] L. Zeng, P. Gupta, Y. Chen, E. Wang, L. Ji, H. Chao, Z. S. Chen, *Chem. Soc. Rev.* (2017) Jun 27. doi: 10.1039/c7cs00195a.
- [15] a) E. Meggers, *Curr. Opin. Chem. Biol.* 11 (2007) 287. b) Z. Adhireksan, G. E. Davey, P. Campomanes, M. Groessl, C.M. Clavel, H. Yu, A.A. Nazarov, C.H. Yeo, W.H. Ang, P. Dröge, U. Rothlisberger, P.J. Dyson, C.A. Davey, *Nat. Commun.* 5 (2014) 3462. c) Ö. Karaca, S. M. Meier-Menches, A. Casini, F. E. Kühn, *Chem. Commun.* 53 (2017) 8249.
- [16] a) N.P. Barry, P.J. Sadler, *Chem. Commun.* 49 (2013) 5106-31. b) G. Gasser, N. Metzler-Nolte, *Curr. Opin. Chem. Biol.* 16 (2012) 84-91. c) G. Gasser, I. Ott, N. Metzler-Nolte, *J. Med. Chem.* 54 (2011) 3.
- [17] a) N. Cutillas, G.S. Yellol, C. de Haro, C. Vicente, V. Rodríguez, J. Ruiz, *Coord. Chem. Rev.* 257 (2013) 2784. b) J. Ruiz, V. Rodríguez, N. Cutillas, K.G. Samper, M. Capdevila, Ò Palacios, A. Espinosa *Dalton Trans.* 41 (2012) 12847. c) V. Novohradsky V. J. Yellol, O. Stuchlikova, M.D. Santana, H. Kostrhunova, G. Yellol, J. Kasparkova, D. Bautista, J. Ruiz, V. Brabec, *Chem. Eur. J.* 2017, DOI: 10.1002/chem.201703581.
- [18] a) M.A. Nazif, R. Rubbiani, H. Alborzina, I. Kitanovic, S. Wölfl, I. Ott, W.S. Sheldrick, *Dalton Trans.* 41 (2012) 5587. b) K.K.-W. Lo, K.K.-S. Tso, *Inorg. Chem. Front.* 2 (2015) 510. c) Y. Gothe, T. Marzo, L. Messori, N. Metzler-Nolte, *Chem. Eur. J.* 22 (2016) 12487.
- [19] M. Dörr, E. Meggers. *Curr. Opin. Chem. Biol.* 19 (2014) 76.
- [20] a) G.S. Yellol, A. Donaire, J.G. Yellol, V. Vasylyeva, C. Janiak, J. Ruiz, *Chem. Commun.*, 49 (2013) 11533. b) J. Yellol, S. A. Pérez, A. Buceta, G. Yellol, A. Donaire, P. Szumlas, P. J. Bednarski G. Makhloufi, C. Janiak, A. Espinosa, J. Ruiz, *J. Med. Chem.* 58 (2015) 7310.
- [21] S. Bose, A. H. Ngo, L. H. Do, *J. Am. Chem. Soc.* 139 (2017) 8792.
- [22] J. M. Zimbron, K. Passador, B. Gatin-Fraudet, C.-M. Bachelet, D. Plazuk, L.-M. Chamoreau, C. Botuha, S. Thorimbert, M. Salmain, *Organometallics* 36 (2017) 3435.
- [23] K.K.-S. Tso, K. K.-W. Lo. *Strategic Applications of Luminescent Iridium(III) Complexes as Biomolecular Probes, Cellular Imaging Reagents, and Photodynamic Therapeutics*, in *Iridium(III) in Optoelectronic and Photonics Applications*. Edited by E. Zysman-Colman. John Wiley & Sons Ltd. 2017. Chichester, UK. doi: 10.1002/9781119007166.ch9
- [24] a) C.-H. Leung, H.-J. Zhong, H. Yang, Z. Cheng, D. S.-H. Chan, V. P.-Y. Ma, R. Abagyan, C.-Y. Wong, D.-L. Ma, *Angew. Chem., Int. Ed.* 51 (2012) 9010. b) G. Miklossy, T. S. Hilliard, J. Turkson, *Nat. Rev. Drug Discovery* 12 (2013) 611.
- [25] a) V. Fernández-Moreira, F. L. Thorp-Greenwood, M. P. Coogan, *Chem. Comm.* 46 (2010) 186. b) K. K.-W. Lo, M.-W. Louie, K. Y. Zhang, *Coord. Chem. Rev.* 254 (2010) 2603. c) K. K.-W. Lo, S. P.-Y. Li, K. Y. Zhang, *New. J. Chem.* 35 (2011) 265. d) K. K.-W. Lo, K. Y. Zhang, S. P.-Y. Li, *Pure Appl. Chem.* 83 (2011) 823.
- [26] a) S. Liu, H. Liang, K. Y. Zhang, Q. Zhao, X. Zhou, W. Xu, W. Huang, *Chem. Commun.* 51 (2015) 7943. b) W. Lv, T. Yang, Q. Yu, Q. Zhao, K. Y. Zhang, H. Liang, S. Liu, F. Li, W. Huang, *Adv. Sci.* 2 (2015) 1500107. c) X. Zheng, H. Tang, C. Xie, J. Zhang, W. Wu, X. Jiang, *Angew. Chem.* 127 (2015) 8212. d) S. Zhang, M. Hosaka, T. Yoshihara, K. Negishi, Y. Iida, S. Tobita, T. Takeuchi, *Cancer Res.* 70 (2010) 4490. e) Y. Zeng, Y. Liu, J. Shang, J. Ma, R. Wang, L. Deng, Y. Guo, F. Zhong, M. Bai, S. Zhang, D. Wu, *PLoS ONE*, 10 (2015) e0121293. f) T. Yoshihara, Y. Yamaguchi, M. Hosaka, T. Takeuchi, S. Tobita, *Angew. Chem. Int. Ed.* 51 (2012) 4148.
- [27] a) D.-L. Ma, S. Lin, K.-H. Leung, H.-J. Zhong, L.-J. Liu, D. S.-H. Chan, A. Bourdoncle, J.-L. Mergny, H.-M. D. Wang, C.-H. Leung, *Nanoscale* 6 (2014) 8489. b) K.-H. Leung, V. P.-Y. Ma, H.-Z. He, D. S.-H. Chan, H. Yang, C.-H. Leung, D.-L. Ma, *RSC Adv.* 2 (2012) 8273. c) K.-H.

- Leung, H.-Z. He, V. P.-Y. Ma, H. Yang, D. S.-H. Chan, C.-H. Leung, D.-L. Ma, *RSC Adv.* 3 (2013) 1656. d) K.-H. Leung, L. Lu, M. Wang, T.-Y. Mak, D. S.-H. Chan, F.-K. Tang, C.-H. Leung, H.-Y. Kwan, Z. Yu, D.-L. Ma, *PLoS One* 8 (2013) e77021. e) H. Huang, P. Zhang, K. Qiu, J. Huang, Y. Chen, L. Ji, H. Chao, *Sci. Rep.* (2016) 6:20887.
- [28] American Cancer Society. *Cancer Facts & Figures 2017*. Atlanta: American Cancer Society; 2017.
- [29] a) D. Wang, S. J. Lippard, *Nat. Rev. Drug Discov.* 4 (2005) 307. b) L. Kelland *Nat. Rev. Cancer* 7 (2007) 573. c) T. C. Johnstone, K. Suntharalingam, S. J. Lippard, *Chem. Rev.* 116 (2016) 3436. d) N. Muhammad, Z. Guo, *Curr. Opin. Chem. Biol.* 19 (2014) 144.
- [30] A. Ali, S. Bhattacharya, *Bioorg. Med. Chem.* 22 (2014) 4506.
- [31] I. Gamba, I. Salvadó, R.F. Brissos, P. Gamez, J. Brea, M.I. Loza, M.E. Vázquez, M. Vázquez López, *Chem. Commun.* 52 (2016) 1234.
- [32] Y. Fan, C. Li, F. Li, D. Chen, *Biomaterials* 85 (2016) 30.
- [33] R. R. Ye, C. P. Tan, L. N. Ji, Z. W. Mao, *Dalton Trans.* 45 (2016) 13042.
- [34] F.-X. Wang, M.-H. Chen, X.-Y. Hu, R.-R. Ye, C.-P. Tan, L.-N. Ji, Z.-W. Mao, *Sci. Rep.* (2016) 6:38954.
- [35] J.-J. Cao, C.-P. Tan, M.-H. Chen, N. Wu, D.-Y. Yao, X.-G. Liu, L.-N. Ji, Z.-W. Mao, *Chem. Sci.* 8 (2017) 631.
- [36] M.H. Chen, F.X. Wang, J.J. Cao, C.P. Tan, L.N. Ji, Z.W. Mao, *ACS Appl. Mater. Interfaces* 9 (2017) 13304.
- [37] X. D. Song, X. Kong, S. F. He, J. X. Chen, J. Sun, B. B. Chen, J. W. Zhao, Z. W. Mao, *Eur. J. Med. Chem.* 138 (2017) 246.
- [38] a) M. Ouyang, L. Zeng, H. Huang, C. Jin, J. Liu, Y. Chen, L. Ji, H. Chao, *Dalton Trans.* 46 (2017) 6734. b) K. Xiong, Y. Chen, C. Ouyang, R. L. Guan, L. N. Ji, H. Chao, *Biochimie* 125 (2016) 186.
- [39] R.R. Ye, J.J. Cao, C.P. Tan, L.N. Ji, Z.W. Mao, *Chem. Eur. J.* (2017) doi: 10.1002/chem.201703157
- [40] C. Caporale, C. A. Bader, A. Sorvina, K. D. M. MaGee, B. W. Skelton, T. A. Gillam, P. J. Wright, P. Raiteri, S. Stagni, J. L. Morrison, S. E. Plush, D. A. Brooks, M. Massi, *Chem. Eur. J.* (2017) doi: 10.1002/chem.201701352.
- [41] S. P. Li, T. S. Tang, K. S. Yiu, K. K. Lo, *Chem. Eur. J.* 18 (2012) 13342.
- [42] L. He, C. P. Tan, R. R. Ye, Y. Z. Zhao, Y. H. Liu, Q. Zhao, L. N. Ji, Z. W. Mao, *Angew. Chem. Int. Ed.* 53 (2014) 12137.
- [43] R. Cao, J. Jia, X. Ma, M. Zhou, H. Fei, *J. Med. Chem.* 56 (2013) 3636.
- [44] J. Yellol, S. A. Pérez, G. Yellol, J. Zajac, A. Donaire, G. Vigueras, V. Novohradsky, C. Janiak, V. Brabec, J. Ruiz, *Chem. Commun.* 52 (2016) 14165.
- [45] I. Salvadó, I. Gamba, J. Montenegro, J. Martínez-Costas, J. M. Brea, M. I. Loza, M. Vázquez López, M. E. Vázquez, *Chem. Commun.* 52 (2016) 11008.
- [46] Y. Hisamatsu, A. Shibuya, N. Suzuki, T. Suzuki, R. Abe, S. Aoki, *Bioconjugate Chem.* 26 (2015) 857.
- [47] Y. Hisamatsu, N. Suzuki, A. A. Masum, A. Shibuya, R. Abe, A. Sato, S. I. Tanuma, S. Aoki, *Bioconjugate Chem.* 28 (2017) 507.
- [48] G. Trapani, N. Denora, A. Trapani, V. Laquintana, *J. Drug Target.* 20 (2012) 1.
- [49] V. Novohradsky, A. Zamora, A. Gandioso, V. Brabec, J. Ruiz, V. Marchán, *Chem. Commun.* 53 (2017) 5523.
- [50] J. S. Desgrosellier, D. A. Cheresh, *Nat. Rev. Cancer* 10 (2010) 9.
- [51] X. Ma, J. Jia, R. Cao, X. Wang, H. Fei, *J. Am. Chem. Soc.* 136 (2014) 17734.
- [52] a) A. Wilbuer, D. H. Vlecken, D. J. Schmitz, K. Kräling, K. Harms, C. P. Bagowski, E. Meggers, *Angew. Chem., Int. Ed.* 49 (2010) 3839. b) A. Kastl, A. Wilbuer, A. L. Merkel, L. Feng, P. Di Fazio, M. Ocker, E. Meggers, *Chem. Commun.* 48 (2012) 1863.

- [53] a) P. Fernandez, X. Farre, A. Nadal, E. Fernández, N. Peiro, B.F. Sloane, G. Sih, H.A. Chapman, E. Campo, A. Cardesa, *Int. J. Cancer* 95 (2001) 51. b) I. Podgorski, B.F. Sloane, *Biochem. Soc. Symp.* 70 (2003) 263. c) J. Ruiz, C. Vicente, C. de Haro, D. Bautista, *Inorg. Chem.* 52 (2013) 974.
- [54] J. S.-Y. Lau, P.-K. Lee, K.H.-K. Tsang, C. H.-C. Ng, Y.-W. Lam, S.-H. Cheng, K. K.-W. Lo, *Inorg. Chem.* 48 (2009) 708.
- [55] J. C. Fuller, N.J. Burgoyne, R. M. Jackson, *Drug Discov. Today* 14 (2009) 155.
- [56] A. A. Ivanov, F. R. Khuri, H. A. Fu, *Trends Pharmacol. Sci.* 34 (2013) 393.
- [57] L.-J. Liu, W. Wang, S.-Y. Huang, Y. Hong, G. Li, S. Lin, J. Tian, Z. Cai, H.-M. D. Wang, D.-L. Ma, C.-H. Leung, *Chem. Sci.* 8 (2017) 4756.
- [58] M.F. Segura, B. Fontanals-Cirera, A. Gaziel-Sovran, M.V. Guijarro, D. Hanniford, G. Zhang, P. González-Gomez, M. Morante, L. Jubierre, W. Zhang, F. Darvishian, M. Ohlmeyer, I. Osman, M.M. Zhou, E. Hernando, *Cancer Res.* 73 (2013) 626.
- [59] H.-J. Zhong, L. Lu, K.-H. Leung, C. C. Wong, C. Peng, S.-C. Yan, D.-L. Ma, Z. Cai, H.-M. D. Wang, C.-H. Leung, *Chem. Sci.*, 6 (2015) 5400.
- [60] G. Civenni, N. Longoni, P. Costales, C. Dallavalle, C. García Inclán, D. Albino, L. E. Nuñez, F. Morís, G. M. Carbone, C. V. Catapano, *Mol Cancer Ther.* 15 (2016) 806.
- [61] T. S. Kang, W. Wang, H. J. Zhong, Z. Z. Dong, Q. Huang, S. W. Mok, C. H. Leung, V. K. Wong, D. L. Ma, *Cancer Lett.* 396 (2017) 76.
- [62] a) B. Vogelstein, D. Lane, A. J. Levine, *Nature.* 408 (2000) 307. b) J. C. Carry, C. García-Echeverria, *Bioorg. Med. Chem. Lett.* 23 (2013) 2480. c) S. P. Deb, *Mol Cancer Res.* 1 (2003) 1009.
- [63] L. J. Liu, B. He, J. A. Miles, W. Wang, Z. Mao, W. I. Che, J. J. Lu, X. P. Chen, A. J. Wilson, D. L. Ma, C. H. Leung, *Oncotarget.* 7 (2016) 13965.
- [64] a) S. Shin, R. Janknecht, *Biochem. Biophys. Res. Commun* 353 (2007) 973. b) C. Harrison, *Nat. Rev. Drug Discovery* 12 (2013) 188.
- [65] L.-J. Liu, L. Lu, H.-J. Zhong, B. He, D. W. J. Kwong, D.-L. Ma, C.-H. Leung, *J. Med. Chem.* 58 (2015) 6697.
- [66] a) W. Fan, P. Huang, X. Chen, *Chem. Soc. Rev.* 45 (2016) 6488. b) W. A. Velema, W. Szymanski, B. L. Feringa, *J. Am. Chem. Soc.* 136 (2014) 2178.
- [67] J. P. Celli, B. Q. Spring, I. Rizvi, C. L. Evans, K. S. Samkoe, S. Verma, B. W. Pogue, T. Hasan, *Chem. Rev.* 110 (2010) 2795.
- [68] R. Weissleder, *Nat. Biotechnol.* 19 (2001) 316.
- [69] a) I. Yoon, J. Zhu Li, Y. Key Shim, *Clin Endosc* 46 (2013) 7. b) A. B. Ormond, H. S. Freeman, *Materials* 6 (2013) 817.
- [70] Y. Chen, R. Guan, C. Zhang, J. Huang, L. Ji, H. Chao, *Coord Chem Review* 310 (2016) 16.
- [71] B. Therrien, *Chem Eur. J.* 19 (2013) 8378.
- [72] J. Zhou, L. Gai, Z. Zhou, J. Mack, K. Xu, J. Zhao, H. Qiu, K. S. Chan, Z. Shen, *RSC Adv.* 6 (2016) 72115.
- [73] S. S. Teneja, J. Bennett, J. Coleman, R. Grubb, G. Andriole, R. E. Reiter, L. Marks, A.-R. Azzouzi, M. Emberton, *J. Urol.* 196 (2016) 1096.
- [74] C. Mari, V. Pierroz, S. Ferrari, G. Gasser, *Chem. Sci.* 6 (2015) 2660. b) E. C. Glazer, *Israel Journal of Chemistry*, 53 (2013) 391.
- [75] a) M. Stephenson, C. Reichardt, M. Pinto, M. Wächtler, T. Sainuddin, G. Shi, H. Yin, S. Monro, E. Sampson, B. Dietzek, S. A. McFarland, *J. Phys. Chem. A* 118 (2014) 10507. b) C. Reichardt, K. R. A. Schneider, T. Sainuddin, M. Wächtler, S.A. McFarland, B. Dietzek *J Phys Chem A.* 121 (2017) 5635.
- [76] a) C. Mari, H. Huang, R. Rubbiani, M. Schulze, F. Würther, H. Chao, G. Gasser, *Eur. J. Inorg. Chem* 2017 (2017) 1745. b) L. Tabrizi, *Dalton. Trans.* 46 (2017) 7242.
- [77] M. A. Baldo, M. E. Thompson, S. R. Forrest, *Nature*, 403 (2000) 750.

- [78] J. B. Waern, C. Desmarets, L.-M. Chamoreau, H. Amouri, A. Barbieri, C. Sabatini, B. Ventura, F. Barigelletti, *Inorg. Chem.* 47 (2008) 3340.
- [79] a) Y. You, *Curr. Opin. Chem. Biol.* 17 (2013) 699. b) R. Gao, D. G. Ho, B. Hernandez, M. Selke, D. Murphy, P. I. Djurovich, M. E. Thompson, *J. Am. Chem. Soc.* 124 (2002) 14828.
- [80] R. C. H. Robin, A. J. Smith, M. P. Murphy, *Antioxid. Redox Signaling*, 15 (2011) 3021.
- [81] a) S. H. Lim, C. Thivierge, P. Nowak-Sliwinska, J. Han, H. van den Bergh, G. Wagnieres, *J Med Chem* 53 (2010) 2865. b) S. Y. Park, K. T. Oh, Y. T. Oh, N. M. Oh, Y. S. Youn, E. S. Lee. *Chem Commun* 48 (2012) 2522 c) K. Han, Q. Lei, S. Wang, J. Hu, W. Qiu, J. Zhu, W. Yin, X. Luo, X. Zhang, *Adv. Funct. Mater.* 25 (2015) 2961.
- [82] R. C. H. Robin, A. J. Smith, H. M. Cochemé, M. P. Murphy, *Cell* 33 (2012) 341.
- [83] S. P.-Y. Li, Chris T.-S. Lau, M.-W. Louie, Y.-W. Lam, S. H. Cheng, Ke. K.-W. Lo, *Biomaterials* 34 (2013) 7519.
- [84] M. Ouyang, L. Zeng, K. Qiu, Y. Chen, L. Ji, H. Chao, *Eur. J. Inorg. Chem.* 2017 (2017) 1764.
- [85] Y. Li, C.-P. Tan, W. Zhang, L. He, L.-N. Ji, Z.-W. Mao, *Biomaterials* 39 (2015) 95.
- [86] Y. Li, B. Liu, X.-R. Lu, M.-F. Li, L.-N. Ji, Z.-W. Mao, *Dalton Trans.* 46 (2017) 11363.
- [87] Y. You, E. J. Cho, H. Kwon, J. Hwang, S. E. Lee, *Chem. Commun.* 52 (2016) 780.
- [88] W. Lv, Z. Zhang, K.Y. Zhang, H. Yang, S. Liu, A. Xu, S. Guo, Q. Zhao, W. Huang, *Angew. Chem. Int.Ed.* 55 (2016) 9947.
- [89] W. R. Wilson, M. P. Hay, *Nat. Rev. Cancer*, 11 (2011) 393.
- [90] J. Tian, L. Ding, H. J. Xu, Z. Shen, H. Ju, L. Jia, L. Bao, J. S. Yu, *J. Am. Chem. Soc.* 135 (2013) 18850.
- [91] L. He, Y. Li, C.-P. Tan, R.-R. Ye, M.-H. Chen, J.-J. Cao, L.-N. Ji, Z.-W. Mao, *Chem. Sci.* 6 (2015) 5409.
- [92] Y. Zheng, L. He, D.-Y. Zhang, C.-P. Tan, L.-N. Ji, Z.-W. Mao, *Dalton Trans.* 46 (2017) 11395.
- [93] N. Zhao, Y.-H. Wu, H.-M. Wen, X. Zhang, Z.-N. Chen, *Organometallics*, 28 (2009) 5603.
- [94] I. Kim, W. Xu, J.C. Reed, *Nat. Rev. Drug. Discov.* 7 (2008) 1013.
- [95] D. Ron, P. Walter, *Nature Rev. Mol. Cell Biol.* 8 (2007) 519.
- [96] a) J. P. Celli, B. Q. Spring, I. Rizvi, C. L. Evans, K. S. Samkoe, S. Verma, B. W. Pogue, T. Hasan, *Chem. Rev.* 110 (2010) 2795. b) C. M. Moore, D. Pendse, M. Emberton, *Nat. Clin. Pract. Urol.* 6 (2009) 18.
- [97] Z. Yu, W. Pan, N. Li, B. Tang, *Chem. Sci.* 7 (2016) 4237.
- [98] S. Mandal, D. K. Poria, R. Ghosh, P. S. Ray, P. Gupta, *Dalton Trans.* 43 (2014) 17463.
- [99] D. Maggioni, M. Galli, L. D'Alfonso, D. Inverso, M. V. Dozzi, L. Sironi, M. Iannacone, M. Collini, P. Ferruti, E. Ranucci, G. D'Alfonso, *Inorg. Chem.* 54 (2015) 545.
- [100] C. Wang, L. Lystrom, H. Yin, M. Hetu, S. Kilina, S. A. McFarland, W. Sun, *Dalton Trans.* 45 (2016) 16366.
- [101] Z. Li, W. G. Zhu, *Int. J. Biol. Sci.* 10 (2014) 757.
- [102] R.-R. Ye, C.-P. Tan, L. He, M.-H. Chen, L.-N. Ji, Z.-W. Mao, *Chem. Commun.* 50 (2014) 10945.
- [103] R. Sing, J. W. Lillard, JR. *Exp. Mol. Pathol.* 86 (2009) 215.
- [104] a) R. Langer, *Acc. Chem. Res.* 26 (1993) 537; b) Z. Ge, S. Liu, *Chem. Soc. Rev.* 42 (2013) 7289.
- [105] Y. Lu, F. Xue, Z. Zhou, M. Shi, Y. Yan, L. Qin, H. Yang, S. Yang, *Chem. Eur. J.* 20 (2014) 16242.
- [106] Q. Yang, M. Shi, H. Zhao, J. Lin, L. An, L. Cui, H. Yang, Z. Zhou, Q. Tian, S. Yang, *Chem. Eur. J.* 23 (2017) 3728.
- [107] H. Xiang, H. Chen, H. P. Tham, S. Z. F. Phua, J.-G. Liu, Y. Zhao, *ACS Appl. Mater. Interfaces* 9 (2017) 27553.
- [108] J. R. McCarthy, F. A. Jaffer, R. Weissleder, *Small* 2 (2006) 983.

- [109] a) T. R. Sathe, A. Agrawal, S. Nie, *Anal. Chem.* 78 (2006) 5627. b) B. S. Kim, T. A. Taton, *Langmuir* 23 (2007) 2198. c) D. K. Yi, S. T. Selvan, S. S. Lee, G. C. Papaefthymiou, D. Kundaliya, J. Y. Ying, *J. Am. Chem. Soc.* 127 (2005) 4990.
- [110] a) S. T. Selvan, P. K. Patra, C. Y. Ang, J. Y. Ying, *Angew. Chem. Int. Ed.* 46 (2007) 2448. b) A. C. Samia, X. Chen, C. Burda, *J. Am. Chem. Soc.* 125 (2003) 15736.
- [111] C.-W. Lai, Y.-H. Wang, C.-H. Lai, M.-J. Yang, C.-Y. Chen, P.-T. Chou, C.-S. Chan, Y. Chi, Y.-C. Chen, J.-K. Hsiao, *small* 4 (2008) 218.
- [112] a) S. Moromizato, Y. Hisamatsu, T. Suzuki, Y. Matsuo, R. Abe, S. Aoki, *Inorg. Chem.* 51 (2012) 12697, b) A. Nakagawa, Y. Hisamatsu, S. Moromizato, M. Kohno, S. Aoki, *Inorg. Chem.* 53 (2014) 409; c) A. Kando, Y. Hisamatsu, H. Ohwada, T. Itoh, S. Moromizato, M. Kohno, S. Aoki, *Inorg. Chem.* 54 (2015) 5342; d) X. Jiang, J. Peng, J. Wang, X. Guo, D. Zhao, Y. Ma, *ACS Appl. Mater. Interfaces* 8 (2016) 3591.
- [113] Z. Feng, P. Tao, L. Zou, P. Gao, Y. Liu, X. Liu, H. Wang, S. Liu, Q. Dong, J. Li, B. Xu, W. Huang, R. W. Y. Wong, Q. Zhao, *ACS Appl. Mater. Interfaces* 9 (2017) 28319.
- [114] W. Fan, P. Huang, X. Chen, *Chem. Soc. Rev.* 45 (2016) 6488.
- [115] P. Majumdar, X. Yuan, S. Li, B. L. Guennic, J. Ma, C. Zhang, D. Jacquemin, J. Zhao, *J. Mater. Chem. B* 2 (2014) 2838.
- [116] J. Wang, Y. Lu, N. McGoldrick, C. Zhang, W. Yang, J. Zhao, S. M. Draper, *J. Mater. Chem. C* 4 (2016) 6131.
- [117] E. Palao, R. Sola-Llano, A. Tabero, H. Manzano, A. R. Agarrabeitia, A. Villanueva, I. López-Arbeloa, V. Martínez-Martínez, M. J. Ortiz, *Chem. Eur. J.* 23 (2017) 10139.
- [118] J. Zhou, L. Gai, Z. Zhou, J. Mack, K. Xu, J. Zhao, H. Qiu, K. S. Chan, Z. Shen, *RSC Adv.* 6 (2016) 72115.
- [119] a) X. Yi, C. Zhang, S. Guo, J. Ma, J. Zhao, *Dalton Trans.* 43 (2014) 1672. b) S. Takizawa, N. Ikuta, F. Zeng, S. Komaru, S. Sebata, S. Murata *Inorg. Chem.* 55 (2016) 8723.
- [120] J. E. Yarnell, C. E. McCusker, A. J. Leeds, J. M. Breaux, F. N. Castellano, *Eur. J. Inorg. Chem.* 2016 (2016) 1808.
- [121] a) Y. Li, N. Dandu, R. Liu, Z. Li, S. Kilina, W. Sun, *J. Phys. Chem. C*, 118 (2014) 6372; b) A. M. Bünzli, E. C. Constable, C. E. Housecroft, A. Prescimone, J. A. Zampese, G. Longo, L. G.-Escrig, A. Pertegás, E. Ortí, H. J. Bolink, *Chem. Sci.* 6 (2015) 2843; c) X. Zhu, L. Lystrom, S. Kilina, W. Sun, *Inorg. Chem.* 55 (2016) 11908; d) L. Wang, P. Cui, S. Kilina, W. Sun, *J. Phys. Chem. C*, 121 (2017) 5719.
- [122] L. Wang, H. Yin, P. Cui, M. Hetu, C. Wang, S. Monro, R. D. Schaller, C. G. Cameron, B. Liu, S. Kilina, S. A. McFarland, W. Sun, *Dalton Trans.* 46 (2017) 8091.
- [123] F. Xue, Y. Lu, Z. Zhou, M. Shi, Y. Yan, H. Yang, S. Yang, *Organometallics* 34 (2015) 73.
- [124] F. Xue, M. Shi, Y. Yan, H. Yang, Z. Zhou, S. Yang, *RSC Adv.* 6 (2016) 15509.
- [125] Z. Li, Y. Zhang, H. La, R. Zhu, G. El-Banna, Y. Weiland, G. Han, *Nanomaterials*, 5 (2015) 2148.
- [126] J. G. J. Raj, M. Quintanilla, F. Vetrone, *J. Mater. Chem. B*, 4 (2016) 3113.
- [127] H. Chen, G. D. Wang, Y.J. Chuang, Z. Zhen, X. Chen, P. Biddinger, *Nano Lett.* 15 (2015) 2249. b) C. Zhang, K. L. Zhao, W. B. Bu, D. L. Ni, Y. Y. Liu, J. W. Feng, *Angew Chem Int Edit.* 54 (2015) 1770. c) L. Ma, X. J. Zou, B. Bui, W. Chen, K. H. Song, T. Solberg, *Appl Phys Lett.* (2014) 105.
- [128] A. Karnkaew, F. Chen, Y. H. Zhan, R. L. Majewski, W. B. Cai. *Acs Nano.* 10 (2016) 3918.
- [129] G. Lan, K. Ni, R. Xu, K. Lu, Z. Lin, C. Chan, W. Lin, *Angew. Chem. Int. Ed.* 56 (2017) 12102.
- [130] B. Gu, W. Wu, G. Xu, G. Feng, F. Yin, P. H. J. Chong, J. Qu, K.-T. Yong, B. Liu, *Adv. Mater.* 170 (2017) 1076.
- [131] H.A. Collins, M. Khurana, E.H. Moriyama, A. Mariampillai, E. Dahlstedt, M. Balaz, M.K. Kuimova, M. Drobizhev, V.X.D. Yang, D. Phillips, A. Rebane, B.C. Wilson, H.L. Anderson, *Nat. Photon.* 2 (2008) 420.
- [132] H. Tian, Y. Feng, *J. Mat. Chem.* 18 (2008) 1617.

- [133] X. Wang, D. M. Nguyen, C. O. Yanez, L. Rodriguez, H. Y. Ahn, M. V. Bondar, K. D. Belfield, *J. Am. Chem. Soc.* 132 (2010) 12237.
- [134] S. Cho, Y. You, W. Nam, *RSC Adv.* 4 (2014) 16913.
- [135] E. M. Boreham, L. Jones, A. N. Swinburne, M. B.-Desce, V. Hugues, C. Terryn, F. Miomandre, G. Lemerrier, L. S. Natrajan, *Dalton Trans.* 44 (2015) 16127.
- [136] L. K. McKenzie, I. V. Sazanovich, E. Baggaley, M. Bonneau, V. Guerchais, J. A. G. Williams, J. A. Weinstein, H. E. Bryant, *Chem. Eur. J.* 23 (2017) 234.
- [137] a) K. Y. Zhang, S. P.-Y Li, N. Zhu, I. W.-S Or, M. S.-H Cheung, Y.-W. Lam, K. K.-W. Lo., *Inorg. Chem.* 49 (2010) 2530. b) K. Qiu, Y. Liu, H. Huang, C. Liu, H. Zhu, Y. Chen, L. Ji, H. Chao *Dalton Trans.* 45 (2016) 16144. b) R. Cao, J. Jia, X. Ma, M. Zhou, H. Fei, *J. Med. Chem.* 56 (2013) 3636.
- [138] X. Tian, Y. Zhu, M. Zhang, L. Luo, J. Wu, H. Zhou, L. Guan, G. Battaglia, Y. Tian, *Chem. Comm.* 53 (2017) 3303.
- [139] J. S. Nam, M.-G. Kang, J. Kang, S.-Y. Park, S. J. C. Lee, H.-T. Kim, J. K. Seo, O.-H. Kwon, M. H. Lim, H.-W. Rhee, T.-H. Kwon, *J. Am. Chem. Soc.* 138 (2016) 10968.
- [140] Y. Yuan, C. J. Zhang, M. Gao, R. Y. Zhang, B. Z. Tang, B. Liu, *Angew. Chem., Int. Ed.* 54 (2015) 1780.
- [141] a) Y. Hong, J. W. Y. Lam, B. Z. Tang, *Chem. Soc. Rev.* 40 (2011) 5361. b) L. Porres, O. Mongin, C. Katan, M. Charlot, T. Pons, J. Mertz, M. Blanchard-Desce, *Org. Lett.* 6 (2004) 47. c) S. Kim, Q. Zheng, G. S. He, D. J. Bharali, H. E. Pudavar, A. Baev, P. N. Prasad, *Adv. Funct. Mater.* 16 (2006) 2317.
- [142] J. Liu, C. Jin, B. Yuan, X. Liu, Y. Chen, L. Ji, H. Chao, *Chem. Comm.* 53 (2017) 2052.
- [143] L. Porres, O. Mongin, C. Katan, M. Charlot, T. Pons, J. Mertz, M. Blanchard-Desce, *Org. Lett.* 6 (2004) 47.
- [144] K. Qiu, M. Ouyang, Y. Liu, H. Huang, C. Liu, Y. Chen, L. Ji, H. Chao, *J. Mater. Chem. B.* 5 (2017) 5488.
- [145] J. Liu, C. Jin, B. Yuan, Y. Chen, X. Liu, L. Jia, H. Chao, *Chem. Commun.* 53 (2017) 9878.
- [146] a) R. J. Holbrook, D. J. Weinberg, M. D. Peterson, E. A. Weiss, T. J. Meade, *J. Am. Chem. Soc.* 137 (2015) 3379. b) S. Le Gac, M. Foucart, P. Gerbaux, E. Defrancq, C. Moucheron, A. Kirsch-De Mesmaeker, *Dalton Trans.* (2010) 9672.
- [147] a) B. S. Howerton, D. K. Heidary, E. C. Glazer, *J. Am. Chem. Soc.* 134 (2012) 8324. b) E. Wachter, D. K. Heidary, B. S. Howerton, S. Parkin, Edith C. Glazer, *Chem. Commun.*, 48 (2012) 9649. c) A. Zamora, C. A. Denning, D. K. Heidary, E. Wachter, L. A. Nease, J. Ruiz, E. C. Glazer, *Dalton Trans.* 46 (2017) 2165.
- [148] N. J. Farrer, L. Salassa, P. J. Sadler, *Dalton Trans* (2009) 10690.
- [149] E. Wachter, E. C. Glazer, *J. Phys. Chem. A*, 118 (2014) 10474.
- [150] J. D. Knoll, B. A. Albani, C. Turro, *Chem. Commun.* 51 (2015) 8777.
- [151] M. Vijayakumar, M. S. Gopinathan, *J. Mol. Struct.: (TEOCHEM)* 361 (1996) 15.
- [152] a) K. K.-S. Tso, K.-K. Leung, H.-W Liua, K. K.-W. Lo, *Chem. Commun.* 52 (2016) 4557 b) A. Leonida, V. Pierroz, R. Rubbiani, Y. Lan, A. G. Schmitz, A. Kaeck, R. K. O. Sigel, S. Ferrari, G. Gasser, *Chem Sci.* 5 (2014) 4044.
- [153] T. Joshi, V. Pierroz, C. Mari, L. Gemperle, S. Ferrari, G. Gasser, *Angew. Chem. Int. Ed.* 126 (2014) 3004.
- [154] A. Borges, M. J. Saavedra, M. Simões, *Curr. Med. Chem.* 22 (2015) 2590.
- [155] L. Viganor, O. Howe, P. McCarron, M. McCann, M. Devereux, *Curr. Top. Med. Chem.* 17 (2017) 1280.
- [156] N. A. Smith, P. Zhang, S. E. Greenough, M. D. Horbury, G. J. Clarkson, D. McFeely, A. Habtemariam, L. Salassa, V. G. Stavros, C. G. Dowson, P. J. Sadler, *Chem. Sci.* 8 (2017) 395.
- [157] L. Ronconi, P. J. Sadler, *Coord. Chem. Rev.* 251 (2007) 1633.
- [158] N. Graf, S. J. Lippard, *Adv. Drug. Delivery Rev.* 64 (2012) 993.

- [159] S. Medicia, M. Peanaa, V. M. Nurchib, J. I. Lachowiczb, G. Crisponib, M. A. Zoroddua, *Coord. Chem. Rev.* 284 (2015) 329.
- [160] F. Li, J. G. Collins, F. R. Keene, *Chem. Soc. Rev.* 44 (2015) 2529.
- [161] B. P. R. Aradhyula, M. Kalidasan, K. Gangele, D. K. Deb, S. L. Shepherd, R. M. Phillips, K. M. Poluri, M. R. Kollipara, *ChemistrySelect* 2 (2017) 2065.
- [162] U. Śliwinska, F. P. Pruchnik, S. Ułaszewski, M. Latocha, D. Nawrocka-Musiał, *Polyhedron* 29 (2010) 1653.
- [163] G. W. Karpin, J. S. Merola, J. O. Falkinham III, *Antimicrob. Agents Chemother.* 57 (2013) 3434.
- [164] P. N. Rao, S. L. Nongbri, J. R. Premkumar, A. K. Verma, K. Bhattacharjee, S. R. Joshi, S. Forbes, Y. Mozharivskyj, R. Thounaojam, K. Aguan, K. M. Rao, *J. Biol. Inorg. Chem.* 20 (2015) 619.
- [165] N. R. Palepu, J. R. Premkumar, A. K. Verma, K. Bhattacharjee, S. R. Joshi, S. Forbes, Y. Mozharivskyj, K. M. Rao, *Arab. J. Chem* (2015), <https://doi.org/10.1016/j.arabjc.2015.10.011>.
- [166] A. B. P. Rao, N. R. Palepu, D. K. Deb, A. Umab, T. Chiranjeevi, B. Sarkar, W. Kaminsky, K. M. Rao, *Inorg. Chim. Acta* 443 (2016) 126.
- [167] P. A. Vekariya, P. S. Karia, J. V. Vaghasiya, S. Soni, E. Suresh, M. N. Patel, *Polyhedron* 110 (2016) 73.
- [168] S. B. Gajera, J. V. Mehta, P. Thakor, V. R. Thakkar, P. C. Chudasama, J. S. Patel, M. N. Patel, *New J. Chem.* 40 (2016) 9968.
- [169] A. B. P. Rao, A. Uma, T. Chiranjeevi, M. S. Bethu, R. J. Venkateswara, D. K. Deb, B. Sarkar, W. Kaminsky, M. R. Kollipara, *J. Organomet. Chem.* 824 (2016) 131.
- [170] L. C. Brown, E. Ressegue, J. S. Merola, *Organometallics* 25 (2016) 4014.
- [171] A. B. P. Rao, K. Gulati, N. Joshi, D. K. Deb, D. Rambabu, W. Kaminsky, K. M. Poluri, M. R. Kollipara, *Inorg. Chim. Acta* 462 (2017) 223.
- [172] M. Pandrala, F. Li, M. Feterl, Y. Mulyana, J. M. Warner, L. Wallace, F. R. Keene, J. G. Collins, *Dalton Trans.* 42 (2013) 4686.
- [173] T. Mukherjee, M. Mukherjee, B. Sen, S. Banerjee, G. Hundal, P. Chattopadhyay, *J. Coord. Chem.* 67 (2014) 2643.
- [174] L. Lu, L.-J. Liu, W.-C. Chao, H.-J. Zhong, M. Wang, X.-P. Chen, J.-J. Lu, R.-N. Li, D.-L. Ma, C.-H. Leung, *Sci. Rep.* 5:14544 (2015) 1.
- [175] N. Jain, P. Alam, I. R. Laskar, J. Panwar, *RSC Adv.* 5 (2015) 61983.
- [176] a) <http://www.alz.org>. b) C. Y. Wong, L.-H. Chung, L. Lu, M. Wang, B. He, L.-J. Liu, C.-H. Leung, D.-L. Ma, *Curr. Alzheimer Res.* 12 (2015) 439.
- [177] G. S. Yellol, J. G. Yellol, V. B. Kenche, X. M. Liu, K. J. Barnham, A. Donaire, C. Janiak, J. Ruiz, *Inorg. Chem.* 54 (2014) 470.
- [178] B. Y.-W. Man, H.-M. Chan, C.-H. Leung, D. S.-H. Chan, L.-P. Bai, Z.-H. Jiang, H.-W. Li, D.-L. Ma, *Chem. Sci.* 2 (2011) 917.
- [179] L. Lu, H.-J. Zhong, M. Wang, S.-L. Ho, H.-W. Li, C.-H. Leung, D.-L. Ma, *Sci. Rep.* (2015) 5:14619.
- [180] J. Kang, S. J. C. Lee, J. S. Nam, H. J. Lee, M.-G. Kang, K. J. Korshavn, H.-T. Kim, J. Cho, A. Ramamoorthy, H.-W. Rhee, T.-H. Kwon, M. H. Lim, *Chem. Eur. J.* 23 (2017) 1645.
- [181] B. B. Aggarwal, *Nat. Rev. Immunol.* 3 (2003) 745.
- [182] R. M. Fleischmann, I. Iqbal, *R.L. Stern, Expert. Opin. Drug Saf.* 3 (2004) 391.
- [183] A. Rubbert-Roth, A. Finckh, *Arthritis Res. Ther.* 11 (2009) (Suppl 1): S1. doi: 10.1186/ar2666.
- [184] H. Mouhsine, H. Guillemain, G. Moreau, N. Fourati, C. Zerrouki, B. Baron, L. Desallais, P. Gizzi, N. Ben Nasr, J. Perrier, R. Ratsimandresy, J.-L. Spadoni, H. Do, P. England, M. Montes, J.-F. Zagury, *Sci. Rep.* (2017) 7:3424.
- [185] C.-H. Leung, H.-J. Zhong, D. S.-H. Chan, D.-L. Ma, *Coord. Chem. Rev.* 257 (2013) 1764.

- [186] T.-S. Kang, Z. Mao, C.-T. Ng, M. Wang, W. Wang, C. Wang, S. M.-Y. Lee, Y. Wang, C-H. Leung, D.-L. Ma, *J. Med. Chem.* 59 (2016) 4026.
- [187] C.-H. Leung, L.-J. Liu, L. Lu, B. He, D. W. J. Kwong, C.-Y. Wong, D.-L. Ma, *Chem. Commun.* 51 (2015) 3973.